May 2014

Optical Studies of Oxidative Stress in Lung Tissue: Rodent Models

Reyhaneh Sepehr
University of Wisconsin-Milwaukee

OPTICAL STUDIES OF OXIDATIVE STRESS IN LUNG TISSUE: RODENT MODELS

by

Reyhaneh Sepehr

A Dissertation Submitted in

Partial Fulfillment of the

Requirements for the Degree of

Doctor of Philosophy

in Engineering

at

The University of Wisconsin-Milwaukee

May 2014

ABSTRACT
OPTICAL STUDIES OF OXIDATIVE STRESS IN LUNG TISSUE:
RODENT MODELS

by

Reyhaneh Sepehr

The University of Wisconsin-Milwaukee, 2014
Under the Supervision of Professor Mahsa Ranji

Objectives: There currently exists a need for reliable measurements of tissue metabolic state at cellular levels. The objective of this research was to study tools capable of evaluating cellular redox states in intact tissue. To meet this goal, three different instruments (cryoimager, fluorometer, and fluorescent microscope) were used to study the metabolism and functions of the mitochondria at different levels and regimes (cryo, *ex vivo*, *in vivo* and *in vitro*).

Introduction: Through optical monitoring of autofluorescent mitochondrial metabolic coenzymes, as well as exogenous fluorophores, the state of mitochondria can be probed in real time in many intact organs and *in vitro*. Autofluorescent mitochondrial metabolic coenzymes, studied here, include NADH (nicotinamide adenine dinucleotide) and FAD (flavin adenine dinucleotide), and the ratio of these fluorophores, referred to as the mitochondrial redox ratio (RR), can be used as a quantitative metabolic marker of the tissue. Exogenous fluorophores include but are not limited to tetramethylrhodamine

(TMRM) and Mito-SOX, which are used to evaluate the mitochondrial membrane potential and level of reactive oxygen species (ROS) in the mitochondria, respectively.

Methods: Different optical imaging and acquisition techniques were studied to evaluate oxidative stress in lung tissue and cells in cryogenic temperatures, *in vivo*, *ex vivo*, and *in vitro*. Though in essence the underlying technological and biological principles appear to be the same, imaging in each of these regimes imposed unique challenges requiring significantly different approaches to system design, data acquisition, and processing. A brief description of each technique is provided here and each is described in detail in the following chapters.

The first device utilized is a cryoimager, which sequentially slices tissue and acquires fluorescence images of up to five fluorophores in cryogenic temperatures (-40^{o}C). Rapid freezing of organs preserves the tissue's metabolic state and subsequent low temperature fluorescence imaging (cryoimaging) provides high fluorescence quantum yield as compared with room temperature. Sequential slicing of the tissue provides 3D spatial distribution of NADH and FAD fluorescence intensities throughout the tissue. These studies were conducted using the cryoimager in the Biophotonics Lab on different models of lung injuries including ischemia, hyperoxia, and BPD (bronchopulmonary dysplasia).

The second device is a fluorometer, which was designed and implemented in the Biophotonics Lab. It is capable of monitoring the dynamics of the metabolism of the tissue through the use of optical surface fluorescence measurements of NADH and FAD. The ratio of these fluorophores, referred to as the mitochondrial redox ratio (RR), can be

used as a quantitative metabolic marker of tissue. Surface fluorescence signals from NADH and FAD were acquired in the absence (baseline) and presence of metabolic perturbers (e.g. pentachlorophenol, rotenone, or potassium cyanide), in the presence of blood, and eventually *in vivo*.

The third instrument, a fluorescent microscope, is used to image slides and dishes containing stained cells (e.g. endothelial cells, perycites, or fibroblasts) from lungs, hearts, and retinas to study their structure and dynamics at cellular level. Images of retinas were classified as normal or injured using developed cytometry tools and morphologic parameters. For heart and lung, the dynamics of concentration of reactive oxygen species (mainly superoxide) and calcium is monitored over time in cultured live cells.

Results: In the cryogenic temperatures, lung treatment with KCN (inhibitor of Complex IV), resulted in an increase in RR and sets the upper limit of the NADH signal level while injured lungs (BPD model, hyperoxia and IR) showed a more oxidized chain compared with control lungs, and as a result more oxidative stress.

In *ex vivo* fluorometric studies, an increase in RR from chain inhibitors (including KCN and rotenone), and a decrease in the same due to an uncoupler (PCP), all from baseline was observed which was consistent with the cryoimaging results. The same experiments in isolated perfused lungs previously treated with hyperoxia showed the same direction but different levels indicating the impairment in different complexes due to hyperoxia.

Segmentation algorithm developed here showed 90% accuracy comparing to manual counting, and studying the cells in retina slides confirms apoptosis and oxidative stress in

retinas from injured mice. In live cells, studying the dynamics of calcium concentration in the presence of different perturbations enabled us to study the behavior of mitochondrial regulated calcium channels. Also, changes in the Mito-SOX channel gave us the dynamics of mitochondrial ROS in the presence of chain perturbers (chemicals and gas).

Conclusion: Optical instrumentation combined with signal and image processing tools provide quantitative physiological and structural information of diseased tissue due to oxidative stress.

TABLE OF CONTENTS

LIST OF FIGURES

LIST OF TABLES

LIST OF ABBREVIATIONS

ADP - Adenosine Diphosphate

APD - Avalanche Photodiode

ATP - Adenosine Triphosphate

BCL-2 -B Cell Lymphoma Gene

DAQ - Data Acquisition Module

DNA - Deoxyribose Nucleic Acid

DNP - Dinitrophenol

DRS - Diffuse Reflectance Spectroscopy

DMEM- Dulbecco's Modified Eagle's Medium

$FADH_2$ - Flavin Adenine Dinucleotide

HBSS - Hank's Balanced Salt Solution

H&E - Hematoxylin and Eosin

IR - Ischemia Reperfusion

KCN - Potassium Cyanide

MTG- Mito-Tracker Green

NADH - Nicotinamide Adenine Dinucleotide

NADPH - Nicotinamide Adenine Dinucleotide Phosphate

NAD(P)H - Combination of NADH and NADPH

P21 - Postnatal Day 21

P42 - Postnatal Day 42

PBS - Phosphate Buffered Saline

PC - Personal Computer

PCP - Pentachlorophenol

PCR - Polymerase Chain Reaction

PMT - Photomultiplier Tube

ROS- Reactive Oxygen Species

TDMS - Technical Data Management Stream

TMRM- Tetramethylrhodamine

ACKNOWLEDGMENTS

I would like to thank my advisor, Dr. Mahsa Ranji, for providing me with the opportunity to design, develop and study the constituent experiments of this thesis. Her high standards and commitment to research set a strong example for me in the lab and provided me with the motivation necessary for the continuation of this work.

The research presented here would not have been possible without the help of our collaborators. I would like to thank Drs. Sheibani and Sorenson from University of Wisconsin Madison, Dr. Audi from Marquette university, Drs. Jacobs and Kondouri from Medical College of Wisconsin and Drs. Holmuhamedov and Jahangir from Aurora healthcare. Their guidance in the biological side of the research and their patience throughout the progress of the work was invaluable. I also would like to sincerely thank all of the members of the Biophotonics Lab for their unending support and insight.

Last but not least I want to thank my family: my best friend and love of my life, Ali, without his endless support I wouldn't be here today; and my parents who have endlessly supported me throughout my life.

I dedicate this thesis to my son, Arad, his love and passion for life made me move at a faster pace in my own life.

Chapter 1

Introduction and Background

1. Introduction and Background

Biophotonics involves the study of the interaction between optical energy and biological tissues [7] and, with the advancement of technology and the increasing understanding of biological systems, is one of the fastest growing research areas. Currently, the majority of research in the field of biophotonics is focused on the determination of tissue properties, and thus tissue disease diagnosis.

Although the most common imaging modalities include X-ray radiography, ultrasound imaging (ultrasonography), X-ray computed tomography (CT), and magnetic resonance imaging (MRI), optical imaging, which is compared with other modalities in table 1, is currently emerging as a promising new addition to medical imaging.

Table 1. Comparison of various Medical imaging Modalities [8].

Characteristics	**X-ray**	**Ultrasonography**	**MRI**	**Optical imaging**
Soft-tissue contrast	Poor	Good	Excellent	Excellent
Spatial resolution	Excellent	Good	Good	Mixed
Maximum imaging depth	Excellent	Good	Excellent	Good
Function	None	Good	Excellent	Excellent
Non-ionizing radiation	No	Yes	Yes	Yes
Data acquisition	Fast	Fast	Slow	Fast
Cost	Low	Low	High	Low

From the table, it can be seen that optical imaging techniques combine safe radiation (non-ionizing) with fast, low-cost and high-contrast imaging. Depending on the

regime of the optical imaging being used (absorption, fluorescence, or Raman scattering), it can even provide biochemical information due relation to molecular conformation. Optical absorption provides contrast for functional imaging since it provides information on the concentration of hemoglobin and oxygen saturation of hemoglobin (particularly important in cancer). Other optical techniques including scattering, polarization and Doppler effect can provide rich information regarding molecular structures of biomarkers, cellular size distribution, blood flow, detection of multiple contrast agents and opportunity for high resolution imaging [8].

The research presented here includes the development of optical instruments in different regimes, conducting experiments, acquiring signals and images and processing them to extract markers for tissue metabolism as well as injuries and diseases. We monitored metabolic states of different tissues, mainly lungs, in diseases of clinically important disorders including cardiopulmonary injuries. The ultimate goal of my research is to translate optical imaging techniques developed to clinical avenues, and to transfer the instruments developed for animal models to bedsides for patient diagnosis.

1.1. My Major Contributions

I have contributed in four major areas:

1- Instrumentation:

I have been involved in the design and implementation of an optoelectronic device called fluorometer. It is designed in such a way to monitor the relative

concentration of two intrinsic fluorophores in the mitochondria of the cell, namely NADH and FAD. I have also been involved in modifying a cryoimager instrument to image different tissue sizes, as well as to improve magnification and resolution by improving the embedding, mounting and imaging of sections.

2- Experimentation, signal and image acquisition:

I have assembled the required tools, and designed experimentation protocols to study the metabolism in different regimes of optical studies, including whole organ cryoimaging, *ex vivo*, *in vivo* and *in vitro* studies. For each regime of studies, unique treatment and preparation of the tissues, as well as proper imaging and acquisition methods are required. The tissues, cell and microscope slides were provided by the VA hospital, the Medical College of Wisconsin, the University of Wisconsin-Madison, and Aurora St. Luke's Health Center.

3- Signal and image processing:

I processed raw pulses and signals acquired from fluorometry as well as the raw images from the cryoimager and microscope to show the dynamics of the metabolism in live tissue, the redox state of frozen tissue, the dynamics of calcium and reactive oxygen species (ROS) in live cells, and tissue properties in fixed slides. The processing was mostly done via algorithms I developed in Matlab with minor steps in ImageJ.

Also, as a side project, I have been working on the problem of figure text resolution detection in figures of biomedical articles in a biomedical figure search engine to improve the accuracy of the search engine, which is a pattern recognition problem.

4- Interpretation of metabolic data in lung injuries:

The focus of this thesis was mainly on the lung tissue and its metabolism, injuries and diseases. Understanding the mechanism and function of this vital organ is of great importance and is essential for designing experiments and injury models and interpreting the results. According to statistics, respiratory disease is a common and important cause of illness and death around the world. In the US, approximately 1 billion "common colds" occur each year [5]. In the UK, approximately 1 in 7 individuals are affected by some form of chronic lung disease, most commonly chronic obstructive pulmonary disease, which includes asthma, chronic bronchitis and emphysema [6]. Respiratory diseases (including lung cancer) are responsible for over 10% of hospitalizations and over 16% of deaths in Canada [7].

Journal Publications and Conference Abstracts

J1- R. Sepehr, K. Staniszewski, S. Audi, E. R. Jacobs, and M. Ranji, "Surface Fluorescence Studies of Tissue Mitochondrial Redox State in Isolated Perfused Rat Lungs," **Ann Biomed Eng**, Dec 13 2012.

J2- R. Sepehr, K. Staniszewski, S. Maleki, E. R. Jacobs, S. Audi, and M. Ranji, "Optical imaging of tissue mitochondrial redox state in intact rat lungs in two models of pulmonary oxidative stress" **Journal of Biomedical Optics**, Vol 17, No. 4, April 2012.

J3- R. Sepehr, S. Audi, S. Maleki, K. Staniszewski, A. L. Eis, G. G. Konduri, M. Ranji ," Optical Imaging of Lipopolysaccharide-induced Oxidative Stress in Acute Lung Injury from Hyperoxia and Sepsis" **JIOHS**, Vol. 06, No. 03, 2013.

J4- R. Sepehr, S. Audi, K. Staniszewski, E. R. Jacobs, and M. Ranji, " Novel Flurometric Tool to Assess Mitochondrial Redox State of Isolated Perfused Rat Lungs after

Exposure to Hyperoxia," to be published in **IEEE Journal** of Translational Engineering in Health and Medicine, 2013.

J5- S. Maleki, **R. Sepehr**, K. Staniszewski, N. Sheibani, C. M. Sorenson, and M. Ranji, "Mitochondrial redox studies of oxidative stress in kidneys from diabetic mice**."** **Journal of Biomedical Optics Express**, Vol. 3, No. 2, pp. 273-281, Feb 2012.

J6- S. Maleki, S. Gopalakrishnan, Z. Ghanian, **R. Sepehr**, H. Schmitt, J. Eells, M. Ranji, "Optical Imaging of Mitochondrial Redox State in Rodent Model of Retinitis Pigmentosa " **Journal of Biomedical Optics**, Vol 17, No. 4, April 2012.

C1- R. Sepehr, et al, "*Fluorometry of ischemia reperfused rat lungs in vivo*", in Proceeding of SPIE Photonices west, 2013.

C2- Z. Ghanian, **R. Sepehr**, et al, "*Optical Imaging of Oxidative Stress in Rodent Model of Retinitis Pigmentosa*", in Proceeding of SPIE Photonices west, 2013.

C3- R. Sepehr, et al, "*Optical studies of tissue mitochondrial redox in isolated perfused rat lungs*", in Proceedings of SPIE 8207D, San Fransisco, 2012;

C4- R. Sepehr, et al, "*Classification of retinopathic injury using image cytometry and vasculature complexity*", in Proceedings of SPIE 8225, San Fransisco, 2012;

C5- S. Maleki, **R. Sepehr**, et al, "*Optical cryoimaging of kidney mitochondrial redox state in diabetic mice models*", in Proceedings of SPIE 8225, San Fransisco, 2012.

C6- K. Staniszewski, **R. Sepehr**, et al, " *Automated Evaluation of Retinopathies Using Image Cytometry*", DAMOR Workshop, Feb 2012.

C7- R. Sepehr, et al, "*Optical Cryoimaging of Kidney Mitochondrial Redox State and the Effect of BCL-2 Family Expression*", BMES Oct 2011.

C8- R. Sepehr, et al, "*Fluorescence Spectroscopy and Cryoimaging of Rat Lung Tissue Mitochondrial Redox State*", in Proceedings of SPIE 80870, Munich, 2011;

1.2. Biological Background

1.2.1. Cell Structure and the Mitochondrion

All biological organisms are made up of cells, the "building block of life" [9]. Figure 1.a shows the diagram of a typical eukaryotic cell [3]. Many injuries and ailments can be traced back to irregularities in the behavior within the cell [10]. Early detection and treatment of such injuries could lead to a significantly lower rate of permanent damage as a result of such injuries and help in reducing further therapy's costs.

Although all sub-cellular organelles are essential for the organism to remain healthy and alive, the mitochondrion (figure 1.b), the power house of the cell [11] that is responsible for metabolic processes [12], is perhaps the most critical. The mitochondria are responsible for the chemical reactions resulting in providing energy for the cells and are necessary for sustaining life in a biological organism [13].

The metabolic process is generally achieved through a series of reactions referred to as aerobic respiration [14]. In this process, a chain of the mitochondrial coenzymes are oxidized resulting in adenosine triphosphate (ATP), which is the unit of energy for the cells. The amount of energy that can be supplied for the cell is positively correlated to the amount of oxygen present in the mitochondria, and an irregular amount of oxygen in the cell and its surrounding environment (**oxidative stress**) leads to perturbation to cell

functions and eventually cell death. The majority of energy in the cell is produced this way via the electron transport chain [12], which is represented in Figure 2 [2].

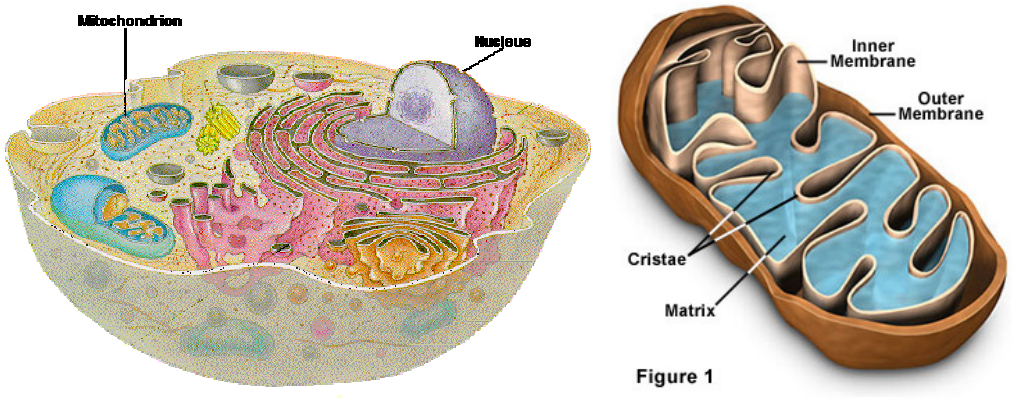

(a) (b)

Figure 1. Cell Structure and Mitochondrion. a) Diagram of the cell including organelles [3] and b) mitochondrion [5].

The electron transport chain is a complex system of chemical reactions that take place in the inner mitochondrial membrane and is used to create a proton gradient across the membrane by pumping excess hydrogen ions into the mitochondria's "intermembrane space" [15]. In the electron transport chain, two proteins, NADH [16] and $FADH_2$ (flavin adenine dinucleotide) [17], are oxidized through a series of protein complexes resulting in a release of protons, which are pumped into the intermembrane space using a portion of the energy released, thus creating a proton gradient.

Finally, ATP is generated by the escape of these protons to the intermembrane space through ATP synthase [12] in conjunction with adenosine diphosphate (ADP) and inorganic phosphate. A change in the oxidation state of these two proteins, or in another

word, a change in the concentration of the oxidized form is a direct marker of a change in tissue oxidation status and metabolism [18].

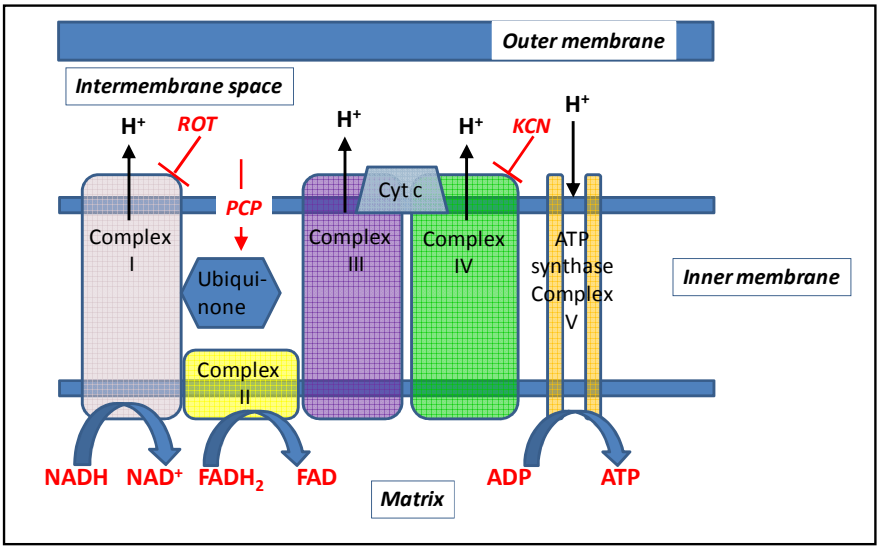

Figure 2. Electron Transport Chain. Schematic representation of subunits of mitochondrial oxidative phosphorylation complexes. Hydrogen ions are transported from the mitochondrial matrix across the inner mitochondrial membrane into the intermembrane space by complexes I, III, and IV. The movement of hydrogen ions down the electrochemical gradient is coupled to the phosphorylation of adenosine diphosphate (ADP) to form adenosine triphosphate (ATP) by complex V. Electrons from the autofluorescent reducing agent, nicotine adenine dinucleotide (NADH), move from complex I through ubiquinone to complex III and then complex IV via cytochrome c (Cyt c). Electrons from succinate, another reducing agent, enter the respiratory chain through flavin adenine dinucleotide (FAD), which is covalently linked to complex II of the respiratory chain. Like NADH, the reduced form of FAD (FADH) is autofluorescent. Rotenone (ROT) and potassium cyanide (KCN) inhibit complex I and IV, respectively. Pentachlorophenol (PCP) is a protonophore which increases membrane proton conductivity, disrupts the proton gradient across the membrane, and as a result uncouples mitochondrial electron transport chain from phosphorylation [146].

Reactive oxygen species (ROS) are chemically reactive molecules containing oxygen. ROS form as a natural byproduct of the normal metabolism of oxygen and have important roles in cell signaling and homeostasis. Oxidative stress, which is often due to an irregularity in the amount of oxygen introduced to the mitochondria, represents an imbalance between production and consumption of ROS. An excessive amount of ROS or the production of peroxides and free radicals, can cause damage to any and all parts of a cell [19]. This is especially important given that a variety of diseases can disrupt the

balance of oxygen flow into and around cells, causing improper function of the mitochondria, and thus an increased rate of cell death via apoptosis or necrosis [20]. A slight increase in oxidative stress leads to mitophagy, in which the mitochondria degrades, but the cell manages to recycle the nutrients released. However, as oxidative stress increases, the cells begin to undergo apoptosis, or programmed cell death, or in extreme cases, necrosis, which is abnormal cell death. In many cases, the amount of oxygen available to a cell can accurately represent the health of the cell and be used as a diagnostic tool. This is especially true in cases related to mitochondrial dysfunction or diseases related to oxidative stress. In these cases, the oxidation state, or redox state, of the tissue serves as a sensitive and reliable measure for the evaluation of cell behavior [21].

1.3. Fluorescence

1.3.1. Description of Fluorescence

Optical fluorescence techniques have the potential to investigate tissue health in real time in a non-destructive manner in intact organs both *in vivo* and *ex vivo* [22-28]. Using the fluorescent signals of intrinsic fluorophores present in the cell, it is possible to determine the oxidation status of the cell. In these studies, fluorescence spectroscopy was mainly used to study lung bioenergetics [29-31].

A fluorophore is a chemical compound which can emit photons with specific wavelengths when excited with specific higher-energy photons [32].

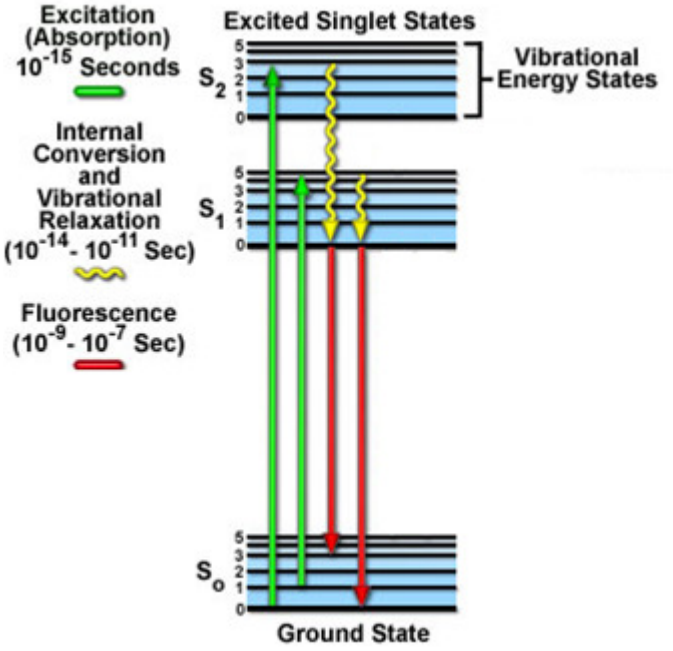

Figure 3. Jablonski Diagram of Fluorescence. Fluorescence as a result of molecule excitation. Green lines indicate excitation, yellow lines relaxation, and red lines emission of fluorescence [4].

Molecules of fluorophores are in some initial energy state, i.e. resting state, prior to being exposed to a source of energy, e.g. a bright light source. When the molecule is exposed to a source of energy, it absorbs the energy from the incident source and goes to an excited energy state. Once there, a portion of the energy is lost to lattice vibrations and other avenues prior to the release of a photon and relaxation to the initial energy state. In the transition back to the ground state, there is a probability, termed the fluorescence quantum yield, of emitting photons of lower energy than the excitation photons, which can be collected by a photoelectric device to quantify the amount of energy released. This process can be seen in Figure 3 [4].

For intrinsically fluorescent molecules, there is a narrow range of photon energies which can cause this excitation, corresponding to the allowable energy states of the

molecule. Since the energy of a photon is inversely proportional to its wavelength, or directly proportional to the frequency, this means that only a specific range of wavelengths can be used to excite a given molecule. In addition, because the emitted fluorescent light has an energy equal to the energy released when the molecule transitions back to its ground state, the wavelength, or color, of this light has a narrow range.

Finally, since the molecule lost some energy along other pathways, the excitation (absorption) and emission spectra must be different, a phenomenon known as the Stokes shift [33]. This phenomenon can be exploited through the use of optical filters or dichroic mirrors to separate the excitation and emission light, so that the only signal that reaches the detector is the emitted fluorescence. The narrow range of both the excitation and emission light is actually beneficial, since multiple molecules can be monitored sequentially, provided that their fluorescence spectra are not completely overlapping [21].

1.3.2. Intrinsic Mitochondrial Fluorophores

In most tissues, there are several intrinsic fluorophores, including NADH, flavins, tryptophan, collagen, and porphyrins, which can be used as structural or physiological tissue parameters. Two of these fluorophores, NADH and FAD (one of the flavins), are of particular interest since they are essential in the metabolic pathway of the mitochondria, as they are located in the first two protein complexes of the electron transport chain [12] and can be used as markers of oxidation of the cell. The spectra of these auto-fluorescent coenzymes are shown in Figure 4 [34, 35].

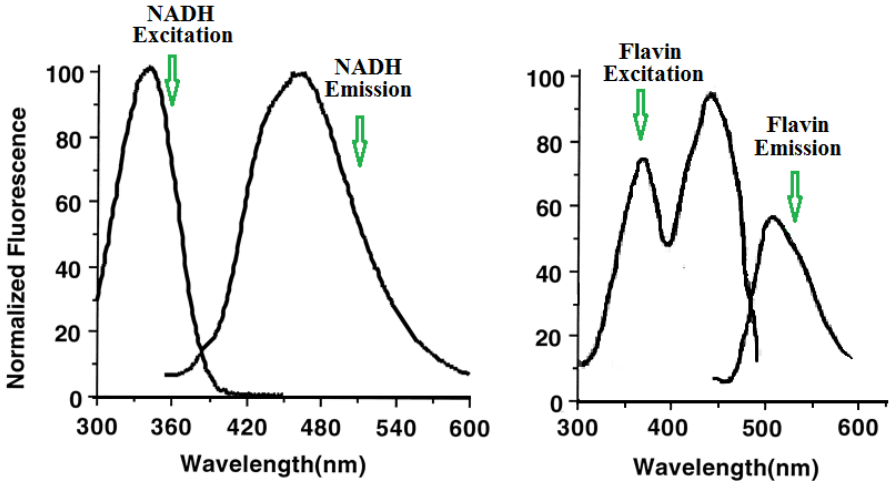

Figure 4. Excitation and emission spectra of NADH (left) and FAD (right).

NADH only fluoresces in its reduced form, whereas FAD only fluoresces in its oxidized form. As a result, the ratio of these two fluorophores, called the mitochondrial redox ratio, is used as a marker of the oxidation state within the tissue [36]. This ratio is beneficial as a quantitative marker of tissue metabolism independent of the number of mitochondria.

NADH and FAD can be excited by filtering a white light such as mercury light at excitation wavelengths. NADH has a maximum in its excitation spectrum at around 340 nm and an emission maximum at 460 nm, and FAD has its excitation maximum at 448 nm and a maximum in the emission spectrum at 520 nm. The overlap between NADH emission and FAD excitation requires that the two fluorophores be excited and detected sequentially, but the fact that the emission spectra don't overlap with each other allows for selective detection of fluorescence between the two fluorophores. Hence, by detecting

the fluorescence of each of these fluorophores, one can obtain a measure of the oxidation state of cells within an organ.

These fluorescent signals are also dependent on the concentration of mitochondria, the presence of absorbing factors such as blood, the movement of the tissue (in *in vivo* experiments), and the presence of interfering factors such as other endogenous fluorophores with the same excitation/emission spectra (namely NADPH and collagen). The first three factors can be effectively canceled out using redox calculations. As for the interfering fluorophores, since they are not involved in the mitochondrial electron transport chain, they would either contribute to the baseline level of the signals or are small enough compared to NADH and FAD fluorescent signals that they can be ignored (see chapter 3 for more details). As a result, the changes in the measured redox ratio are due to changes in the mitochondrial redox state, and are not impacted by the other endogenous fluorophores present in the tissue [21].

1.4. Florescence imaging techniques

Fluorescence imaging techniques provide both anatomical and functional information of tissue via intrinsic fluorophores or exogenous tagged proteins [60]. These techniques are widely used to probe tissue redox state and energy homeostasis in organs such as the heart [26], brain [28], kidney [27, 61], liver [62], skeletal muscle [63], cervix [64], and colon [65] as well as to diagnose diseases such as breast cancer tumor localization and oxygenation [66, 67]. Furthermore, these techniques have been shown to

have a high sensitivity and specificity for discriminating between diseased and non-diseased tissue [68].

Fluorescence spectroscopy and imaging of intrinsic molecules *in vivo* as intracellular oxygen indicators was first introduced by Britton Chance and colleagues [37-42]. Their pioneer work on spectroscopic monitoring of mitochondrial redox state in isolated mitochondria in vitro [38, 39], and in vivo in various organs (e.g., brain, kidney, heart) [43-49] has shaped our understanding of cellular bioenergetics under different physiological conditions.

Tissue metabolic state, which is an indicator of cellular oxygen consumption, can be extracted from fluorescence images of intrinsic fluorophores [69, 70]. The mitochondrial metabolic coenzymes NADH and $FADH_2$ are the primary electron carriers in oxidative phosphorylation and a change in the mitochondrial redox ratio (RR = NADH/FAD) is an indicator of a change in lung tissue bioenergetics [18]. NADH and FAD (the oxidized form of $FADH_2$) are autofluorescent and can be monitored without exogenous labels by noninvasive optical techniques [25]. The fluorescence signals of these intrinsic fluorophores have been used as indicators of tissue metabolism in injuries due to hypoxia, ischemia, and cell death [71]. Ranji et al. demonstrated that the ratio of these fluorophores, RR, is a marker of the mitochondrial redox and metabolic state of myocardial tissue in intact hearts or *in vivo* situations [36, 72-74].

Different groups have used optical monitoring of cancer tissue in different diseases. Mycek et al. have used optical spectroscopy in studies of pancreatic cancer in clinical practice [50-52]. Ramanujam et al. have shown the ability of endogenous redox

imaging to differentiate normal, precancerous, and cancerous squamous epithelial tissues by multiphoton microscopy[53, 54]. Mayevsky's group has used NADH spectroscopy and blood oxygenation in brain tumor metabolism studies in vivo [55, 56]. Kortum's group examined optical imaging for diagnosis of cervical, esophageal, and oral cancer [57,58]. Georgakoudi et al. have studied endogenous redox ratio in human epithelial cell apoptosis studies [59, 60]. we have used optical biopsy, cryoimaging and fluorescence spectroscopy for cardiovascular and pulmonary diseases. [34, 35, 61-67].

1.1. Lung tissue, injury models and diseases

Exposure to elevated O_2 (hyperoxia) is a common and necessary therapy for adult and pediatric patients with acute respiratory distress syndrome (ARDS) to restore blood oxygen tension (PO_2) to a level that sustains vital organ metabolic requirements [6, 37]. However, sustained exposure to high O_2 concentrations (> 50%) causes lung O_2 toxicity injury. This injury, which is the result of enhanced production of reactive O_2 species (ROS), i.e. oxidative stress, may further impair lung function and contribute to the very dysfunction that it is intended to alleviate [38, 39].

Reactive oxygen species (ROS) have been implicated in the pathogenesis of many acute and chronic pulmonary disorders such as acute lung injury (ALI) in adults and bronchopulmonary dysplasia (BPD) in premature infants. Bacterial infection and oxygen toxicity, which result in pulmonary vascular endothelial injury, contribute to impaired vascular growth and alveolar simplification seen in the lungs of premature infants with

BPD. Hyperoxia induces ALI, reduces cell proliferation, causes DNA damage, and promotes cell death by causing mitochondrial dysfunction.

BPD is a chronic lung condition that affects premature infants who receive supplemental oxygen (hyperoxia) or ventilator support for long periods of time. Studies have shown that the premature lung can be acutely injured by either oxygen or mechanical ventilation, resulting in interference with or inhibition of lung alveolar and vascular development [40-42]. Premature infants are also more likely to be exposed to infection *in utero* or during postnatal life, which accelerates the subsequent development of BPD.

Lipopolysaccharide (LPS) is an endotoxin, which is derived from the cell wall of gram-negative bacteria and induces the release of cytokines and ROS such as superoxide, hydroxyl radicals, and peroxynitrite. The endothelial injury caused by LPS stimulation contributes to vascular remodeling by inhibiting endothelial cell proliferation, migration and angiogenesis, which together contribute to impaired lung growth in BPD.

ARDS, a manifestation of ALI, is a serious illness associated with severe and diffuse injury to the alveolar-capillary membrane of adult lungs. In ARDS, organs are deprived of the required amount of O_2, which impairs their proper function. Despite the high morbidity and mortality rates of this illness, the mechanisms underlying the development of ARDS/ALI are not completely understood [43-46]. Respiratory distress syndrome (RDS) in neonates occurs due to surfactant deficiency and immaturity of the lung parenchyma and vasculature. The course of RDS is characterized by parenchymal lung injury, which leads to impaired gas exchange, neutrophil accumulation in the lung,

the expression of pro-inflammatory mediators, increased vascular permeability and damage to the lung epithelium and endothelium. One of the contributing factors in the development of ALI in neonates is exposure to bacterial infections, including endotoxins from gram-negative bacteria. [43-45, 47-49]. Exposure to supplemental oxygen, which is often used in the treatment of RDS, can also contribute to lung injury.

As previously reported, LPS induces elevated ROS levels in endothelial cells. Decreased antioxidant capacity of pulmonary vascular tissue along with increased production of ROS contributes to the injury seen in LPS-induced ALI/BPD [44, 50-55]. ROS generated by LPS exposure in endothelial cells is regarded as a key to the modulation of the pulmonary vascular endothelial damage, which leads to higher oxidative stress. Increased ROS may cause cell injury, activate the inflammatory response, promote cytotoxicity, and activate signaling pathways that lead to pro-apoptotic signaling. Thus, LPS has been considered the principal component in the induction of ALI and BPD in adults and premature infants, respectively [47, 50, 56, 57].

Ischemia-reperfusion (IR) injury of lung tissues is commonly encountered clinically in conditions such as lung transplantation, necrotizing pneumonias, or crush injury to the chest [58]. Approximately 1,500 lung transplants are successfully performed each year in the US [59] with many times that number lost due to prohibitive ischemic times.

In all these lung injuries, we have studied the effect of the damage on the electron transport chain and cell viability. We monitored the metabolic activities in these

clinically important cardiopulmonary disorders and injuries using optical imaging tools with the future goal of translation to clinical avenues.

Chapter 2

Cryoimaging

2. Cryoimaging

2.1. Introduction

The cryoimager (Barlow scientific, Olympia, WA), described and used in this chapter, sequentially slices the frozen tissue and acquire fluorescent images in up to five channels from each slice [149]. It was first developed and used in studying organ blood flow in small laboratory animals using microspheres [150]. The instrument determines regional blood flow by using the locations of fluorescent microspheres deposited in perfused rat hearts. Image analysis of fluorescent microspheres is much faster and less labor intensive than traditional indirect microsphere-based flow measurements while providing higher quality data [149]. The modified version of the instrument used in this chapter, is imaging endogenous coenzymes (NADH and FAD) concentration to acquire metabolic states of the tissue under study, with higher magnifications up to cell resolution.

As previously mentioned, NADH and FAD are autofluorescent and can be monitored without exogenous labels by noninvasive optical techniques [25]. The fluorescence signals of these intrinsic fluorophores have been used as indicators of tissue metabolism in injuries due to hypoxia, ischemia, and cell death [71]. There is more than one definition for redox ratio, including the normalized redox ratio (NADH/(NADH + FAD)) [71]; the definition that is used in this study (NADH/FAD) is chosen since the FAD signal in lung tissue, as compared to the NADH signal, is significantly smaller than

in other organ tissues such as the heart. Thus, the normalized redox ratio would be less sensitive to a change in mitochondrial redox state than NADH/FAD.

Rapid freezing of organs in liquid nitrogen temperatures preserves the tissue metabolic state [75]. Subsequent slicing and low temperature fluorescence imaging (cryoimaging) is advantageous since it provides high fluorescence quantum yield of NADH and FAD as compared with room temperature, and 3D spatial distribution of tissue NADH and FAD fluorescence intensities [36, 76, 77].

Use of supplemental O_2 in patients who suffer from hypoxemia and RDS is often life saving since it is necessary to restore blood pO_2 to a level that supports the metabolic requirements of vital organs. However, prolonged exposure to higher concentrations of O_2 or hyperoxia leads to enhanced production of ROS and lung injury at the cellular level associated with mitochondrial dysfunction, decreased cell proliferation, DNA damage and alveolar epithelial and endothelial cell death [78-83]; in another word, mitochondrial dysfunction is a cardinal feature of a spectrum of lung injuries including hyperoxia and Ischemia reperfusion (IR) [84, 85].

We are focusing on ROS as the final causative molecule in the pathogenesis of lung injury caused by LPS or exposure to higher O_2 concentrations. Although ROS generation after exposure of cells to LPS is well documented by *in vitro* investigations, *in situ* evidence is, so far, lacking [43, 44, 50, 51, 94]. Using optical cryoimaging, we investigated *in situ* ROS detection in intact rat lungs treated with higher O_2 concentrations and LPS.

Bcl-2 is the founding member of a family of proteins with anti-apoptosis and anti-oxidant effects [91]. Expression of bcl-2 may also act as a protective mechanism for endothelial cells under oxidative or mechanical stress [92]. The bcl-2 knocked-out lungs were also compared to normal lungs as another model of BPD in mice pups. It has been hypothesized that mice lacking bcl-2 display a BPD-like phenotype [93].

Although much work has been done in cell cultures and tissue homogenates, studies for probing key tissue mitochondrial functions and the effect of oxidant injury in the intact lungs are limited [6]. Thus, the objective of this chapter was to utilize cryoimaging to evaluate the effects of *in vivo* exposure of rats to hyperoxia or lung IR on lung tissue mitochondrial RR. We also investigated whether the changes in metabolic state can be used as a marker of oxidative stress caused by bacterial lipopolysaccharide (LPS) exposure in neonatal rat lungs combined with hyperoxia. We investigated the hypothesis that the effects of LPS on the immature lung are amplified when exposed to hyperoxic conditions during postnatal life compared to the hypoxic *in utero* environment of the fetus [50, 86-88] and showed NADH RR serves as a quantitative marker of oxidative stress level in lung injury caused by clinically important conditions including hyperoxia and LPS exposure.

Neonatal rodent pups have been extensively used as a model to study the effects of hyperoxia on lung injury and growth. Previous studies have demonstrated an arrest of lung alveolar and vascular growth with the exposure of neonatal rat lungs to hyperoxia for a period of 7-10 days [89]. Since rat pups at birth have lung development at the saccular stage similar to premature babies [90], the disruption of development by

hyperoxia parallels the changes seen in premature babies with BPD. We therefore, selected this model to investigate mitochondrial redox state during hyperoxia induced BPD.

The results of this chapter will provide a basis to apply optical fluorescent techniques for evaluating the effects of these and other models of lung injury on lung tissue mitochondrial RR *ex vivo* and eventually *in vivo*.

2.2. Tissue Preparation

All animal experiments were performed under the approval of Institutional Animal Care and Use Committee (IACUC) review boards and in compliance with the National Research Council's Guide for the Care and Use of Laboratory Animals at Milwaukee Zablocki VA Hospital, University of Wisconsin Madison and Medical College of Wisconsin.

Lung tissues from mice, neonatal rats, as well as mature rats were used in the frozen tissue studies. Each set of tissues has been prepared distinctly; a brief description of our tissue preparation protocols follows.

2.2.1. Mice Lungs (BCL-2 knocked out)

Bcl-2 mutant mice were maintained and screened as previously described [95] at the University of Wisconsin-Madison. Briefly, bc1-2 (+/-) animals were interbred, producing bc1-2 (+/+), bc1-2 (+/-), and bc1-2 (-/-) mice. The genotypes of the offspring were determined by PCR using genomics DNA prepared from tail biopsies [96, 97].

Lungs were surgically removed from mice at the age of 3 weeks and were frozen for subsequent cryoimaging.

2.2.2. Hyperoxia exposure and LPS administration in neonate rat

Neonatal rats were randomly assigned at birth to either postnatal normoxia (21%) or hyperoxia exposure (90%) from birth to 10 days of postnatal age. Each group was further subdivided to intra-peritoneal (IP) LPS injection (10 μg) on postnatal day seven, or to IP injection of equal volume of saline. This study design yielded four different groups of rats consisting of normoxia +/- LPS and hyperoxia +/- LPS.

Hyperoxic rat pups were reared from birth in a Plexiglas chamber with air and oxygen flow at a sufficient rate (3 L/min) to prevent CO_2 accumulation in the chamber. Openings in the chamber at the top allowed ambient air in the chamber to be replaced with fresh flow of gas. Air and oxygen were mixed to maintain an oxygen (O_2) concentration of 90% inside the chamber. Ambient temperature was kept at 27 ± 1º C in the chamber. The chamber was large enough to house the mother and pups for 10 days. Since adult rats are more vulnerable to oxygen injury, mothers were taken out of the chamber for a period of 2 hours per day to normoxia while the pups were kept in the hyperoxia chamber. Cages were cleaned quickly during this interruption to hyperoxia. Oxygen concentration in the chamber returned to 90% level 15 minutes after the chamber was opened to remove or return the mother to hyperoxia chamber. Normoxic pups were kept in a similar chamber with 21% O_2 exposure.

Bacterial LPS (E. coli, 0111:B4, sigma, St. Louis, MO, USA) was suspended in sterile pyrogen-free 0.9% saline. A dose of 10 μg LPS or equal volume of saline (control) was injected IP into rat pups at 7 days postnatal age. The pups were allowed to continue under hyperoxia (or normoxic) condition for three additional days after the intra peritoneal injection of LPS or saline.

2.2.3. Hyperoxic exposure for adult rats:

Sprague-Dawley rats (275-350 g, males) were housed in a Plexiglass chamber maintained at 85% O_2 balance N_2 for 7 days as previously described [98]. Age-matched control rats were exposed to room air (21% O_2) and referred to as normoxic rats. This O_2 level and exposure period were chosen for several reasons. First, Crapo et al. provide detailed description of histologic and morphometric changes in lungs of rats exposed to this injury model [37] . Second, it has been demonstrated that rat exposure to this hyperoxia model alters the activities of lung tissue mitochondrial complexes I, III, and IV [98]. Third, the rats are unique in that if pre-exposed to 85% O_2 for 7 days they develop tolerance to the otherwise lethal effects of exposure to 100% O_2 [37, 98]. Lungs were isolated immediately following the seven-day exposure to controlled environmental gases.

2.2.4. IR injury:

Adult Sprague-Dawley rats (~300 g) were anesthetized with isoflurane, an endotracheal (ET) tube was secured for ventilation and the rat placed in a prone position as previously described [84]. The left anterior chest was opened to access the left hilum. The left hilum, including the main stem bronchus, left PA (pulmonary artery) and left pulmonary veins,

was located and clamped for 60 minutes after which time the vascular clamp was removed and the surgical wound closed. Lungs for imaging studies were harvested 24 hours later, following the procedure for isolated perfused studies described before.

2.2.5. Isolated lung perfusion in adult rats

Lungs from adult rats from control, IR, and hyperoxic groups were all perfused before freezing as previously described [99] and summarized below. Each rat was anesthetized with pentobarbital sodium (40 mg/kg body wt. intraperitoneal), after which the chest was opened. Heparin (0.7 IU/g body wt.) was injected into the right ventricle. Cannulas were placed in the pulmonary artery and the trachea, and the pulmonary venous outflow was accessed via a cannula in the left atrium. The lungs were removed from the chest and attached to a ventilation and perfusion system. The perfusate was Krebs-Ringer bicarbonate solution containing (in mM) 4.7 KCl, 2.51 $CaCl_2$, 1.19 $MgSO_4$, 2.5 KH_2PO_4, 118 NaCl, 25 $NaHCO_3$, 5.5 glucose, and 3% bovine serum albumin (BSA) [100]. The ventilation gas mixture was 15% O_2, 6% CO_2 in N_2. The perfusate was pumped (at 10 mL/min) through the lung until it was clear of blood, after which the flow and ventilation were stopped. The lung was then partially deflated by disconnecting the tracheal cannula from the ventilation system and then rapidly frozen as described below. The ventilation with room air (pO_2 ~ 115 mmHg) lasted for ~15 minutes, and should have no effect on the mitochondrial redox state since the PO_2 at which mitochondrial complex IV activity is inhibited and the electron transport chain reduced is < 2 mmHg [18].

2.2.6. KCN administration

To determine the ability of the cryoimaging technique to detect a change in mitochondrial NADH and FAD redox state, as well as capturing the dynamic range of the metabolic state of lung, the lungs from a group of normoxic adult rats as well as from a group of normoxic pups were perfused *ex vivo* as described above. However, instead of perfusion with buffer alone, these lungs were perused for 10 minutes with Krebs Ringer bicarbonate solution containing potassium cyanide (KCN, complex IV inhibitor, 2 mM), and then frozen. This treatment was employed to reduce the respiratory chain, and hence increase the NADH signal, decrease the FAD signal, and as a result increase RR. The perfusate was pumped into the lungs at a flow rate of 1 mL/min for 10 min. During this period, the lungs were ventilated (15% O_2, 6% CO_2, balance N_2) at 80 breaths/min. At the end of the perfusion period, the lungs were rapidly frozen for cryoimaging as described below.

2.2.7. Freezing Protocol and Embedding

Freezing: Rapid freezing in chilled isopentane (2-methyl butane, Fisher Scientific, IL) within liquid nitrogen (LN_2, -196^{o}C) preserved the metabolic state of the lung tissue. The tissue was immersed in isopentane for one minute followed by permanent storage in LN_2. For fluorescence imaging, the tissue was embedded in a customized black mounting medium (that is not fluorescent in the excitation wavelengths) and placed on a chilled aluminum plate to keep the tissue in place for freezing and slicing.

Mounting medium: The mounting medium is prepared in the Biophotonics Lab (UWM), using Polyvinyl Alcohol (PVA, Grade 71-30, PVOH7130, Chemical Store Inc., Clifton, NJ), distilled water and carbon black powder (Daniel Smith Dry Pigment, 284030040, Daniel Smith Inc., Seattle, WA). To make one liter of the embedding medium, 80 g of PVA is added to 920 g of boiling distilled water and stirred to make a homogeneous transparent medium. The solution is then allowed to cool, and 80 g of carbon black is added and mixed thoroughly. The mixture is refrigerated for 4-5 days before use.

Embedding: The embedding process starts with freezing the base medium, then embedding the tissue and fixing its position by adding more black medium around the tissue. After embedding, the tissue was stored in an ultralow freezer (-80^{o}C) for at least 24h prior to imaging. The lungs were imaged within a week with each injury group imaged along with its corresponding control group. The plate was installed in the cryoimager such that the surface of the black medium is parallel to a microtome.

2.3. Imaging and Image Processing

2.3.1. Cryoimager

Low temperature fluorescence imaging (cryoimaging) provides both three-dimensional fluorescence images of cryo-preserved intact organs and a higher quantum yield of fluorescence of NADH and FAD as compared to room temperature [77, 101, 102]. The cryoimager (figure 5) collects 3-D fluorescence images of frozen tissue's

intrinsic or extrinsic fluorophores. The instrument consists of an Aqua Exi CCD camera (Q-imaging, Aqua Exi, 14 bit, 6.45 μm pixel), a workstation (Dell Computer), a mercury arc lamp (200W, Oriel), an excitation (EX) filter wheel (which provides up to five excitation wavelengths), an emission (EM) filter wheel with synchronized rotation to EX wheel, and a cryo-microtome. Fluorescence images are acquired with the digital camera (1392×1040 pixel array) with a 200-mm Nikkor lens (Nikon, Tokyo, Japan). Two motorized filter wheels containing excitation and emission filters are mounted in front of the light source and camera, respectively. The motor-driven microtome sequentially sections frozen tissue at the desired slice thickness while filtered light from the arc lamp excites fluorophores in the exposed surface of the tissue block for up to five distinct fluorophores. The microtome is housed in a freezer unit that maintains the sample at -40^{o}C during sample slicing and image acquisition. Computer control of the microtome motor and filter wheels as well as image capture and display is accomplished through LabVIEW (8.6 National Instruments) [103].

The excitation band pass filter used for NADH is 350 nm (80 nm bandwidth, UV Pass Blacklite, HD Dichroic, Los Angeles, CA) and for FAD is 437 nm (20 nm bandwidth, 440QV21, Omega Optical, Brattleboro, VT). The emission filter for NADH is 460 nm (50 nm bandwidth, D460/50M, Chroma, Bellows Falls, VT) and for FAD is 537 nm (50 nm bandwidth, QMAX EM 510-560, Omega Optical, Brattleboro, VT). At each slice, the camera records fluorescence images of the tissue block in pixel dimensions of 22 μm × 22 μm. The resolution in the z-direction of microtome slices can be as small as 10 μm. For this study, a resolution of 25 μm was used in the z-direction, which resulted

in ~ 1000 z-slices per adult rat lung (and <1000 for rat pups and mice lung). Images are acquired with exposure times of 1.5 s for FAD and 1 s for NADH. Accounting for the time to rotate the filter wheels, as well as moving and slicing the sample, this results in 3-4 h (depending on the size of the lung) for imaging a whole adult rat lung [103-105].

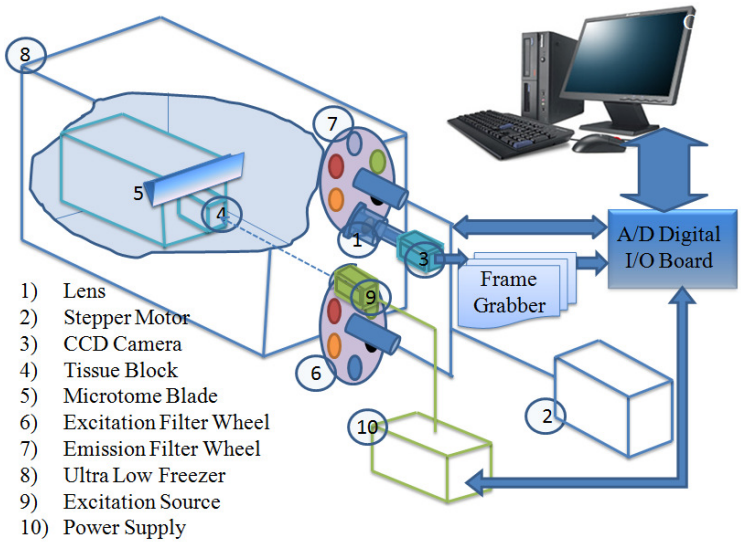

Figure 5. Schematic of Cryoimager. This device sequentially slices the tissue, imaging the surface between each successive slice, in as many as 5 channels. The images are then displayed and saved to a computer where they can be processed to create 3D renderings of the tissue [33].

2.3.2. Calibration

A calibration method was designed to compensate for day-to-day variation of light intensity, mirror angle, and non-uniformity of the illumination pattern.

At the beginning of each experiment and before slicing the tissue, a piece of graph paper was placed in the tissue position to set the focus of the lens and determine the

resolution. Then, one image was taken with the lamp shutter closed and the camera lens covered, referred to as the dark image.

Next, a uniform fluorescent flat acrylic plate was placed in the same position and imaged in all channels to acquire the illumination pattern. Because of the fluorescence of the standard in both the NADH and FAD channels and its high resistance to photobleaching, it also accounts for day-to-day light intensity changes in both channels. The acrylic plate is also advantageous in that it allows for imaging with camera settings in the same range as those used for tissue without causing saturation of the resulting image. Acquisition of the tissue sections then followed calibration.

When the tissue has been completely imaged, each individual slice first has the dark image subtracted from it, followed by correction for the non-uniformity of the illumination pattern by division to the image of the flat plate captured in the same channel.

2.3.3. Image Processing

FAD and NADH autofluorescence images from each lung were processed using MATLAB (r2008a, The MathWorks, Inc., Natick, MA). The composite images were created using all the image slices for each lung, for both NADH and FAD signals. The ratio of NADH and FAD (RR) [74, 106], was calculated voxel by voxel, using Matlab, according to equation (1).

$$\text{Redox Ratio} = RR = NADH / FAD \quad (1)$$

For each lung, a histogram of RR values was created, and the mean (first moment) of this histogram was calculated for the whole volume of the tissue according to equation (2).

$$Mean = \frac{1}{N_x \times N_y \times N_z} \sum_{i=1}^{N_x} \sum_{j=1}^{N_y} \sum_{k=1}^{Nz} Lung\_Volume(i, j, k) \quad (2)$$

Where N_x, N_y and N_z are the number of voxels in x, y and z directions, respectively and the voxel size in x, y and z direction is 22μm, 22μm and 25μm, respectively. Only the tissue volume was included in the calculation of the mean value and the background (from black medium) is excluded.

For the IR lungs, the left and right lobes were separated to examine similarities and differences between the injury region and the normal region. This was performed by defining a plane that separates the two lobes (using the voxels' inherent coordinate geometry), and collecting data on either side of the plane separately [83].

Statistical comparisons were carried out using ANOVA followed by Tukey's test, with $p < 0.05$ as the criterion for statistical significance.

2.4. Results

As the first set of imaging, mice lungs lacking bcl-2 (a BPD-like phenotype) is compared to normal mice lungs of the same age (21 days) and the result is presented in figure 6. The first two panels shows 3D rendering of NADH and FAD fluorescence

signals and their ratio (RR = NADH/FAD) from representative control and bcl-2 knocked out mice lungs. As expected, mice lacking bcl-2 shows a decreased NADH signal and increased FAD signal and as a result decreased RR (43%) which implies more ROS generation and oxidative stress.

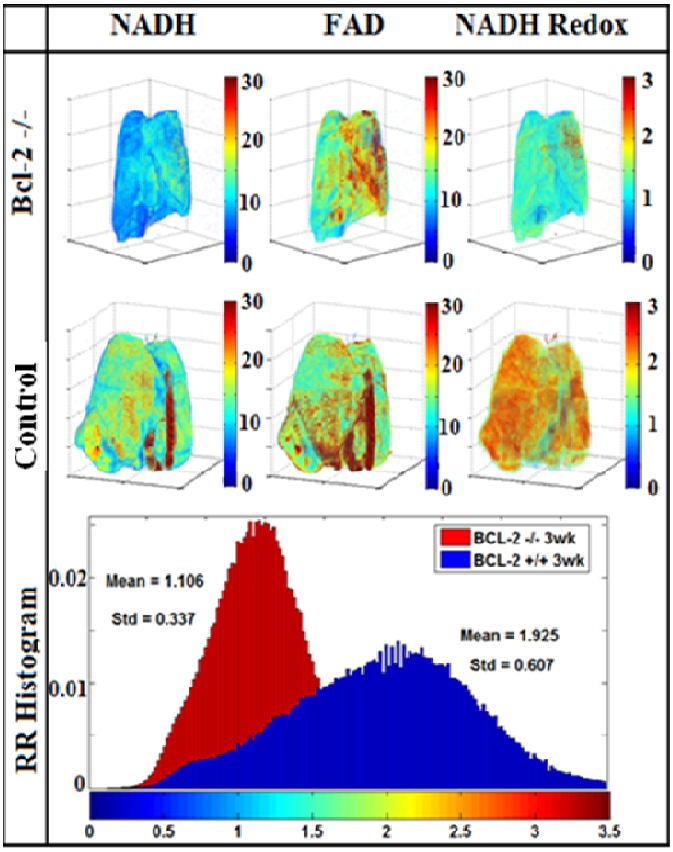

Figure 6. 3D representative and histograms of Bcl-2 lungs. Representative 3D reconstructions of lungs from each of two groups (Bcl-2 knocked out and control). From left to right, images shown are NADH, FAD, and mitochondrial redox ratio (RR) for bcl-2 knocked out lung (top) and control littermates (bottom). The histogram on NADH redox voxels distribution is also shown in the bottom panel, along with mean values of the two groups of lungs.

Figure 7 shows the 3D rendering of NADH and FAD fluorescence signals and their ratio (RR = NADH/FAD) from representatives of each of the four groups (normoxic,

normoxic + KCN, hyperoxic, and IR) of adult rat lungs and figure 8 shows histograms of RR for the four sets of lungs in figure 7.

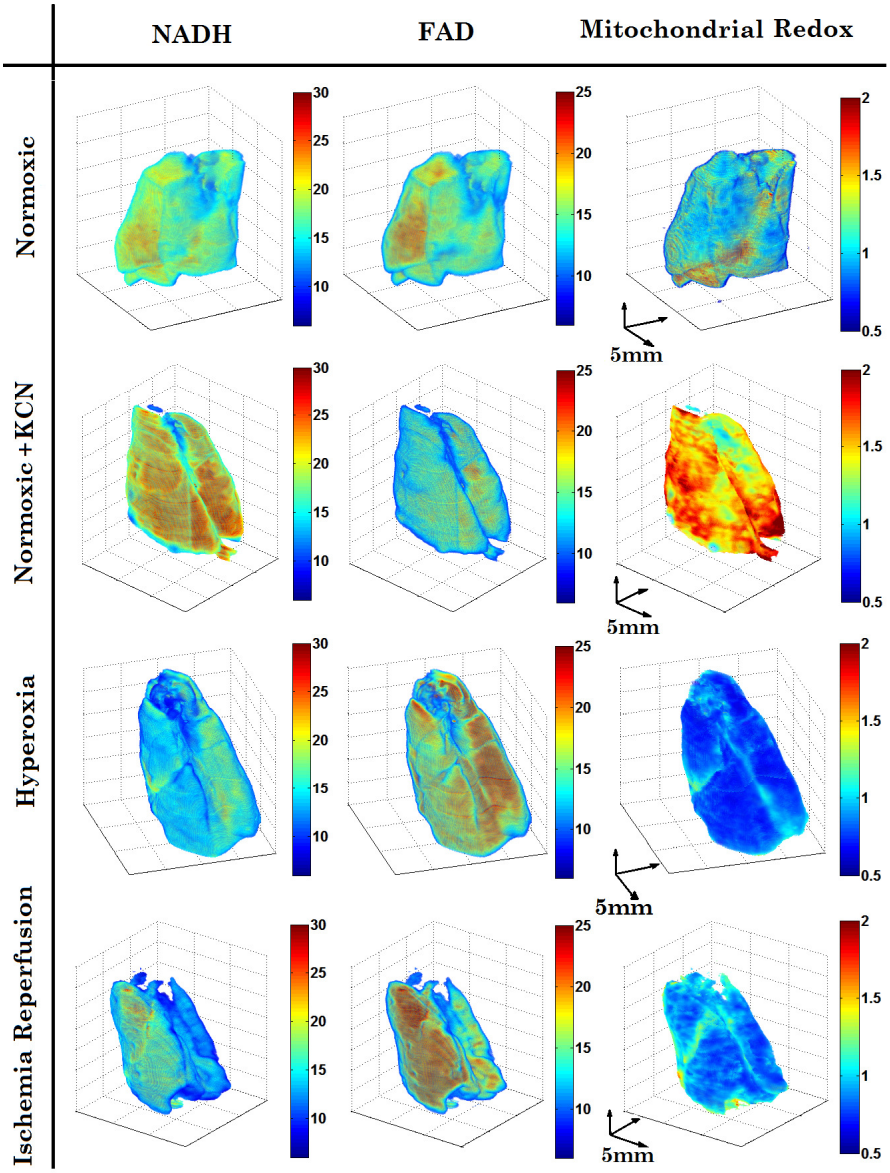

Figure 7. Representative 3D reconstructions of IR and Hyperoxic lungs. Represented lungs from each of four groups (from top to bottom: normoxic, normoxic + KCN, hyperoxic, and IR) is shown. From left to right, images shown are NADH, FAD, and mitochondrial RR [29].

For the IR lung, the histogram in figure 7 is that of both the injured lobe (left lobe) and normal lobe like the other sets. Despite the localized nature of the IR insult, all

areas of the lung show a difference when compared to a normal lung. For each histogram, the mean value was calculated as described in the image processing section. In this figure, the counts of each bin have been normalized to the total number of pixels in the lung. As a result of this normalization, the value of each bin corresponds to the percent of voxels in the lung with intensities falling within the given range. In this manner, the histogram can be thought of as a scaled probability density function of mitochondrial redox ratio intensities for a lung. The mean values of these histograms suggest a more reduced mitochondrial redox state for normoxic lungs treated with KCN (which inhibits complex IV and hence oxidizes the chain), and more oxidized mitochondrial redox state for hyperoxic and IR lungs as compared to normoxic lungs.

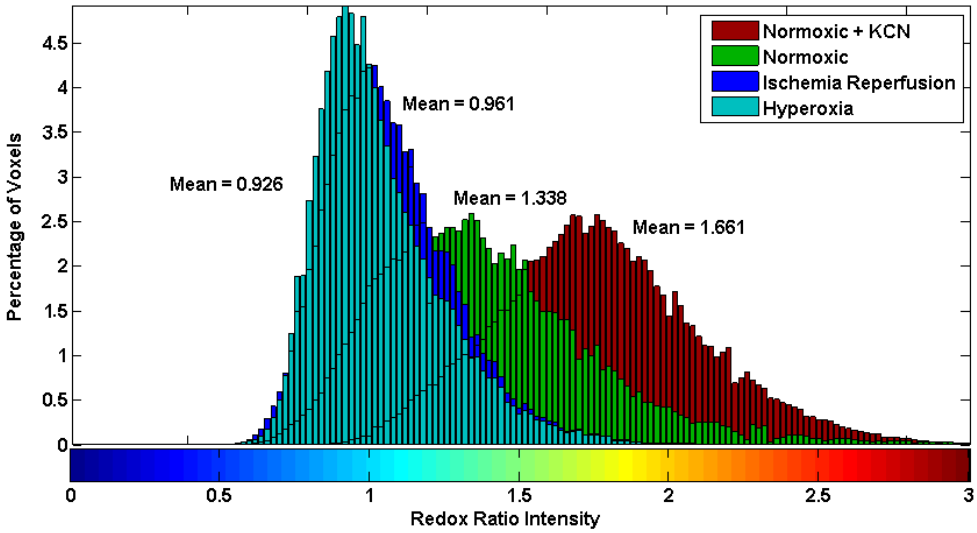

Figure 8. Histogram distribution of Redox ratio for the four lungs exemplified in Figure 7 [29].

Figure 9 shows the average ± SE (standard deviation over the number of samples) of the mean values of the redox ratio histograms for four groups of rats in figure 7. Each lung was calibrated to correct for day-to-day variations as described in the signal

processing section. In this figure, only the injured lobe of the lung was considered when generating the histograms of the IR lungs. Inhibition of complex IV with KCN increased the mean value of the RR histogram by 30% compared to normoxic lungs. On the other hand, hyperoxia and IR decreased the mean values of the RR histograms by 23% and 20%, respectively, compared to normoxic lungs.

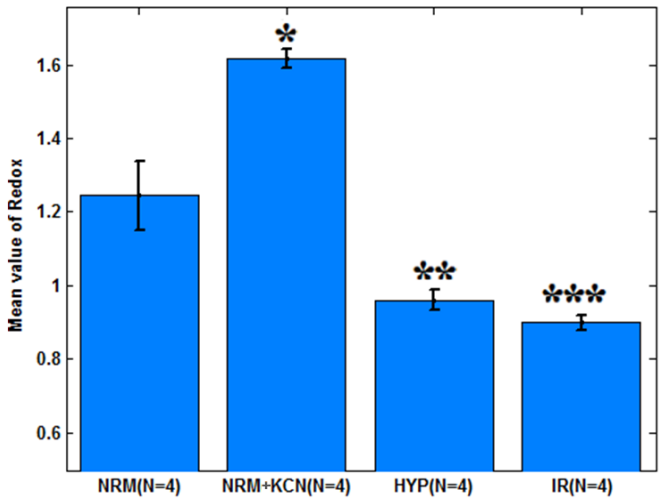

Figure 9. Bar graph showing the average values and standard errors of the mean value of the histogram of the mitochondrial redox ratio for each of the four groups of lungs. The results show a difference between normoxic (NRM) and NRM + KCN (* $p < 0.005$), NRM and hyperoxic (HYP) (** $p < 0.01$), and NRM and IR (*** $p < 0.01$). p values were obtained from post-hoc testing of a balanced one way ANOVA using Tukey's honestly significant difference criterion [29].

Figure 10 displays a bar graph plot comparing the contralateral (non-ischemic) lobe to the injured lobe of lungs subjected to ischemia-reperfusion. The figure shows that both NADH and FAD signals were decreased for the injured lobe as compared to the non-ischemic lobe. However, the mitochondrial redox ratio was only minimally impacted.

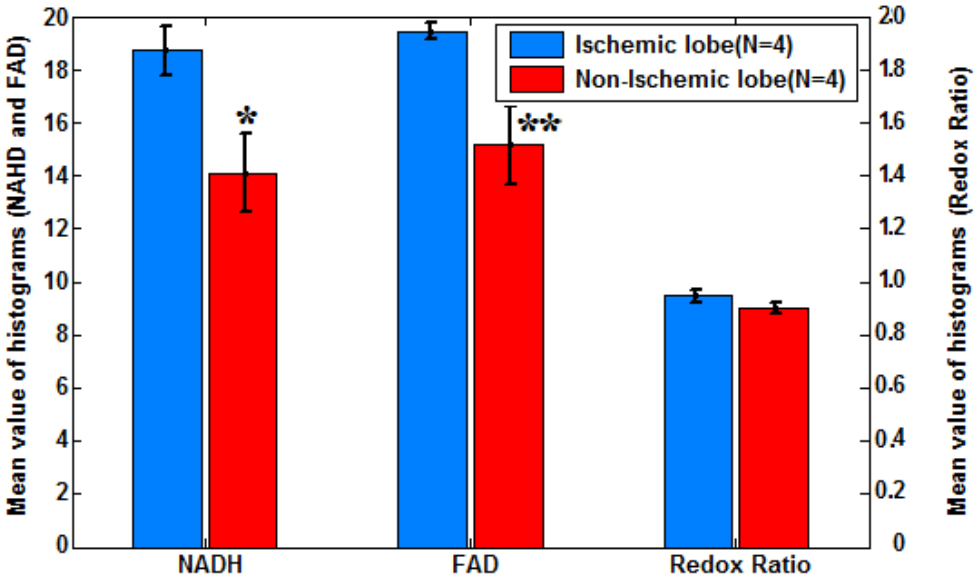

Figure 10. Bar graph plot of the mean value of normal and IR lobe in IR lungs. The results show a difference between non-ischemic (contralateral) and injured ischemic lobe in NADH (* $p < 0.01$) and FAD (** $p < 0.05$). P values were obtained from a *paired one-tailed student's t-test* [29].

Figure 11 shows the 3D volume rendering of NADH, FAD, and NADH redox for a representative lung from each of the normoxic+KCN, normoxic, normoxic+LPS, hyperoxic, and hyperoxic+LPS lung groups, in decreasing order of RR, and figure 12 shows the NADH redox histograms of the representative lungs presented in Fig. 11. The normoxic lungs treated with KCN again show the highest levels of NADH RR compared to other lungs, establishing an upper limit for NADH RR in this study. The lungs in the normoxic and normoxia+LPS group (second and third rows in Fig. 11) show a lower concentration of FAD and a higher concentration of NADH compared to hyperoxic and hyperoxia+LPS groups (fourth and fifth row in Fig. 12). Thus, the NADH RR is lower (more oxidized) in the hyperoxia +/- LPS groups compared to the normoxic +/- LPS groups.

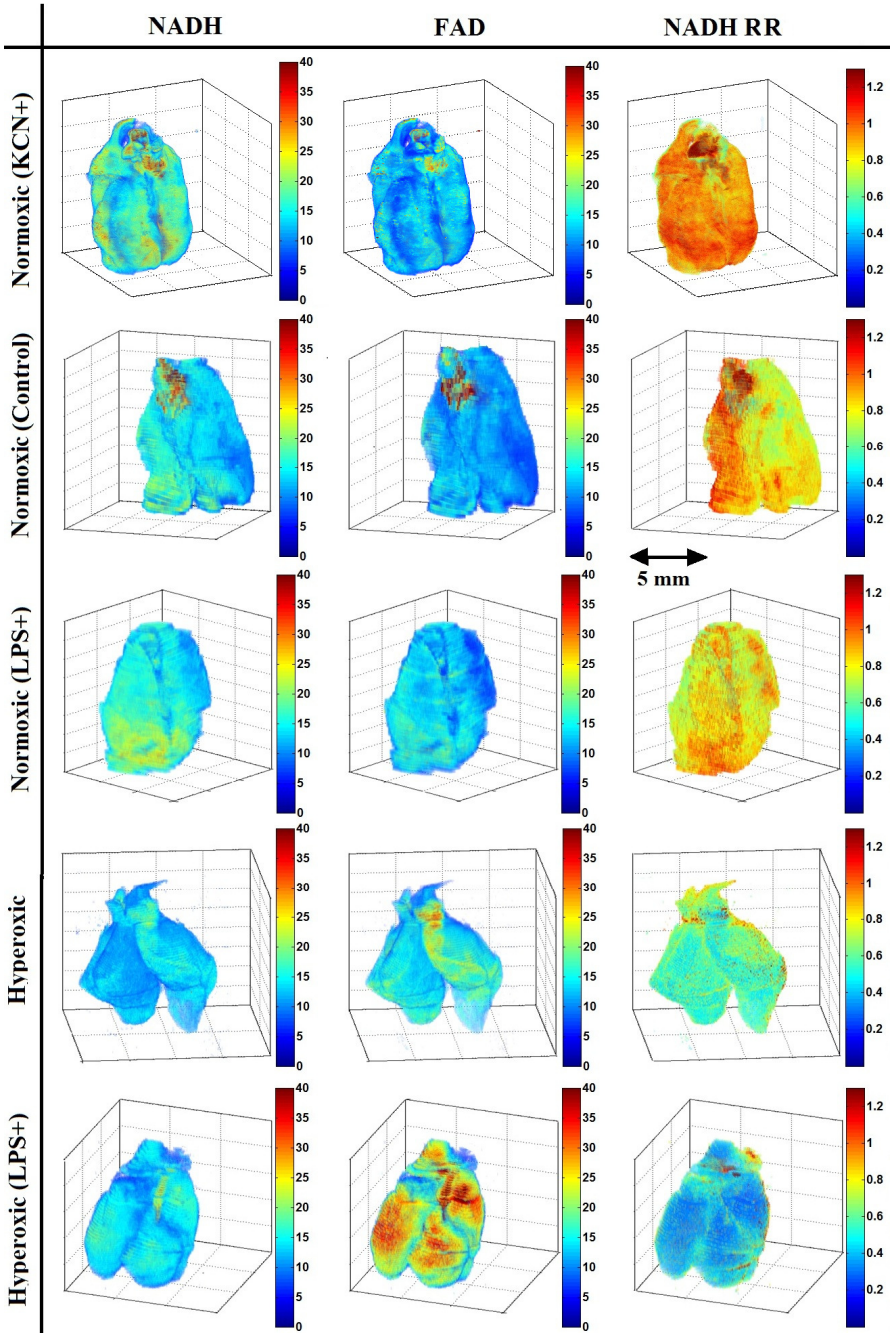

Figure 11. Volume rendering of NADH, FAD, and RR of a representative lung in each group of neonate rat pups [145].

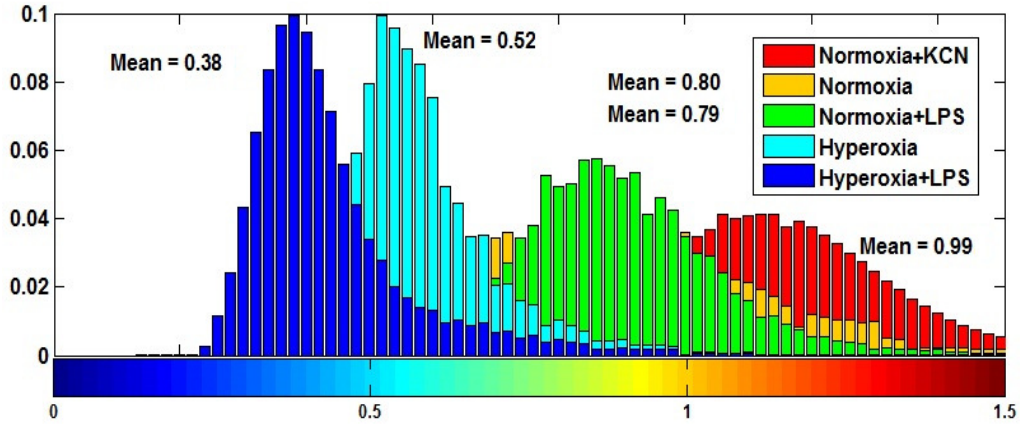

Figure 12. NADH redox histograms for a representative lungs of figure 11 [145].

The mean values of NADH RR for all the lungs are shown in a bar graph including the standard errors, in Figure 13.

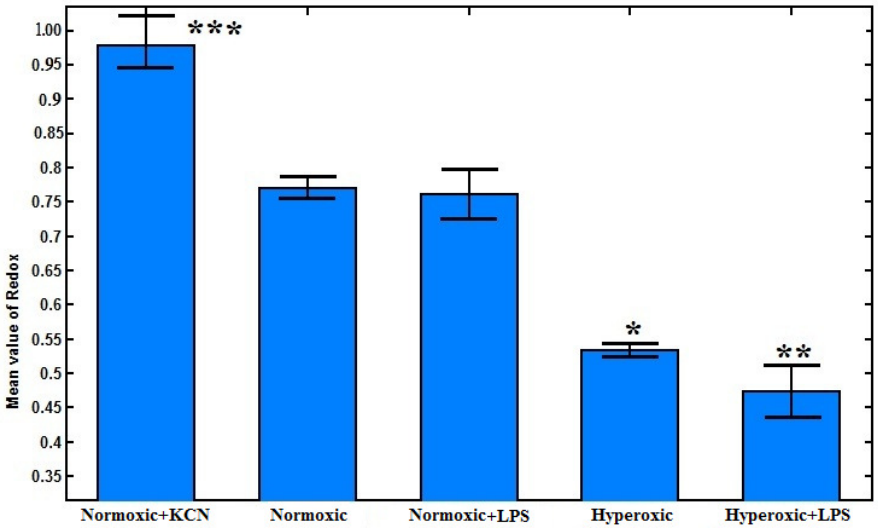

Figure 13. Bar graph showing the means and standard errors of the mean value of mitochondrial redox ratio for each of the five groups of lungs. The number of lungs N = 3, 5, 4, 4, and 4 for normoxic+KCN, normoxic, normoxic+LPS, hyperoxic, and hyperoxic+LPS, respectively. The results show a significant difference between normoxic and hyperoxic (*p < 0.01), normoxic and hyperoxic +LPS (**p < 0.01), and normoxic and normoxic+KCN lungs (***p < 0.01) [145].

KCN perfused lungs showed the highest NADH redox, which is 29% more reduced than that for normoxic lungs. Comparing the normoxic lungs to normoxic+LPS lungs, the results show no significant change in the biochemical state of the tissue, which indicates that stimulating the lung with LPS has no significant effect on the redox status of the respiratory chain of the lung. NADH RR values for hyperoxic+LPS lungs were lower (more oxidized) than hyperoxic lungs but were not significantly different. Thus, comparing the results for all lungs (hyperoxic+LPS+/- versus normoxic LPS+/-), it can be concluded that there is a higher level of oxidative stress in the hyperoxic+LPS lung versus the normal+LPS lung compared to their controls (hyperoxic and normoxic lungs, respectively). Comparing the mean values of normoxic versus hyperoxic lung, it can be seen that the NADH RR indicates a 31% more oxidized chain in hyperoxic lungs compared with normoxic lungs.

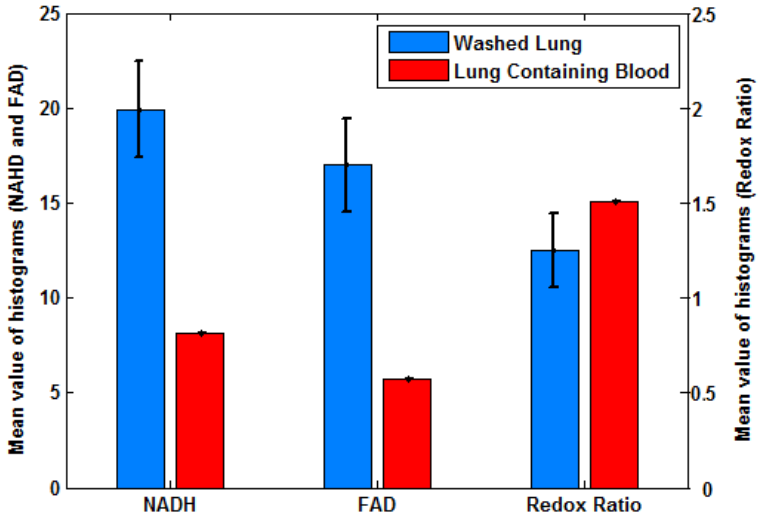

Figure 14. Mean values of NADH, FAD, and RR histograms of two groups of normoxic lungs plus the standard deviation of the mean value for the first group. For the first group (washed lungs) the blood was washed out of the lungs (n=4) by perfusing with Krebs bicarbonate solution. For the second (lung containing blood), the lung (n=1) was not perfused and was frozen immediately after it was removed from the chest [145].

Figure 14 demonstrates the effect of having blood present in the tissue, as would be the case for any in vivo study. The overall fluorescence signal decreased in both channels; however, the RR change is relatively small.

2.5. Discussion

The results of this study demonstrate the utility of cryoimaging for evaluating the redox status of tissue mitochondrial coenzymes NADH and FAD in intact lungs. The redox ratio (RR), NADH/FAD, is an index of lung tissue mitochondrial redox state, which is an important determinant of mitochondrial bioenergetics.

Oxygen therapy has been used in clinical medicine for many years despite the recognition of pulmonary oxygen toxicity as a problem for nearly 70 years. Cellular metabolism under hyperoxic conditions leads to an increase in the rate of formation of oxygen free radicals and results in oxygen-induced lung injury. Bacterial LPS is a major factor in causing ALI and induces the release of reactive oxygen species, which in turn may lead to higher oxidative stress in the lung tissue. LPS exposure is a common factor involved in ALI and results in endothelial apoptosis and mitochondrial dysfunction. Our hypothesis is that LPS accentuates a preexisting insult to lungs caused by hyperoxia.

Hyperoxia leads to enhanced production of ROS and the results revealed that both chronic hyperoxia and IR injury decreased lung RR due to mitochondrial dysfunction caused by oxidative stress. Although these two injury models produce the same mitochondrial dysfunction and caused oxidative stress, it is possible that they might be

distinguished due to the heterogeneity of the IR injury. However, the present goal of this study is to quantify oxidative lung injury regardless of cause.

Previously, it was demonstrated that adult rat exposure to 85% O_2 for 7 days decreased complex I activity by 50% and increased complex III and IV activities by 56% and 90%, respectively, as compared to normoxic lungs [98]. These changes would be expected to lead to a more oxidized chain downstream from complex I and hence to a decreased RR ratio consistent with the results from this study. Although redox state of mitochondrial respiratory chain does not directly measure ROS, our observation suggests a possible mechanism for higher prevalence of lung diseases with the use of high concentrations of supplemental oxygen.

Prediction of hyperoxia induced lung injury is difficult because the susceptibility of individuals to hyperoxia is quite variable. Serial surface fluorescence measurements that can be obtained from catheter probes inserted through tube thoracostomies could provide critical real time information regarding the development of oxidative lung injury over days in patients at risk.

The IR model also causes a depression in complex I activity which would also be expected to oxidize the chain and decrease RR [21]. Our results show that RR decreased equally for both the ischemic and non-ischemic lungs. This suggests that the IR injury was not limited to the ischemic lung. This is consistent with previous results which demonstrated an increase in caspase 3 activity and influx of neutrophils in *both* lungs in this IR model [84], demonstrating bilateral injury. The anesthesia "preconditioning" effects on the IR lungs tissue caused by isoflurane are minimized after 24 hour recovery

period following the surgery. The left (ischemic and reperfused) and right (non-ischemic) lungs would exhibit identical preconditioning effects if there are any.

Because IR is associated with alveolar hemorrhage [84, 85] and in vivo estimates of RR would unavoidably be acquired in the presence of blood, we determined the effect of blood on RR as follows. We conducted cryoimaging for one control lung which was not washed free of blood and compared its NADH, FAD and RR to those of control lungs that were washed of blood. Figure 14 demonstrates the effect of having blood present in the tissue, as would be the case for any in vivo study. The result of this experiment is consistent with the results from a study by Chance et al. in which they showed that perfusion of isolated organs (e.g. liver) with perfusate containing red blood cells decreases NADH and FAD signals but does not change the redox ratio [36]. They concluded that the RR in the presence of blood is still a faithful indicator of oxidation-reduction and can compensate for interfering factors such as light scattering, hemoglobin, etc. that exist under in vivo conditions [36] still several methods exist to correct for these factors [108, 109] (more on this subject in chapter 3 for in vivo fluorometry studies).

In order to show the dynamic range of mitochondrial redox state, we demonstrated changes in the redox ratio of normoxic adult rat lung when perfused with KCN (potassium cyanide), as a negative control (the most reduced state). KCN is a complex IV inhibitor of the respiratory chain which reduces the chain, and hence provides an upper boundary on NADH RR [29, 110, 111]. KCN was chosen since in a previous study [111], comparing perfusion with KCN, anoxia (95% N2 and 5% CO2) and CO (95% CO, 5% CO2), the KCN group showed the largest inhibitory effect on the

redox state of the lung tissue. In the present study, hyperoxia and KCN had the opposite effects on lung NADH RR, which was higher (more reduced) in KCN+normoxic lungs and lower (more oxidized) in hyperoxic lungs as compared to that in normoxic neonate lungs [29].

Cytosolic NADPH, which has the same fluorescence characteristics as NADH, could be contributing to the signal attributed to NADH in this study. However, Chance et al. demonstrated that the fluorescence signal originates mostly from NADH in the mitochondria and the contribution of NADPH - present in cytosol - is very small [112]. The fluorescence signal is mainly from NADH since its quantum yield is much higher than NADPH (1.25 to 2.5), its concentration is 5 times larger than NADPH, and is the only one affected by metabolic perturbations [113-115]. Thus, NAPDH contribution to the NADH signal and the change in the NADH signal due to hyperoxia or IR in this study is assumed to be small and was ignored.

Other endogenous flurophores that may contribute to the NADH signal include collagen and elastin, which are present in the tissue [116]. However unlike NADH, collagen and elastin contribution would not be expected to change with variations in mitochondrial redox state [116, 117]

The current study demonstrates the utility of RR to detect lung mitochondrial oxidant injury under ideal conditions that optimize the quantum yields of NADH and FAD and minimize the effects of confounding factors such as blood. We have not evaluated the effect of temperature on the quantum yields of NADH and FAD. However, Chance et al. addressed this question and demonstrated a high correlation between the RR values in

room temperature compared to cryogenic temperatures [36]. In addition, we have developed a fluorometer to measure lung surface NADH and FAD signals from an isolated perfused lung at 37^{o}C and the results using this system in presented in the next chapter.

Chapter 3

Ex vivo and *in vivo* studies -

Fluorometry: Fluorescence spectroscopy

3. *Ex vivo* and *in vivo* studies - Fluorometry: Fluorescence spectroscopy

3.1. Introduction

Fluorometry is the monitoring of concentrations of fluorophores using their fluorescence properties. We designed a fiber-optic-based optoelectronic fluorometer to measure emitted fluorescence from the previously mentioned auto-fluorescent electron carriers NADH and FAD of the mitochondrial electron transport chain (ETC). We evaluated the fluorometer by measuring the fluorescence intensities of NADH and FAD at the surface of rat lungs both isolated perfused (*ex vivo*) and in IR injury (*in vivo*).

This technique was first implemented by Chance, et al [119] in the early 1950s to monitor biochemical states of NADH *in vitro* and later in 1970s *in vivo* in rat brains. The first implementation (figure 15.a) of this device used a pneumatic wheel to time share signals from fluorescence and reflectance on one photomultiplier tube (PMT). The device showed the ability to monitor concentrations on NADH *in vivo* (figure 15.b). His group then advanced their design (figure 15.c) to use a separate PMT for reflectance and gain. This design first split the signal using a trifurcated fiber bundle, but was later modified to split the signal using a beamsplitter (figure 15.d). Similar devices have been designed by other groups [109, 120-122], as well. We have designed our fluorometer in Biophotonics Lab and modified it over time. Further details of each design is provided before and a

summary along with the description of the final design is presented in the following section [21].

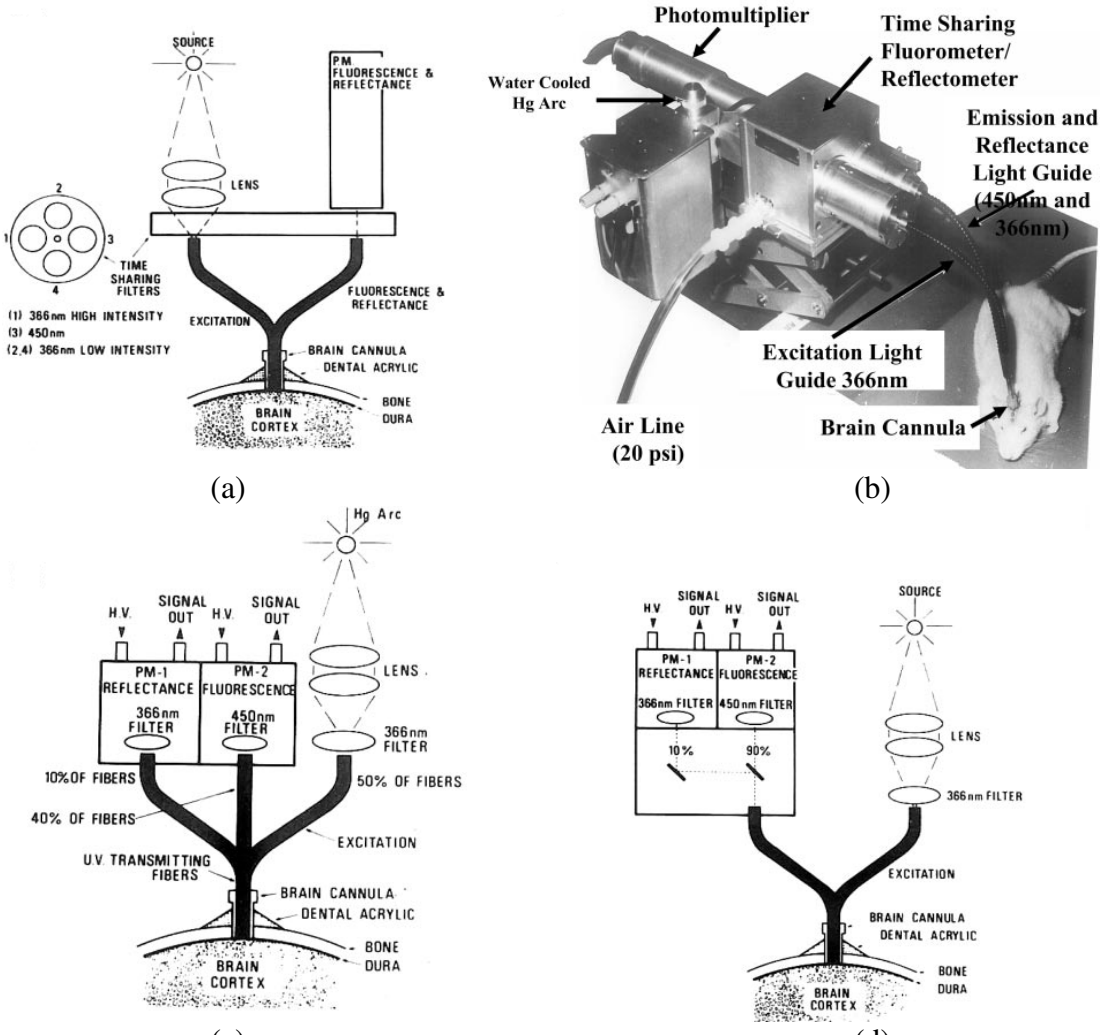

Figure 15. Previous fluorometer designs. Early designs of fluorometer devices used by Chance, et al. a) schematic of original implementation. b) Picture of a. c) Second iteration of fluorometer. d) Current implementation [1].

The objective of the fluorometry studies is to demonstrate the utility of these optical fluorescence techniques to evaluate lung tissue mitochondrial redox state (NADH/FAD) in isolated perfused rat lungs in control and injured lungs with high

sensitivity, and quantify the impact of blood on NADH and FAD fluorescence signals and their ratio and finally *in vivo* evaluation of IR injury. Isolated perfused lungs are particularly attractive to study in this regard since perfusate and/or ventilation gas composition can be altered to modify the oxido-reductive state of tissue mitochondria.

Our results demonstrate the ability of these techniques to detect a change in lung tissue mitochondrial redox state in isolated perfused lungs. We further utilized optical fluorometry to evaluate the effect of rat exposure to hyperoxia (>95% O_2 for 48 hours) on lung tissue mitochondrial redox status in a nondestructive manner in intact lungs, with a long term goal of understanding the role of mitochondrial dysfunction in the pathogenesis of lung O_2 toxicity as well as developing a diagnostic modality of oxygen toxicity.

3.2. Fluorometer

3.2.1. Optoelectronic design

The fiber-optic-based fluorometer device designed for this study has undergone several improvements and iterations over our original design [19, 20]. The initial design included a pneumatic filter wheel which was used both for filtering of excitation and emission fluorescence. However, to eliminate the need for compressed air to use the device, the second design replaced the pneumatic filter wheel with two synchronized electric filter wheels. After further investigation, it became apparent that the use of separate detectors for each fluorophore would be beneficial. Therefore, the emission filter wheel was supplanted by the combination of a dichroic mirror and static filters. Finally,

to correct for interfering factors such as hemodynamics, a beam splitter was added to detect diffuse reflectance from the tissue. A schematic for this iteration of the fluorometer device used in this study is shown in Figure 16.a. Excitation light is generated from a mercury arc lamp (Intensilight, Nikon, Tokyo, Japan), and coupled to a liquid light guide. The light is then fed into a filter wheel (Lambda-3, Sutter Instrument, CA), where the appropriate excitation wavelength can be selected. On the other side of this filter wheel is one leg of a bifurcated fiber bundle (Newport Instrument, NJ) with a distal end of 3.2 mm inner diameter. This distal tip is brought into contact with the tissue under investigation to deliver the appropriate excitation light and collect the corresponding fluorescence emission. The emitted light, along with reflection of the excitation is then delivered through the other leg of the bifurcated fiber bundle to the detection optics. After the light exits the fiber bundle, it is collimated and split using a beam splitter (UVBS14-1, Newport Instruments, CA). Half of the light is then incident on an avalanche photodiode (PDA25K, ThorLabs, NJ) for detection of reflected light. The other half of the light then passes through a dichroic mirror (DMLP505R, ThorLabs, NJ) to separate the NADH and FAD channels. In either of the channels, the light is then filtered to select the emitted fluorescence, remove any remaining reflection as background, and is finally incident on a photomultiplier tube (PMT; PMM02, ThorLabs, NJ). Synchronization of excitation and detection is achieved through the use of a custom LabVIEW program. To optimally excite the fluorophores of interest, NADH and FAD, using the mercury arc lamp, the excitation filters used were centered at 370 nm (FF01-370/36, Semrock, NY) and 452 nm (FF01-452/45, Semrock, NY), with bandwidths of 40 nm and 50 nm, respectively. The

dichroic mirror used to separate the emission of each fluorophore has its transition wavelength at 505 nm. Finally, the filters used to detect the emitted fluorescence are centered at 460 (D460/40M, Chroma, VT) and 520 nm (D520/40M, Chroma, VT), respectively, each with a bandwidth of 40 nm. To control all of the hardware used, as well as record the necessary signals and display them in real time, a LabVIEW program has been designed as well [21]. The fluorometer is used in a dark room to minimize stray-light effects [71, 73, 123]. At the beginning of each experiment, NADH and FAD fluorescence standards were measured to account for day-to-day variations in light intensity. Surface fluorescence was then measured by placing the fiber optic probe against the pleural surface of the right lobe (figure 18.a).

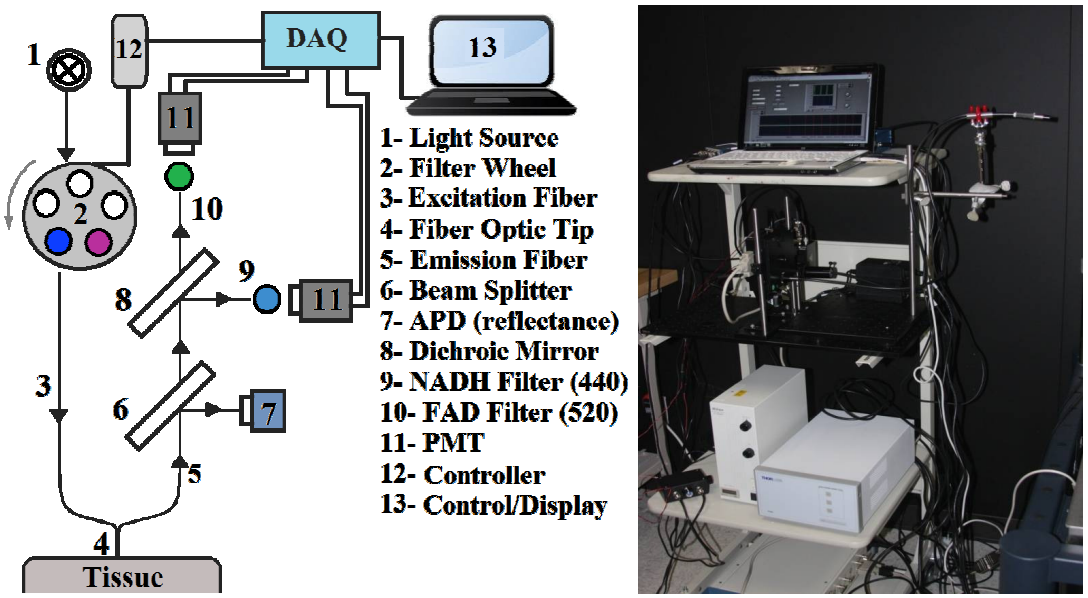

(a) (b)

Figure 16. a) Fluorometer Schematic [146] and b) actual implementation.

3.2.2. Signal processing

The stored files containing the recorded data are saved to the computer in National Instrument's "technical data management stream" (TDMS) file format. This type of file is ideal in that it is optimized for rapid storage of measurement data, and the output can be relatively easily read. To read the files, our chosen method is to import the TDMS file into the familiar excel format, where the first sheet of a workbook contains information about the data, such as sampling rate and the time of collection, and the second sheet contains the saved data.

From here, the data is easily read into MATLAB, where it can be managed to allow for powerful and easy display customization. However, we must again sort through the data to eliminate the zeros and pulses to show the actual trend of the data (figure 17.a). This is done by looping through the data one column at a time, and extracting the maximum value of each pulse (figure 17.b). This is achieved by defining the start and end point of any pulse as the first and last values after or before a zero. This trend was then smoothed out using a fourth order median filter followed by a fourth order moving average filter. The resulting NADH and FAD signals were then normalized by dividing each by its baseline value (signal level in the absence of any metabolic inhibitor or uncoupler). The normalized signals were then used to calculate the mitochondrial RR, RR = (normalized NADH)/(normalized FAD), which has a baseline value of 1.

Reflectance signal: For experiments in which blood was added to the perfusate as well as in vivo studies, the NADH and FAD reflectance signals were also measured in both channels. The quenching effect of blood on the surface fluorescence NADH and FAD signals was then

corrected for, either by dividing the normalized reflectance signals by the normalized fluorescence signals or by subtraction of the reflectance signals from the fluorescence signals [124] according to the following equations, respectively.

$$RR = \frac{\text{Normalized NADH Fluorescence / Normalized NADH Reflectance}}{\text{Normalized NADH Fluorescence / Normalized NADH Reflectance}} \quad (3)$$

$$RR = \frac{(\text{Normalized NADH Fluorescence} - \text{Normalized NADH Reflectance}+1)}{(\text{Normalized NADH Fluorescence} - \text{Normalized NADH Reflectance}+1)} \quad (4)$$

Statistical evaluation of data: Data are presented as means ± standard error (SE) unless otherwise stated. Statistical comparisons were carried out in each group using a two-tailed student's *t*-test or one way ANOVA followed by Tukey's HSD (Honestly Significant Difference) post-hoc test, with $p < 0.05$ as the criterion for statistical significance.

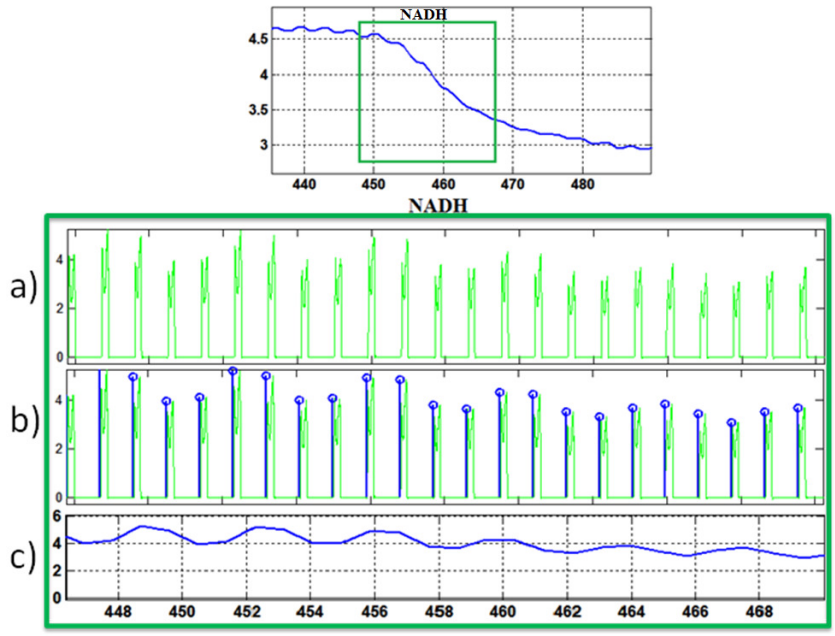

Figure 17. Fluorometry data processing. Extraction of the trend of fluorescent signals from the raw data produced by the fluorometer. Top shows the final trend of the data and bottom step of signal processing to get the final result shown on top: a) Raw data recorded. b) Detection of maximum value of pulses corresponding to active channel periods. c) Extraction and filtering of data trend.

3.2.1. Fluorometer linear response

To evaluate the linearity and sensitivity of the fluorometer to a change in NADH or FAD signal, we measured the NADH and FAD fluorescence signals in cuvettes containing aqueous solution with different NADH and/or FAD concentrations. The range of NADH and FAD concentrations studied encompassed the NADH and FAD concentrations in lung tissue [6, 125]. In one cuvette, the solution of fixed 6.7 μM NADH, and incrementally added FAD, led to concentrations ranging from 0-270 nM. Similarly, the second cuvette with fixed 30nM FAD solution, and sequentially added NADH resulted in concentrations ranging from 0-26 μM. The tip of the fluorometer probe was placed in contact with the wall of the cuvette, and the experiments were performed in a dark room to minimize background signal due to ambient light.

3.3. Tissue Preparation and signal acquisition

3.3.1. Materials

Fatty-acid free bovine serum albumin (Standard Powder, BSA) was purchased from Serologicals Corp. (Gaithersburg, MD). All other reagent grade chemicals were purchased from Sigma Chemical Company.

3.3.2. Chain perturbation in control and hyperoxic lungs *ex vivo*

For normoxic (control) lung studies, adult male Sprague-Dawley rats (Charles River; 300-350 g) were exposed to room air. For the hyperoxic lung studies, age matched

rats were housed in a Plexiglass chamber maintained at >95% O_2 for 48 hours (hyperoxic) [126]. The total gas flow was 3.5 liters/min and the chamber CO_2 level was maintained at < 0.5%. The temperature within the chamber was 20-22^{o}C. Every other day, the rats were weighed, and their cage, food, water, and CO_2 absorbent were changed. All rats were kept on a 12:12-h light-dark cycle. A total of 17 normoxic and 16 hyperoxic rats were studied. All the lungs were perfused clear of blood with the perfusion-ventilation langendorff system described in the previous chapter. The isolated perfused lung preparation allows for manipulation of lung tissue mitochondrial redox state without disrupting the multi-cellular environment of the lung through the addition of metabolic inhibitor(s) to the recirculating perfusate and/or alteration of the composition of the ventilation gas [127].

For a given lung, NADH and FAD surface fluorescence signals were first acquired under resting conditions (lung perfused with control perfusate and ventilated with 15% O_2, 6% CO_2 balance N_2 ventilation gas), and then following the addition of one or more of the following agents (rotenone, potassium cyanide, and pentachlorophenol) to the recirculation perfusate. Rotenone (20 μM) was used to inhibit mitochondrial complex I activity, which would be expected to increase NADH signal by reducing the chain upstream from complex I, and decrease FAD signal from lipoamide dehydrogenase (LipDH) [128], which is an element of the pyruvate dehydrogenase complex [129]. As a mitochondrial complex IV inhibitor, potassium cyanide (KCN, 2 mM) would be expected to reduce the chain upstream from complex IV and hence increase NADH signal and decrease FAD signal from LipDH, succinate dehydrogenase (complex II), and electron

transfer flavoproteins (ETF) which are the main sources of FAD signal [128]. Uncoupled mitochondrial condition was achieved by the addition of pentachlorophenol (PCP, mitochondrial uncoupler; 3 mM) to the recirculating perfusate and by ventilation of the lungs with 95% O_2: 5% CO_2 to maximize the oxidation of the electron transport chain. As a protonophore, PCP should oxidize the chain and hence decrease NADH signal and increase FAD signal. In some experiments, KCN was added after the initial addition of rotenone or PCP. The above concentrations of rotenone, KCN, and PCP were chosen to achieve maximal inhibition or uncoupling and hence maximal changes in NADH and/or FAD signal [6, 99].

3.3.3. Lung perfusion with blood

To evaluate the quenching effect of blood on the NADH and FAD signals, surface fluorescence measurements were carried out in a separate group of lungs first perfused with control perfusate, then following the addition of autologous blood to the recirculating perfusate in ~ 0.5 ml increments to achieve perfusate hematocrit (Hct) levels of ~ 0.5%, 1.0%, 1.5%, 2%, 2.5%, 3.5%, and 4%. This range of perfusate hematocrit was chosen based on the results of a previous study by Chance et. al [36]. At the end of this protocol, KCN was added to the recirculating blood-containing perfusate to evaluate the ability of the system to detect a change in NADH, FAD, and RR = NADH/FAD in the presence of red blood cells (4 % Hct).

3.3.4. Ischemia reperfusion injury in rat lungs *in vivo*

Male Sprague-Dawley rats (275-350 g; Charles River) were used for this study. Rats were anesthetized with isoflurane, an ET tube was secured for ventilation and the rat was placed in a prone position as previously described [15]. The ventilation gas was room air. The left anterior chest was opened to access the left hilum including the main stem bronchus, left PA (pulmonary artery) and left pulmonary veins. Next, surface NADH and FAD fluorescence signals were acquired by placing the fiber optic probe against the pleural surface of the left lobe (figure 18.b). Once the signal settled to a stable level, a vascular clamp was carefully placed across the hilum for 10 minutes, after which time it was removed. Signals were collected continuously prior to, during and following clamping.

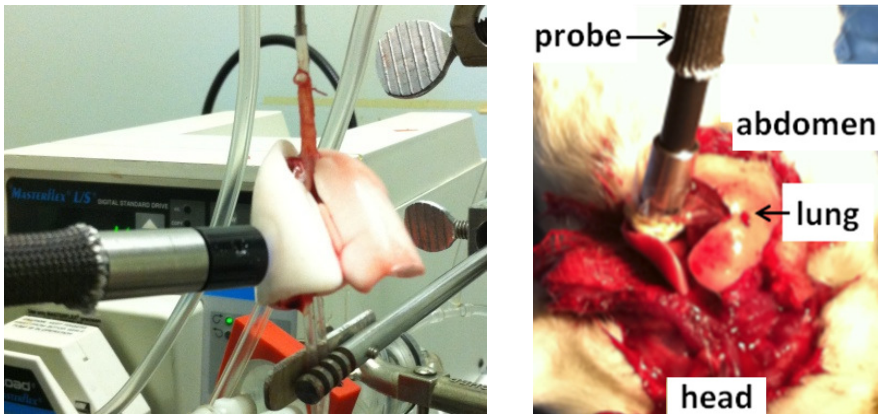

(a) (b)

Figure 18. Probe head on the lung during an (a) ex vivo and (b) in vivo experiment.

3.3.5. Complex I and II Assays:

For a separate sets of normoxic and hyperoxic lungs the activities of mitochondrial complex I and II were determined as previously described [21, 22]. Briefly, lungs were

isolated and washed free of blood with perfusate containing (in mM) 4.7 KCl, 2.51 $CaCl_2$, 1.19 $MgSO_4$, 2.5 KH_2PO_4, 118 NaCl, 25 $NaHCO_3$, 5.5 glucose, and 2.5% Ficoll. Lungs were then removed from the perfusion system, weighed, minced, and homogenized with buffer (pH 7.2) containing (in mM) 225 mannitol, 75 sucrose, 5 3-[N-morpholino] propanesulfonic acid, 20 ethylene glycol-bis (B-aminoethyl ether)-N,N,N',N'-tetraacetic acid, 2% fatty-acid free BSA, and 0.02 ml per ml protease inhibitor cocktail set III (Calbiochem, La Jolla, CA), utilizing a Polytron tissue homogenizer. Lung homogenates were centrifuged at 1,500 g for 5 min at 4°C, and the resulting supernatants were centrifuged again at 13,000 g for 30 min at 4°C to obtain a crude mitochondrial fraction (P2). The P2 fractions were washed twice by resuspension in 8 ml ice-cold homogenization buffer without BSA and then centrifuged (13,000 g for 20 min at 4°C). The final P2 fractions were resuspended in 1-ml BSA-free homogenization buffer. Mitochondrial complex I (NADH dehydrogenase) activity (nmol NADH oxidized$\cdot min^{-1}\cdot$mg $protein^{-1}$) was determined as the difference between the rates of NADH oxidation in the presence and absence of rotenone over the linear portion of the reaction progress curve as we have previously described [21]. Mitochondrial complex II (succinate-coenzyme Q reductase) activity was determined as the difference between the rates of reduction of the artificial electron acceptor 2,6-dichlorophenolindophenol (DCPIP) in the presence and absence of thenoyltrifluoroacetone (TTFA, complex II inhibitor) over the linear portion with succinate as donor [22]. The protein concentrations were determined colorimetrically as previously described [21].

3.4. Results

3.4.1. System Linearity

In order to verify that the response of the fluorometer has a linear relationship with the concentration of the fluorophores of interest, the sensitivity curves of each fluorophore were determined and plotted as shown in figure 19. In one plot, sequentially increasing concentrations of NADH were tested and plotted while the concentration of FAD was held approximately constant. The second plot, on the other hand, contains data from sequentially increasing concentrations of FAD while the concentration of NADH is held approximately constant. The values of the coefficient of determination, R^2, (0.999 for NADH and 0.996 for FAD) demonstrates a linear response to a change in the concentration of NADH (or FAD) in the presence of FAD (or NADH) over a wide range of NADH and FAD concentrations. The results presented here from the fluorometer indicate that it has great potential as a diagnostic tool in clinical settings. The linearity of the response of both the NADH and FAD signals to increasing concentrations of either fluorophore is essential to this possibility. The importance of this linearity is especially useful given that the range of concentrations used is similar to the range seen in typical tissue, meaning that the device is capable of detecting changes in the concentration of either fluorophore in tissue. In addition, the figure shows that changing the concentration of one fluorophore has a minimal impact on the signal corresponding to the other fluorophore.

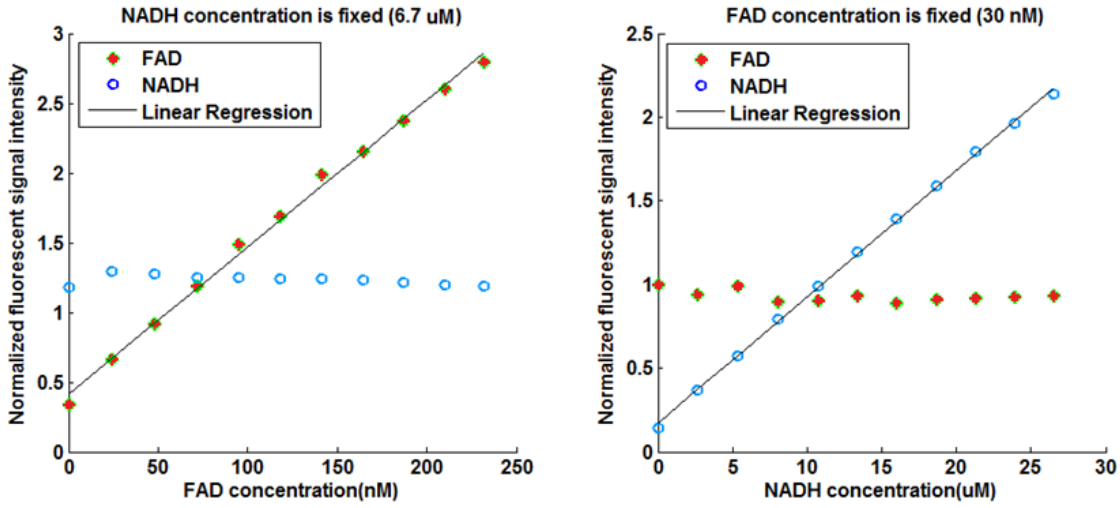

(a) (b)

Figure 19. Fluorometer Linearity Response. Linearity response of the fluorometer when tested on sequentially increasing concentrations of FAD (a) or NADH (b). While one fluorophore concentration is increased, the other is held approximately constant to show the minimal crosstalk of the system. The fluorescence signal intensity is normalized to a concentration typically found in tissue [110].

3.4.2. Chain perturbations using inhibitors and uncouplers

For both normoxic and hyperoxic lungs, the response of both NADH and FAD lung surface signals to lung perfusion with rotenone, KCN, or PCP appeared within a minute of adding the chemical to the perfusate reservoir (figure 20).

An increase (from baseline) in NADH fluorescence signal indicates reduction of the electron transport chain (figure 20), whereas an increase in the FAD fluorescence signal indicates oxidation of the electron transport chain. In this study, the change in NADH signal in the presence of rotenone or KCN is considered a measure of mitochondrial complex I activity, and the change in the FAD signal in the presence of KCN is considered a measure of mitochondrial complex II activity.

For normoxic lungs (figure 20 and table 2), lung perfusion with rotenone (complex I inhibitor) reduced the electron transport chain (ETC) upstream from complex I resulting in an increase in NADH signal by 20.2 ± 2.3 (SE) %, with no effect on FAD signal. Lung perfusion with KCN (complex IV inhibitor) reduced the ETC resulting in a 21.7 ± 2.5 % increase in NADH and 6.8 ± 1.6 % decrease in FAD. Lung perfusion with PCP, which uncoupled ETC from phosphorylation, decreased NADH signal by 19.7 ± 2.1% with no effect on FAD signal. The addition of KCN to PCP-treated lungs reversed the effect of PCP on the redox status of the ETC, increasing NADH signal by 25.7 ± 2.6% and decreasing FAD signal by –9.3 ± 1.0%.

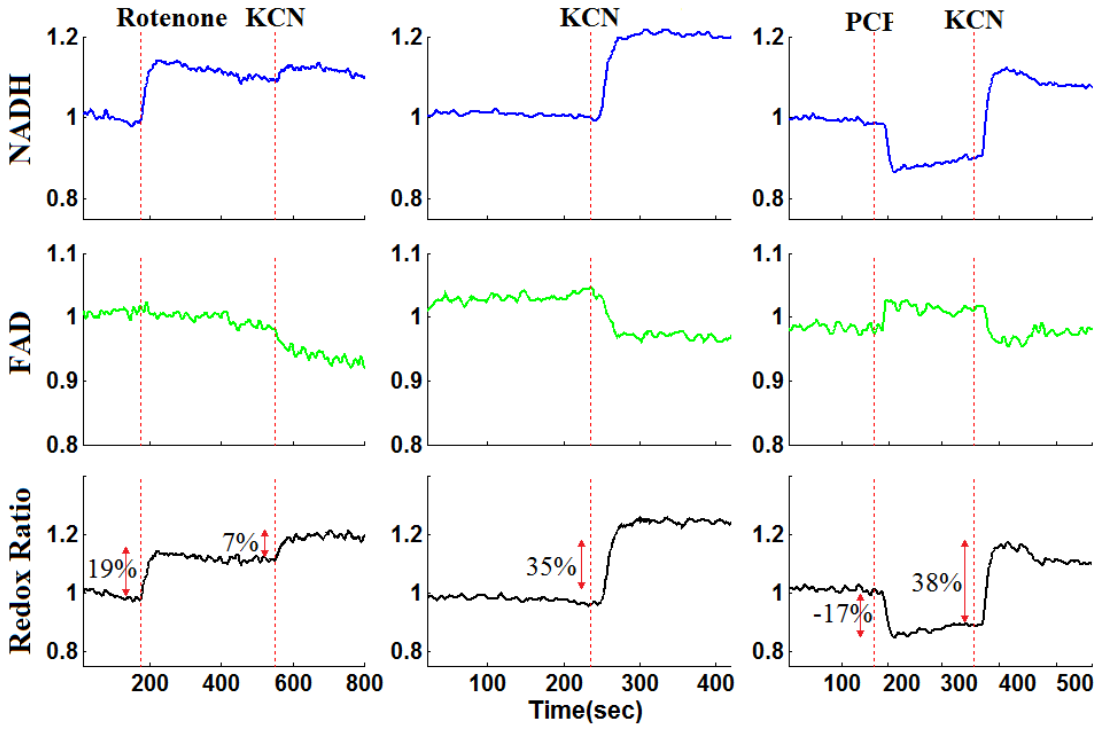

Figure 20. Representative fluorometer response to perfusion with chemical inhibitors and uncouplers in a normoxic lung [110].

In the presence of rotenone, KCN resulted in a small but significant decrease (−3.3 ± 0.8%) in lung surface FAD signal and increase (4.6 ± 1.0%) on NADH signal as compared to values in the presence of rotenone only.

3.4.1. Chain perturbations in hyperoxic lungs

For hyperoxic lungs (figure 21, table 2), lung perfusion with rotenone increased NADH signal by 7.5 ± 1.1%, which is 63% lower than in normoxic lungs, with no effect on FAD signal. Lung perfusion with KCN increased NADH by 9.2 ± 1.2%, which is 58% lower than in normoxic lungs. KCN effect on FAD signal in hyperoxic lungs was not significantly different from that in normoxic lungs.

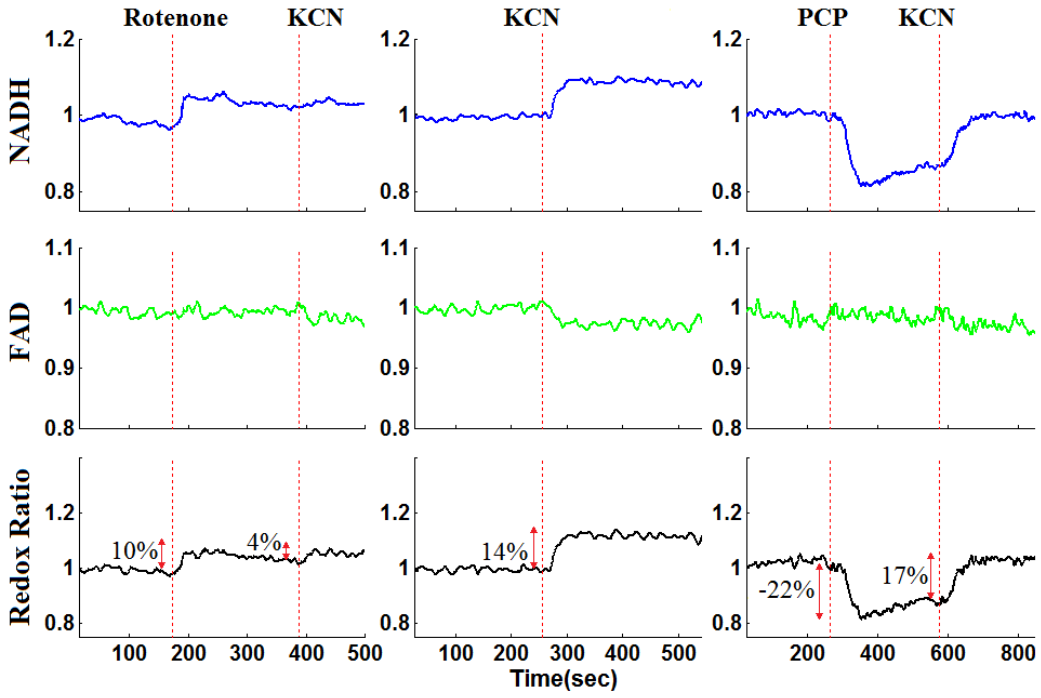

Figure 21. Representative fluorometer response to perfusion with chemical inhibitors and uncouplers in a hyperoxic lung [146].

Lung perfusion with PCP had the same qualitative and quantitative effects on NADH and FAD signals as in normoxic lungs. The addition of KCN to PCP-treated hyperoxic lungs increased NADH by 9.0 ± 1.0%, which is 65% smaller than that in normoxic lungs. Furthermore, KCN decreased FAD signal by 4.2 ± 0.7%, which is 55% smaller than in normoxic lungs. These results are consistent with a more reduced chain upstream from complex I and II in hyperoxic lungs as compared to normoxic lungs, and suggest a decrease in complex I and II activities in hyperoxic lungs.

Table 2. The effects of metabolic inhibitors and uncoupler on the lung tissue surface FAD and NADH fluorescence signals of normoxic and hyperoxic rats [146].

	FAD %		NADH%		RR (NADH/FAD)%	
	NRM	**HYP**	**NRM**	**HYP**	**NRM**	**HYP**
PCP	1.4 ± 1.0	-2 ± 1.3	-25.4 ±3.7 $^{\delta}$	-26.2 ±1.9 $^{\delta}$	-27.2 ±2.9 $^{\delta}$	-23.8 ±3.1$^{\delta}$
Rotenone	0.3 ± 0.3	-0.3 ± 0.3	21.5 ± 2.5$^{\delta}$	7.5 ±1.1$^{*\delta}$	21.3 ±2.7 $^{\delta}$	7.8 ± 1.1$^{*\delta}$
KCN	-7.4 ±1.8 $^{\delta}$	-5.4 ± 0.7 $^{\delta}$	21.7 ± 2.5$^{\delta}$	9.2 ±1.2$^{*\delta}$	31 ±2.1 $^{\delta}$	14.8 ±1.6$^{*\delta}$
PCP+KCN	-9.6 ±1.1 $^{\delta}$	-4.2 ± 0.7$^{*\delta}$	27.2 ± 2 $^{\delta}$	9 ± 1 $^{*\delta}$	38.9 ±0.8 $^{\delta}$	13.2 ±1.3$^{*\delta}$
Rotenone+ KCN	-3.1 ±0.9	-3.8 ±0.6 $^{\delta}$	4.0 ±0.9	2.8 ±1.2	7.0 ±0.3 $^{\delta}$	5.8 ±1.1 $^{\delta}$

- Values are mean ± SE.
- The number of lungs for each condition is greater than 4 (5,6,4,4,7,5,4,5,6,4 for PCP in normal and hyperoxic lungs, rotenone in normal and hyperoxic lungs, KCN in normal and hyperoxic lungs, PCP followed by KCN in normal and hyperoxic lungs and rotenone followed by KCN in normal and hyperoxic lungs, respectively).
- * : $p<0.05$ (two-tailed student's *t*-test) between normal and hyperoxic lungs.
- δ: $p<0.05$ (two-tailed student's *t*-test) showing each condition is significantly different than zero.

Table 3 shows that complex I and II activities normalized to protein were ~ 77% and 63% lower, respectively, in P2 fractions derived from hyperoxic than those of normoxic lungs.

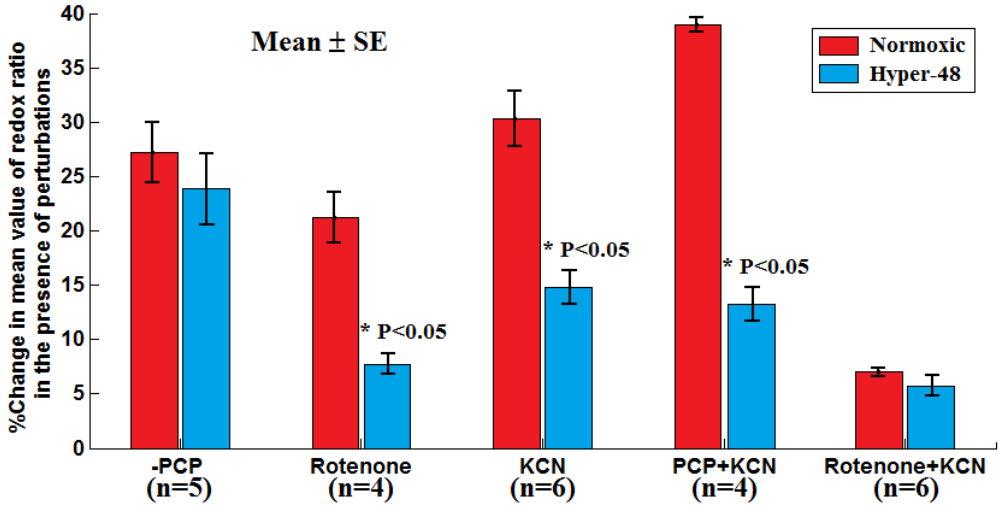

Figure 22. Bar graph of the fluorometer response (RR) to perfusion with uncouplers and inhibitors in normoxic and hyperoxic lungs. The p values (one-way student t-test) shows the significant changes between normal and hyperoxic lungs.

Table 3. Mitochondrial complex I and complex II activity measured in P2 fractions of lung homogenate [146].

	Complex I (nmol/min/mg protein)	**Complex II (nmol/min/mg protein)**
Normoxic	37.6 ± 3.2	79.1 ± 5.9
Hyperoxic	8.6 ± 0.7*	28.5 ± 2.3*

Values are mean ± SE. n = 4 and 3 for normoxic and hyperoxic lungs, respectively. *indicates value significantly different from the corresponding normoxic value ($p < 0.05$; t-test).

3.4.2. Effect of Blood

Perfusion of the lungs with buffer results in clean fluorescence signals, but the effect of blood should be considered for *in vivo* studies. To evaluate the ability of the fluorometer to operate *in vivo*, the fluorometer was tested in the presence of blood. The sequentially increasing amount of blood was studied to determine its effect on the signals, as well as evaluate a few methods to compensate for this effect. Figure 23 shows surface

fluorescent signals of the lung before (left) and after correction using division (middle) and subtraction (right) methods.

Addition of blood to the control perfusate quenched the lung surface NADH and FAD signals (Figure 23). Increasing perfusate hematocrit (Hct) level from 0% (control perfusate) to 1% decreased NADH and FAD signal by ~40%. Further increases in perfusate Hct had a smaller effect on the signals, with the NADH and FAD signals approaching a steady state value at ~ 4% perfusate hematocrit. This exponential relationship between the degree of quenching of NADH and FAD fluorescence signal and perfusate Hct level is consistent with Beer's law [130]. The effect of blood on RR was relatively small and was independent of perfusate Hct within the range of Hct studied. This result is consistent with results by Chance et al. [36].

The majority of this large attenuation in the fluorescence signals due to the change in the blood concentration is corrected in the corrected signals. It is notable that the NADH redox is independent of the blood concentration and is almost constant throughout the experiment. The results in figure 23 also show that correcting the NADH or FAD normalized fluorescence signal using corresponding reflectance signals did not completely eliminate the quenching effect of blood, especially that which occurred between 0% and 1% Hct.

To further evaluate the ability of the fluorometer to measure the signals in the presence of blood, KCN was administered to the lung following perfusion containing blood at 4% hematocrit. This level of hematocrit was chosen since the previous result indicates that the fluorescence signals are independent of blood concentration past this point. Figure 24

shows that potassium cyanide increased RR by ~26% in a lung perfused with blood-containing perfusate (4% Hct). This increase in RR is within the 31 ± 2.1 % (SE) range measured in lungs perfused with blood-free perfusate (table 2).

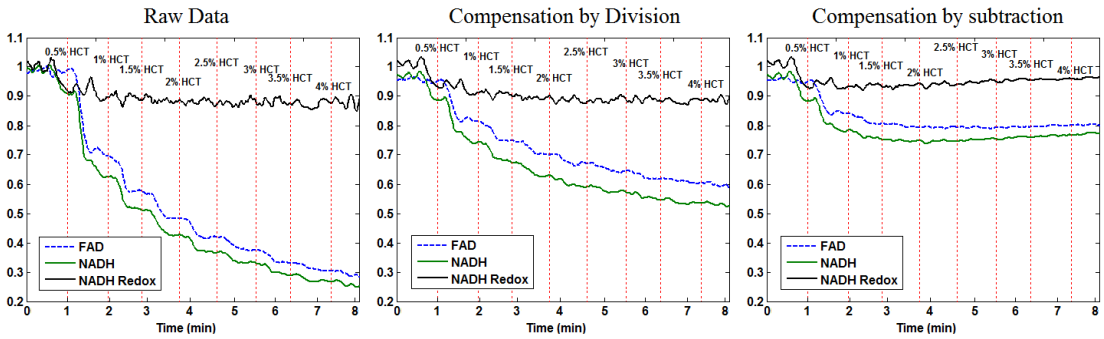

Figure 23. Lung surface NADH, FAD, and RR signals in the presence of blood. The figure shows basline followed by sequantial addition of blood up to 4% hematocrit to isolated perfused lungs. Left is the raw fluorescent signals and right is the corrected signals using the division method described in Equation 1 [147].

3.4.1. Ischemia reperfusion *in vivo*

Figure 25 shows representative surface fluorescence data (NADH, FAD and mitochondrial RR) from in vivo lung tissue, under control conditions and after clamping and unclamping of the left hilum. The data show that clamping, which reduces the chain (and as a result reduces NADH and FADH2) increased NADH signal, decreased FAD, and thus increased RR by 60%. The return of the fluorescence signals toward their original baseline as a result of unclamping indicates that the effect of clamping on lung surface NADH and FAD fluorescence is reversible by unclamping the left hilum (for short clamping intervals).

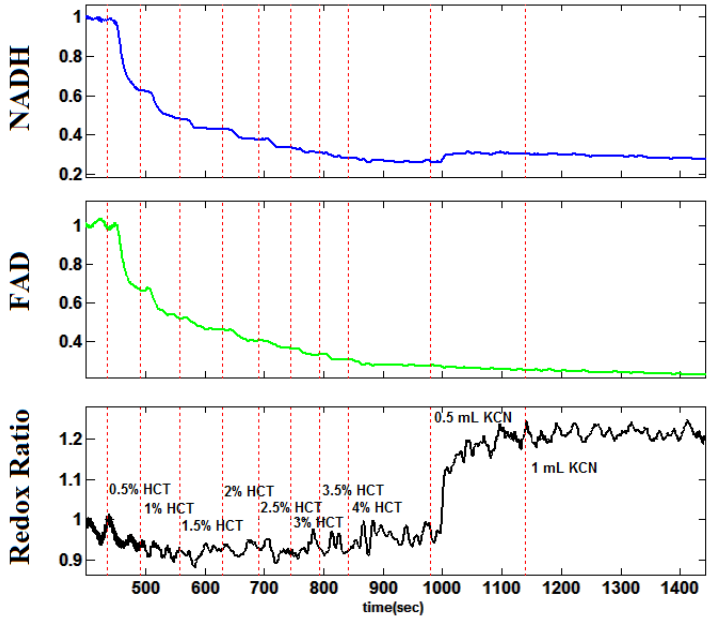

Figure 24. Chemical Addition in the Presence of Blood. Response of the fluorometer to KCN and PCP in the presence of blood. Although blood initially decreases both of the fluorescence signals, the change due to the addition of KCN and PCP is detected with similar percentage changes as what was seen in the case without blood [147].

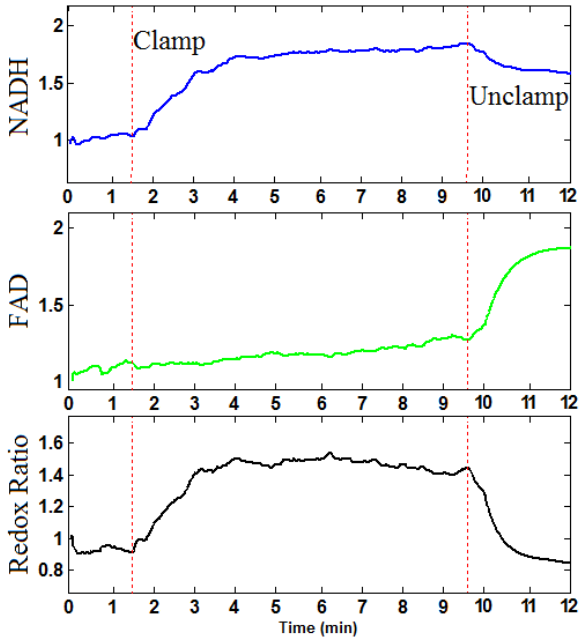

Figure 25. Fluorometry in vivo experiment. Lung surface NADH (top panel), FAD (middle panel), and mitochondrial redox ratio (RR) (bottom panel) signals for baseline, followed by clamping the left hilum and subsequent unclamping after 10 minutes [147].

3.5. Discussion

The results of this study demonstrate the ability of optical fluorescence techniques to detect a change in the redox state of the mitochondrial electron transport chain as measured by lung surface NADH and FAD fluorescent signals. The measured changes in NADH and FAD surface fluorescence following lung treatment with rotenone, KCN, or PCP are qualitatively consistent with the known effects of these metabolic inhibitors on the redox status of the mitochondrial electron transport chain.

3.5.1. Metabolic Inhibitors

Optical fluorescence techniques have been widely used to probe tissue redox state and energy homeostasis in organs such as the heart and liver, but have not been fully used in lungs [6]. The lung tissue presents a greater challenge for quantitative fluorescence studies than metabolically active tissues such as the heart or liver. The reasons include the low mitochondrial density of lung cells compared with metabolically active organs such as the heart [131, 132], the lungs' air content and high perfusion to metabolic needs ratio, and the lungs' high collagen content which contributes to high background fluorescence [6]. To the best of our knowledge, the 1976 study by Fisher et al. [6] is the only study in the literature in which lung surface fluorometry was used to probe the redox status of lung tissue NADH. They reported relatively small changes in the NADH signal (table 3) in response to lung treatment with metabolic inhibitors that are known to oxidize or reduce the mitochondrial electron transport chain. As shown in table 3, the results of the present study represent a substantial improvement in our ability to detect a change in

NADH redox status in response to lung treatment with metabolic inhibitors as compared to what Fisher et al. [6] had reported. This increased sensitivity is mostly due to the use of optical fibers and highly sensitive PMTs. The fiber-optic design injects light into the tissue allowing fluorescence emission to be more heavily weighted from the mitochondrial containing parenchymal tissue than from the surface connective tissue fluorescence as is the case with the lens-based optics approach used by Fisher et al. [6].

Table 4. The comparison of the percentage change in the NADH signal in the presence of metabolic inhibitors and uncoupler in the lung tissue surface fluorescence between our fluorometer and previous results (Fisher et al. [6]) [110].

Treatment	N	%Change in NADH (Fisher and Chance[6])	N	%Change in NADH (Present study)
Potassium cyanide	11	6.7 ± 0.7	6	22.0 ± 2.9
Amytal/(Rotenone)	5	5.0 ± 1.2	4	21.5 ± 2.5
Pentachlorophenol	3	-4.3 ± 0.5	5	-25.4 ± 3.7

Values are mean ± SE for N experiments.

Our assumption in this study is that changes in the mitochondrial pool of NADH is a key contributor to the measured changes in the NADH fluorescence signal since the metabolic inhibitors target the mitochondrial electron transport chain [133, 134]. However, cytosolic NADH also contributes to the lung surface NADH signal. There are multiple processes that determine cytosolic NADH concentration, including NADH reduction during glycolysis, and NADH oxidation by lactate dehydrogenase. Another important cytosolic process that alters both cytosolic and mitochondrial NADH concentration is the malate-aspartate shuttle which transfers electrons across the mitochondrial membrane from cytosolic NADH, which is oxidized to NAD^+, to mitochondrial NAD^+, which is reduced to NADH [135]. Lung treatment with rotenone,

KCN, or PCP decreases mitochondrial ATP production, stimulates glucoses [136, 137], and hence could alter cytosolic NADH concentration. Data in this report do not permit us to distinguish the contribution of these sources of NADH to the signal used to calculate RR values.

NADPH, which has the same fluorescence characteristics as NADH, may also contribute to the lung surface signal attributed to NADH in this study. The major cytosolic source is the pentose pathway, which requires glucose [128, 138, 139]. Other cytosolic sources include the malic enzyme and $NADP^+$ dependent isocitrate dehydrogenase [128, 138, 139]. These enzymes use citrate acid cycle metabolites to generate NADPH, and hence do not require glucose. Mitochondrial NADPH is generated by energy-dependent mitochondrial nicotinamide nucleotide transhydrogenase, which catalyzes the interconversion of NADH to NADPH. Fisher et al. [139] showed that treatment of isolated perfused rabbit lungs with potassium cyanide, an uncoupler, or antimycin (complex III inhibitor) decreased the rate of the NADPH dependent mixed-function oxidation of p-nitroanisole to p-nitrophenol by 50% to 77% with glucose as substrate. Thus, the increase in lung surface NADH signal in the presence of cyanide (Table 1) cannot be attributed to an increase in the NADPH signal since cyanide decreased the rate of the NADPH-dependent mixed-function oxidation of p-nitroanisole to p-nitrophenol [139]. On the other hand, the decrease in measured lung surface NADH signal in the presence of the uncoupler (table 2) could be in part due to a decrease in NADPH since lung treatment with the uncoupler decreased the rate of the NADPH dependent reaction. However, the fact that KCN and PCP had opposite effect on the lung

surface NADH signal (table 1), but the same effect on the rate of the NADPH-dependent reaction may suggest that NADPH is not contributing much to the measured NADH signal.

Unlike the NADH signal which has cytosolic and mitochondrial components, the FAD signal derives only from the mitochondria [140]. To the best of our knowledge, this study is the first to measure lung surface FAD fluorescence. Compared to NADH, the change in the FAD signal in response to lung treatment with the various metabolic inhibitors was relatively small (table 1). One reason could be due to the lower lung tissue concentration of FAD as compared to NADH. In fact, the FAD baseline signal is small relative to the NADH signal as evidenced by the difference in signal amplification for the NADH and FAD channels (10^3 for NADH compared to ~6 x 10^5 for FAD).

Sources of redox-sensitive flavoprotein (FAD) include succinate dehydrogenase (complex II), lipoamide dehydrogenase (LipDH), and electron transfer flavoprotein (ETF) [141, 142]. Treatment with rotenone (complex I inhibitor), which raises mitochondrial NADH/NAD^+, should decrease LipDH flavoprotein fluorescence signal [128]. In the present study, rotenone had no effect on FAD signal (table 2), suggesting that lung mitochondrial LipDH does not contribute much to the measured lung surface flavoprotein signal.

The contribution of ETF, a fatty-acid oxidizing flavoprotein, to the measured flavoprotein signal can be evaluated by lung treatment with potassium cyanide (complex IV inhibitor), which reduces ETF, and complex II flavoprotein signal [128]. Thus, the cyanide-dependent decrease in FAD signal measured in the present study (table 2) could

be due to ETF and/or complex II flavoprotein signal. For lung tissue, glucose is the major oxidizable substrate under normal physiological conditions [139]. Since glucose was the only oxidizable substrate in our perfusate, change in FAD signals (Table 1) in the presence of cyanide should be attributed to complex II flavoprotein rather than ETF flavoprotein.

The contributions of complex II, LipDH, and ETF to the measured lung surface flavoprotein signal in the present study are different from those reported by Kunz and Kunz [141]. Whether this difference in the contributions of these flavoprotein enzymes is attributable to a difference between intact lungs and isolated mitochondria, tissue differences [142], or other factors, is not known. Finally, lung treatment with PCP had no effect on the FAD surface fluorescence signal (table 3). This could be because most of the flavoproteins (FAD + $FADH_2$) are in the oxidized (FAD) form.

The measured changes in NADH and FAD fluorescence signals in response to the treatments in the present study are qualitatively and quantitatively similar to those obtained from rat hippocampal slices [143]. Gerich et al. showed that treatment with rotenone (20 μM) increased NADH signal by ~ 10% with no effect on FAD. Potassium cyanide (100 μM or 1 mM) increased NADH by ~ 20% and decreased FAD signal by ~ 9%. Treatment with the uncoupler carbonyl cyanide 4-(trifluoromethoxy) phenylhydrazone (FCCP, 1 μM) decreased NADH by ~ 12% with no effect on FAD. Using isolated rat ventricular trabeculae, Brandes and Bers [135] demonstrated using fluorescence spectroscopy that treatment with KCN increased $NADH/NAD^+$ by 31%,

whereas treatment with the uncoupler FCCP decreased the ratio by 49%. These results are again consistent with the results from the present study (table 2).

The lung surface optical imaging data measured in this study does not provide information about the specific types of lung cells contributing to the measured NADH and FAD signals, although endothelial cells would be expected to contribute significantly because of their relatively large surface area and fraction of total lung cells [37]. Although determining the contributions of specific lung cell types to the measured signal is potentially important, the global oxidoreductive state of the lung tissue is a highly valuable piece of information irrespective of the individual cell types contributing to the redox ratio. Another limitation of optical surface fluorescence imaging is that it *may* not detect deeper than 500 μm, with an initial diameter of 3.2 mm, for a volume of ~ 4 mm^3. However, this resolution is more than sufficient for determining the RR of parenchymal tissue which has a thickness (air to plasma) of 1.6 μm [37]. That said, central lung lesions without pleural extension would not be expected to be detected by surface fluorescence measurements such as those used in the present study.

3.5.2. Hyperoxic lungs

Hyperoxic lung fluorometry demonstrates the utility of optical fluorescent studies for evaluating the effect of subacute rat exposure to hyperoxia on the redox state of lung tissue mitochondrial electron transport chain (ETC) in a non-destructive manner in isolated perfused lungs. The results suggest a hyperoxia-induced decrease in complex I and II activities, and demonstrate the ability of this approach to detect a change in mitochondrial redox state in the early phase of hyperoxic lung injury.

NADH signal and complex I activity:

Surface fluorometry results establish that rat exposure to >95% O_2 for 48 hours decreased the change in NADH signal in the presence of KCN or rotenone by 58% and 63%, respectively, as compared to those of normoxic lungs. A similar decrease (65%) in NADH signal was also measured following the addition of KCN to PCP-treated hyperoxic lungs as compared to normoxic lungs. Rotenone- or KCN-induced change in NADH signal is a measure of complex I activity. Thus these result suggest that the ETC upstream from complex I is more reduced in intact hyperoxic lungs than in normoxic lungs, and that complex I activity is lower in hyperoxic lungs. This is consistent with the 77% decrease in mitochondrial complex I activity per mg protein which is measured in P2 fractions derived from hyperoxic lungs as compared to normoxic lung.

The measured hyperoxia-induced change in complex I redox state (table 3) could be due to a change in complex I protein and/or change in rate of NADH production. The latter could result from impairment to the Krebs cycle and/or change in cytoslic $NADH/NAD^+$ which could affect mitochondrial NADH level via the malate-aspartate shuttle. However, the hyperoxia-induced change in complex I redox state is most likely due to a change in complex I protein since for the complex I assay (P2 fraction), the NADH concentration used was the same for both normoxic and hyperoxic lung mitochondrial preparations (P2 fractions). The results of this assay (Table 2) show that the measured hyperoxia-induced change in complex I activity is qualitatively and quantitatively consistent with the hyperoxia-induced change in complex I redox state measured on the surface of the lung (table 2).

The sulfhydryl-containing Krebs cycle enzymes pyruvate and alpha-ketoglutarate dehydrogenase and their coenzymes CoA and lipoic acid are sensitive to oxidative stress [23]. Previous studies evaluated the effect of rat exposure to 100% O_2 for 24 hrs on these and other Krebs cycle enzymes [15, 23, 24]. Gardner et al. [24] reported a 73% decrease in lung aconitase activity after 24 hrs of rate exposure to 100% O_2. This decrease is consistent with the increase in citrate level (aconitase substrate) in lung tissue under the same exposure conditions as reported by Bassett et al. [23]. This impairment to the Krebs cycle could affect NADH supplied to the electron transport chain and in turn complex I redox state. However it is not known whether this impairment to aconitase activity persists after 48 hrs of exposure to 100% O_2 or whether it is sufficient to account for the measured hyperoxia-induced change in complex I redox state. In another study, Bassett et al. [15] reported that rat exposure to 100% O_2 for 24 hrs had no effect on the activities of the Krebs cycle enzymes succinate dehydrogenase, isocitrate dehydrogenase or α-glycerophosphate dehydrogenase. In the present study we report a 64% decrease in succinate dehydrogenase (complex II) activity after 48 hrs of exposure to 100% O_2. Additional studies would be needed to evaluate the effect of rat exposure to 100% O_2 for 48 hrs on the activities of Krebs cycle enzymes isocitrate dehydrogenase, α-glycerophosphate dehydrogenase, and aconitase to determine the potential contribution of impaired production of NADH by the Krebs cycle to the measured change in complex I redox state.

Fisher AB [16] reported that rat exposure to 100% O_2 for 48 hrs increased lung lactate production rate (78%) and lactate to pyruvate ratio (108%). Since lactate to

pyruvate ratio is proportional to cytosolic NADH/NAD^+, the increase in lactate to pyruvate ratio suggests an increase in cytosolic NADH transported to the mitochondria matrix via the malate-aspartate shuttle. This shuttle provide more cytosolic NADH to mitochondria when the cytosolic NADH/NAD^+ is higher than in the mitochondrial matrix. Thus the hyperoxia-induced increase in cytosolic NADH/NAD^+ could contribute to the measured change in complex I redox state in hyperoxic lungs.

Rat exposure to hyperoxia had no effect on the change in NADH signal in the presence of PCP as compared to that in normoxic lungs as a measure of the coupling between ETC and phosphorylation. This observation implies that rat treatment with hyperoxia (>95% O_2 for 48 hours) did not alter the coupling between respiration and phosphorylation in lung tissue despite the apparent decrease in complex I activity. However, since the ETC upstream from complex I is more reduced in hyperoxic lungs than in normoxic lungs, one would expect a larger PCP-induced decrease in NADH signal in hyperoxic lung. Currie et al. demonstrated that rat exposure to 100% O_2 for 48 hours decreased ADP-stimulated O_2 consumption (state 3) by ~50% with a-ketoglutarate as an NAD-linked substrate [25]. Together these results support a decreased tightness of coupling between respiration and phosphorylation in hyperoxic lungs as compared to normoxic lungs.

There is ample evidence that increased production of reactive oxygen species (ROS) is a major pathophysiological factor in the genesis of hyperoxic lung injury [3, 26-28]. Thus, one strategy that cells may have evolved to protect against hyperoxic lung injury is to mitigate the activities of ROS sources [12, 29-31]. Mitochondrial electron

transport complex I is a major source of ROS [3, 27, 32]. Moreover, studies have shown that the rate of ROS formation at complex I in endothelial cells increased with an increase in O_2 tension, and that complex I inactivation using rotenone decreased ROS generation in sheep pulmonary microvascular endothelial cells exposed to hyperoxia (100% O_2 for 30 min) [27, 32, 33]. Thus the measured decrease in complex I could be an adaptive mechanism by the cells to decrease the rate of ROS formation at complex I under hyperoxic conditions.

On the other hand, the measured decrease in complex I activity could represent hyperoxia-induced injury leading to increases in the rate of ROS formation. Mitochondrial DNA (mDNA) is highly sensitive to ROS [34]. Hyperoxia-induced increase in the rate of ROS formation could damage mDNA and as a result compromise complex I activity since 7 out of 45 subunits of complex I are encoded by mDNA [34, 35]. Hyperoxia-induced increase in ROS formation could also cause direct damage to complex I activity by oxidizing cardiolipin, which is sensitive to ROS [36, 37]. This phospholipid is important for the function of complex I [38]. In addition, oxidation of this lipid could lead to increase in the loss of electrons at complex I and in the rate of mitochondrial superoxide formation at complex I [36, 37].

Ratner et al. demonstrated that exposure of neonatal mice to hyperoxia (75% O_2 for 72 hours) decreases complex I activity in lung homogenates by ~70%, and that this decrease compromises mitochondrial oxidative phosphorylation and contributes to alveolar development arrest [7]. Fisher AB [16] showed that rat exposure to 100% O_2 for 48 hours had no effect on lung tissue ATP content as compared to normoxic lungs,

although there was an increase (105%) in lactate/pyruvate ratio indicating an increase in ATP production via glycolysis. He suggested that the increased lactate/pyruvate ratio could be due to demand for glycolytic ATP and/or decrease in ATP production via oxidative phosphorylation which is compensated for by an increase in ATP production via glycolysis.

FAD signal and complex II activity:

Compared to NADH, the measured change in the FAD signal in response to lung treatment with the metabolic inhibitors was relatively small for normoxic and hyperoxic lungs (Table 1). One reason for this observation could be lower lung tissue concentration of FAD as compared to NADH. In fact, the FAD baseline signal is small relative to the NADH signal as evidenced by the difference in signal amplification for the NADH and FAD channels (10^3 for NADH compared to ~6 x 10^5 for FAD) [18].

Lung treatment with KCN, which reduces the ETC upstream from complex IV, should reduce complex II and as a result decrease FAD signal. Just as a change in NADH tracks complex I activity, a change in FAD signal reflect complex II activity. Rat exposure to hyperoxia had no significant effect on the change in FAD signal in the presence of KCN as compared to that in lungs from normoxic rats. However, the change in FAD signal following the addition of KCN to PCP-treated lungs was 56% lower in hyperoxic lungs than normoxic lungs. It could be that lung treatment with PCP, which simulates the flow of reducing equivalents through the chain, fully oxidized the chain and as a result exposed the difference in the capacities of complex II between normoxic and

hyperoxic lungs. Regardless, this apparent decrease in complex II activity is consistent with the 63% decrease in mitochondrial complex II activity per mg protein in P2 fractions derived from hyperoxic lungs as compared to normoxic lung (Table 2).

The measured hyperoxia-induced change in FAD signal in the presence of (PCP + KCN) could be due to a direct oxidant-induced inhibition of complex II or indirect inhibition of complex II by impairment of Krebs cycle enzymes/coenzymes that result in a decrease in succinate concentration or increase in the concentration of oxaloacetate (OAA). Complex II activity is inhibited by a high level of OAA. However the results of the mitochondrial isolates (P2 fractions) suggest that the hyperoxia-induced change in complex II redox state is most likely due to impairment of complex II itself since for this assay the concentrations of succinate and the electron acceptor (DCPIP) used were the same for the mitochondrial isolates from both normoxic and hyperoxic lungs and should be in excess of what is required for maximal function of complex II. The measured decrease in complex II activity using this assay (Table 2) is qualitatively and quantitatively consistent with the measured hyperoxia-induced decrease in FAD signal in the presence of PCP + KCN as a measure of complex II activity (Table 1).

Complex II is the only ETC complex that is completely encoded by nuclear DNA [39]. Hence, damage to mDNA due to hyperoxia-induced increase in the rate of ROS formation should have no effect on complex II. Since electrons channeled through complex II produce 4-fold more mitochondrial superoxide than electrons channeled through complex I [40], the apparent decrease in complex II activity could be a means by the cells to reduce ROS formation under hyperoxic conditions.

Additional studies are needed to evaluate the effect of the depression in complex I and complex II activities observed in hyperoxic lungs on ROS production at complex I and III and mitochondrial bioenergetics, and to determine whether this depression is an injury or an adaptive response to the hyperoxic environment.

Sources of NADH and FAD surface fluorescent signals:

Our assumption in this study is that changes in the mitochondrial pool of NADH is a key contributor to the measured changes in the NADH fluorescence signal since the metabolic inhibitors we used target the mitochondrial electron transport chain [18]. Another source of NADH signal is the cytosolic pool of NADH. Fisher et al. [41] demonstrated that rat lung treatment with KCN increased lung lactate/pyruvate by 4-fold. In this study, lung perfusion with KCN increased lung surface NADH signal by 22% in normoxic lungs. Since lactate/pyruvate ratio reflects cytosolic NADH/NAD^+ [42, 43], this suggests that cytosolic NADH did not contribute significantly to the measured lung surface NADH signal.

Unlike the NADH signal which has cytosolic and mitochondrial components, the FAD signal derives only from the mitochondria [18, 44]. Sources of redox-sensitive flavoprotein (FAD) include succinate dehydrogenase (complex II), lipoamide dehydrogenase (LipDH), and electron transfer flavoprotein (ETF) [18, 45, 46]. However, as previously discussed, most of the measured lung surface FAD signal is from complex II flavin [18].

Fisher AB demonstrated that rat exposure to 100% O_2 for 48 hours stimulated glycolysis as measured by ~105% increase in the lung lactate/pyruvate ratio [16]. Since

this ratio is a measure of cytosolic NADH/NAD^+, this suggest that lung tissue cytoplasm is more reduced in hyperoxic lungs than normoxic lungs. Thus, coupled with the results of the present study, the data document that both tissue cytosolic and mitochondrial compartments are more reduced in hyperoxic lungs than normoxic lungs.

The hyperoxia-induced decrease in complex I and II activities in the present study represents a relatively early *in situ* metabolic consequence of hyperoxia in that it precedes effects on lung histology, hemodynamic and functional endpoints observed with rat exposure to >95% O_2 for > 48 hours [8, 47]. Of the few studies evaluating the metabolic consequences of hyperoxia in the 18-48 hr period, a decrease in serotonin clearance and an increase in lactate production have been observed in lungs from rats exposed to 100% O_2 for 18 and 36 hrs, respectively [16, 48]. Audi et al. reported that rat exposure to hyperoxia (85% O_2 for 48 hours) results in 47% decrease in the capacity of complex I mediated coenzyme Q_1 (amphipathic homolog of ubiquinone) reduction on passages through the pulmonary circulation as compared to that in lungs of normoxic rats [11]. Additionally, Klein et al. demonstrated a decrease in the metabolism of prostaglandin E_2 metabolism in intact lungs of rats exposed to > 97% O_2 for 36 hrs [49].

3.5.1. Blood Effect

Since *in vivo* estimates of RR are unavoidably acquired in the presence of blood, we determined the effect of blood in perfusate on NADH and FAD lung surface fluorescence signal, and on RR. The results of the study show an exponential relationship of the quenching effect of red blood cells on NADH and FAD fluorescence signals, consistent with Beer's law [130]. However, the effect of blood on RR is relatively small and

appears to be independent of blood hematocrit level. Although the range of Hct studied (0-4%) is much lower than rat blood Hct (44%) [131], the plateau seen in the results at 4% Hct (Figure 5) indicates that higher perfusate Hct will have a minimal additional quenching effect on the NADH and FAD fluorescence signals. These results are consistent with those from a study by Chance et al. in which they showed that perfusion of isolated organs (e.g., liver) with perfusate containing blood (0-4% Hct) decreased NADH and FAD signals but did not change the redox ratio [36]. Thus, we expect that the presence of blood in perfusate will have no significant effect on the percentage changes in RR (tables 2 and 3).

3.5.1. *In vivo* studies

Ischemia-reperfusion is a clinically relevant injury and its effects on lung tissue mitochondrial redox is evaluated here using optical fluorometry *in vivo*. Under ischemic conditions (cessation of both blood flow and ventilation), insufficient oxygen supply to the mitochondrial chain should induce reduction in the mitochondrial chain and restoring blood and oxygen flow should reoxidize the chain. The surface fluorometry results are consistent with the expected effects of ischemic conditions in lung tissue.

The results of this study demonstrate the utility of fluorometry for measuring lung tissue NADH and FAD redox state, and lung tissue mitochondrial RR *in vivo*. These data will be important for future studies designed to evaluate the effect of IR injury (e.g. lung transplantation, necrotizing pneumonias, or crush injury to the chest [58]) on lung tissue mitochondrial redox state [99].

Chapter 4

In vitro and cell studies:

Time-lapse microscopy

4. *In vitro* and cell studies: Time-lapse microscopy

4.1. Introduction

In this study, endothelial and fibroblast cells of mice retina, rat lung and heart were assessed either on fixed slides or using live cell treatment and imaging.

Cytometry is an image processing technique to measure various parameters of cells. Some of these parameters are cell size, the stage of the cell cycle, the DNA content of the cell, and the existence or absence of specific proteins on the cell surface or in the cytoplasm. It is a common method of quantifying injured retinas compared to those that are healthy. One way to measure the amount of injury sustained in the retina is through the analysis of its cellular and vascular morphological parameters [7], but quantifying these parameters has proven a difficult task. In addition, the current gold standard method for measuring all of these parameters is the tedious process of manual counting and analysis. This is a difficult task, which leads to errors in the quantification process, and prohibits the measurement of some more complex parameters. As the first stage of cell studies I have developed algorithms and tools to quantify these parameters (including number of cells and their location) automatically using Matlab.

Changes in the cytoplasmic free Ca^{2+} concentration ($[Ca^{2+}]_c$) constitute one of the main pathways by which information is transferred from extracellular signals received by animal cells to intracellular sites. In eukaryotic cells, one major route for Ca^{2+} influx is through store-operated calcium released activated channels (CRAC), which are activated following a fall in Ca^{2+} content within the endoplasmic reticulum. Mitochondria are key regulators of this ubiquitous Ca^{2+} influx pathway [148]. In the next step, the role of mitochondria in regulating the activity and dynamics of calcium channels through time lapse fluorescence microscopy and cytometry is evaluated. The hypothesis is that alterations in the various ion channels of the cell membrane by chemical stress would result in dynamically changing concentrations of cytosolic calcium. In addition, inhibition of one of these channels using a mitochondrial uncoupler will result in a smaller change in concentration compared to normal conditions.

As previously discussed, reactive oxygen species (ROS) are chemically reactive molecules containing oxygen and have important roles in cell signaling and homeostasis. Oxidative stress, often due to an irregularity in the level of oxygen introduced to the mitochondria, represents an imbalance between production and consumption of this species. As the final step in cell studies, the dynamics of production of ROS are studied in different stress conditions (modeling oxidative stress) including the addition of chain perturbers (PCP and KCN) in fibroblasts to be further compared with differentiated cells.

4.2. Cell Preparation

4.2.1. Fixed cells (microscope slides)

As a preliminary test of the developed algorithm for retinal image analysis, microscope slides were prepared from transgenic mice eyes. The slides consisted of a total of four groups as follows: 3 week old complete BCL-2 gene knockout, 3 week old partial BCL-2 gene knockout, 6 week old complete BCL-2 gene knockout, and 6 week old partial BCL-2 gene knockout. The BCL-2 gene is one of the most important genes in regulating apoptosis, and is thus expected to impact the cell count and vasculature within the retina [7]. The complete gene knockouts generally show increased apoptosis, leading to fewer cells and a less dense vasculature than their wild type counterparts. Dr. Sheibani's lab prepared retina samples and fixed them in 4% paraformaldehyde for at least 24 hours. The eyes were then bisected equatorially and the entire retina was removed under the dissecting microscope. Following completion of digestion, retinal vessels were flattened by four radial cuts and were mounted on glass slides [5].

4.2.2. Live cells preparation

Fibroblasts of heart and lung and pulmonary arterial endothelial cells (PAEC) are cultured and kept in the incubator (5% CO2, 37^{o}C) for future imaging. The bottom glass 35 mm MatTek dishes were coated with 70 uL of 0.02% collagen in acetic acid and used for plating the next day. The frozen cells were thawed, the old media was removed after 15 minutes and 5 minutes, for fibroblast and PAEC, respectively in the centrifuge (1500 rpm), cells were counted using the hemocytometer, and the cell suspension with the 30,000 cell/mL was prepared using fresh medium including 5 mL pen/strep, 50 mL

bovine serum, and 500 mL ATCC Dulbecco's Modified Eagle's Medium (DMEM) and was added to 4-7 dishes of MatTek dishes depending on the total number of the cells (2 mL = 60,000 cells per dish). Some of the PAEC were plated in 4-well glass bottom dishes to study the effect of drugs simultaneously. Before each experiment and fluorescent imaging, the cells are loaded with proper fluorescent dyes (depending on the experiment) as described below.

For CRAC studies the cells were loaded with the following dyes in 2 mL DMEM and were incubated for 30 minutes. The main dye is Fluo-4 (2 uM), which is an exogenous tag used to probe calcium concentration in the GFP channel (Ex: 470, Em: 522) in the cells. The cells were also tagged with 0.5 uM Hoechst and 2 uM TMRM (tetramethylrhodamine) for probing nuclei and mitochondrial membrane potential to be imaged in blue (Ex: 360, Em: 460) and TxR (Ex: 540, Em: 620), respectively. The dyes were washed twice after incubation, and KRH (10x Krebs-Ringer-Hepes Ca^{2+} free) was added to the MatTek dish for imaging.

To evaluate the production of ROS in oxidative stress models in fibroblasts, the cells were loaded with 0.5 uM Hoescht and 2 uM fluo-3 AM (Hoescht only for PAEC) in DMEM and were incubated for 30 minutes, after which they were washed then Hank's Balanced Salt Solution (HBSS) was added for subsequent fluorescent imaging.

4.3. Image acquisition and microscopy

4.3.1. Fluorescence microscope:

Our Nikon Ti-E inverted microscope, used in the cell studies, includes four fluorescent interchangeable filter cubes in addition to the standard DIC and bright-field channels. It is commonly used to study normal cell processes as well as those of diseases, cell signaling, neurobiology, molecular pathology, and so on in cellular and sub-cellular resolution.

The bright field images are acquired using an overhead halogen lamp, whereas the fluorescent images use a mercury arc lamp, to take advantage of halogen's intense peaks in the ultraviolet regime. Each image was acquired at a magnification of 20× to 40× to capture a high level of detail, while maintaining a large field of view. All images were acquired using a charge-coupled device camera (Q-imaging, Aqua Exi, 14 bit, 6.45 μm pixel) with exposure time and gain set to ensure proper use of the dynamic range of the camera, while avoiding saturation and photo-bleaching. The excitation spectra in the blue, green, and red channels are 340-380 nm, 455-485 nm, and 528-553 nm, respectively while the emission spectra are 435-485 nm, 500-545 nm, and 590-650 nm, again in blue, green, and red channels, respectively.

4.3.2. Fixed cells imaging:

The slides of the retina were imaged using bright field and fluorescence illumination using the Nikon Ti-E inverted microscope, the results of which can be seen in Figure 24. The figure shows an example of cellular (in bright-field) and vasculature (in TxR) images of the retina slides.

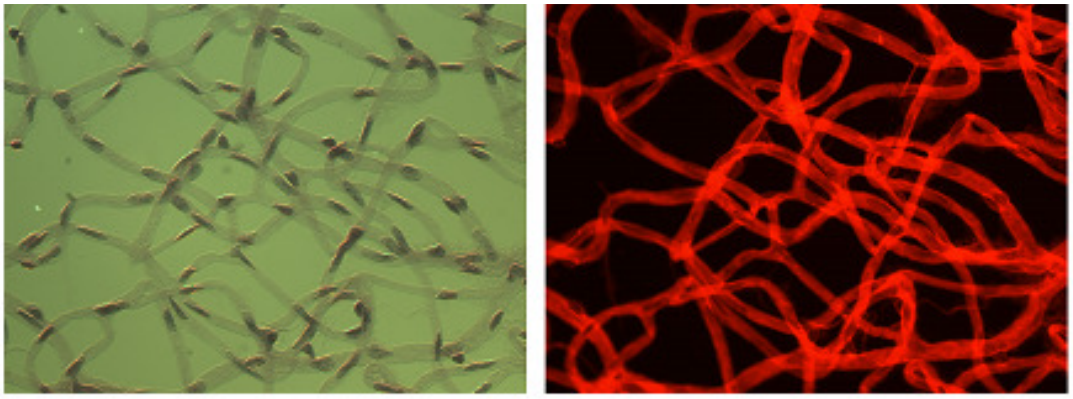

(a) (b)

Figure 24: Example Retinal Images. Examples of the a) bright field and b) fluorescent images used to detect cells and vasculature, respectively.

4.3.3. Live cell imaging

The wells of the cells were imaged in bright field illumination and three channels of fluorescence illumination using the microscope, the results of which can be seen in figures 25 and 26 for CRAC studies and ROS production studies, respectively. For each field of view, the bright field image is captured first, followed by a series of time-lapse imaging in the blue (Hoechst), green (Fluo-3 or Mito-tracker green) and red (TMRM or Mito-SOX) channels in 1 minute intervals to monitor nuclei, calcium concentration or mitochondrial ROS, and mitochondrial membrane potential or ROS levels respectively.

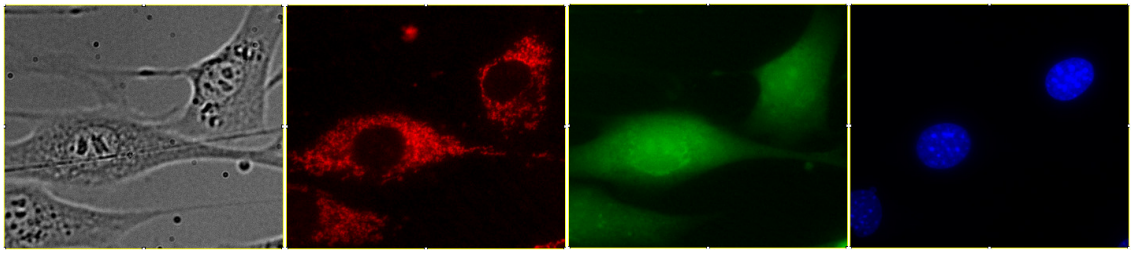

Figure 25. The result of cell imaging in CRAC studies. From left to right, are cell images in bright-field, red (TMRM), green (Fluo-3) and blue (Hoechst) fluorescent channels.

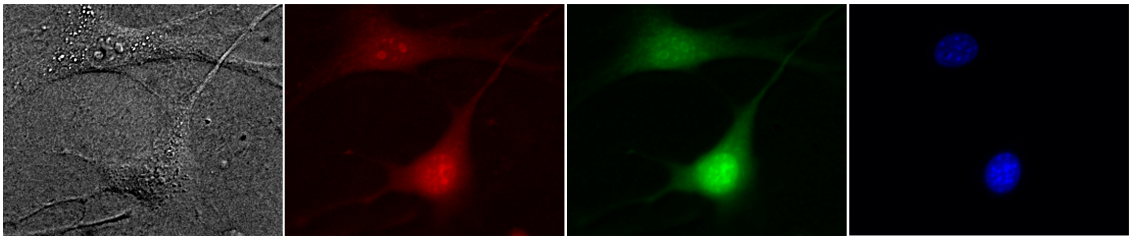

Figure 26. The result of fibroblast imaging in ROS studies. From left to right, are cell images in bright-field, red (Mito-SOX), green (Fluo-3), and blue (Hoechst) fluorescent channels.

One plate of cells was loaded with Mito-SOX, Hoechst, and Mito-Tracker green and imaged in red, blue, and green channels, respectively, to ensure the localization of the Mito-SOX dye in the mitochondria by comparing the red channel to the green channel; the result of this is shown in figure 27.

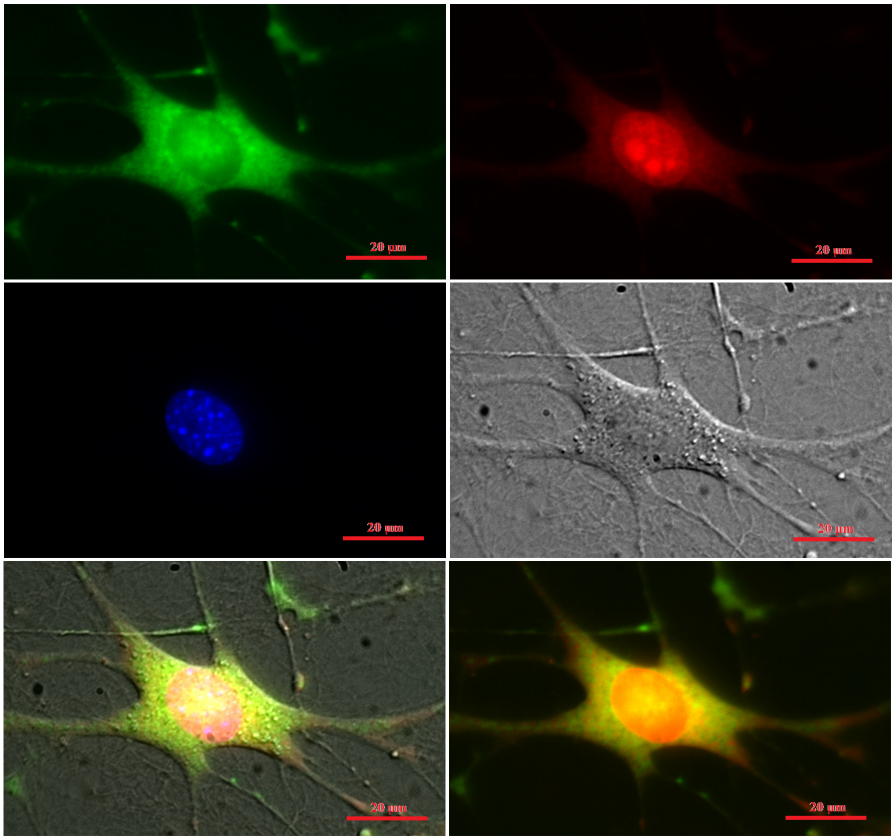

Figure 27. The result of mitochondria imaging. Top left and right shows Mito-tracker green and Mito-SOX in green and red channels, the middle panel shows cell nuclei in blue and left whole cell in bright-field. The bottom panel shows the overlay of different channels, left: all four channels mentioned above and right only red and green channels.

For CRAC studies, the cells were treated with thapsigargin, calcium, and ionomycin with and without dinitrophenol (DNP) to study their effect on the calcium concentration within the cytoplasm as well as CRAC channel dynamics.

For ROS studies the cells were loaded with Mito-SOX after acquiring the baseline images followed by treating with KCN, Rotenone or PCP (either right after Mito-SOX or 20 minutes after it) to study the ROS production (mainly superoxide) in the mitochondria as indicated by fluorescence intensity.

Before the addition of each drug, the old imaging medium or drug was removed from the plate using the insert system implemented in Biophotonics lab as shown in figure 28, and the new drug was added immediately using the same system.

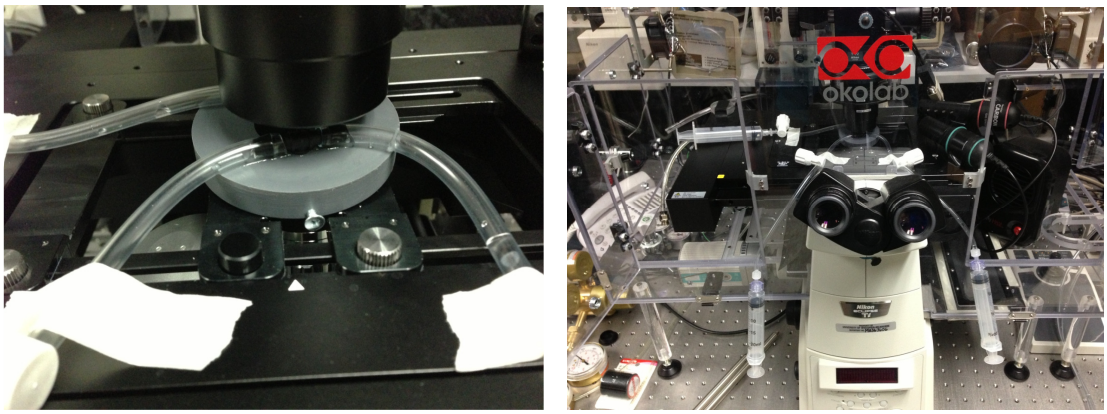

(a) (b)

Figure 28. a) insert system b) in the microscope. The insert system enables us to add or remove drugs to the system without movement of the plate.

4.4. Image Processing

The image processing techniques, including cell segmentation, were developed and tested on fixed cells, and later applied to live cells to detect the cells and study the dynamics of the cells over time.

4.4.1. Fixed cells: Segmentation

An image cytometry algorithm (segmentation of the cell borders) has been developed to analyze cells' response to oxidative stress in eyes. The details of the segmentation algorithm are as follows (also depicted in figure 29). First, the location of foreground markers (cells) is detected by applying an FIR semi-Laplacian filter, the center and surround filter, to enhance the contrast of the circular objects (figure 29.b). The impulse response of the filter emphasizes circular objects by leaving pixels in a central circle unchanged, while negating pixels outside of the central circle to create a high contrast around circular objects in the image. With the location of the cells detected by thresholding the filtered image (figure 29.c), a distance transform is calculated for the resulting image, in which each pixel value is transformed into the distance to the nearest cell (figure 29.d). Background markers are then computed by applying watershed detection on the resultant distance image from the previous stage (figure 29.e). Watershed detection is a technique which finds the "ridges" in an image, which in this case leads to areas where the distance to the nearest cell is maximal. The resulting background markers are the lines that separate the image into individual cells, while maintaining the maximum distance between any line and the nearest cell. Then the gradient of the image is calculated (figure 29.f) and modified so that its intensity becomes zero in both foreground

and background objects. Finally, the watershed transform of the modified gradient image is computed, which results in a binary mask containing the borders of the objects.

In addition to segmenting the cells, the software is capable of counting the number of cells, and the location and shape of each cell.

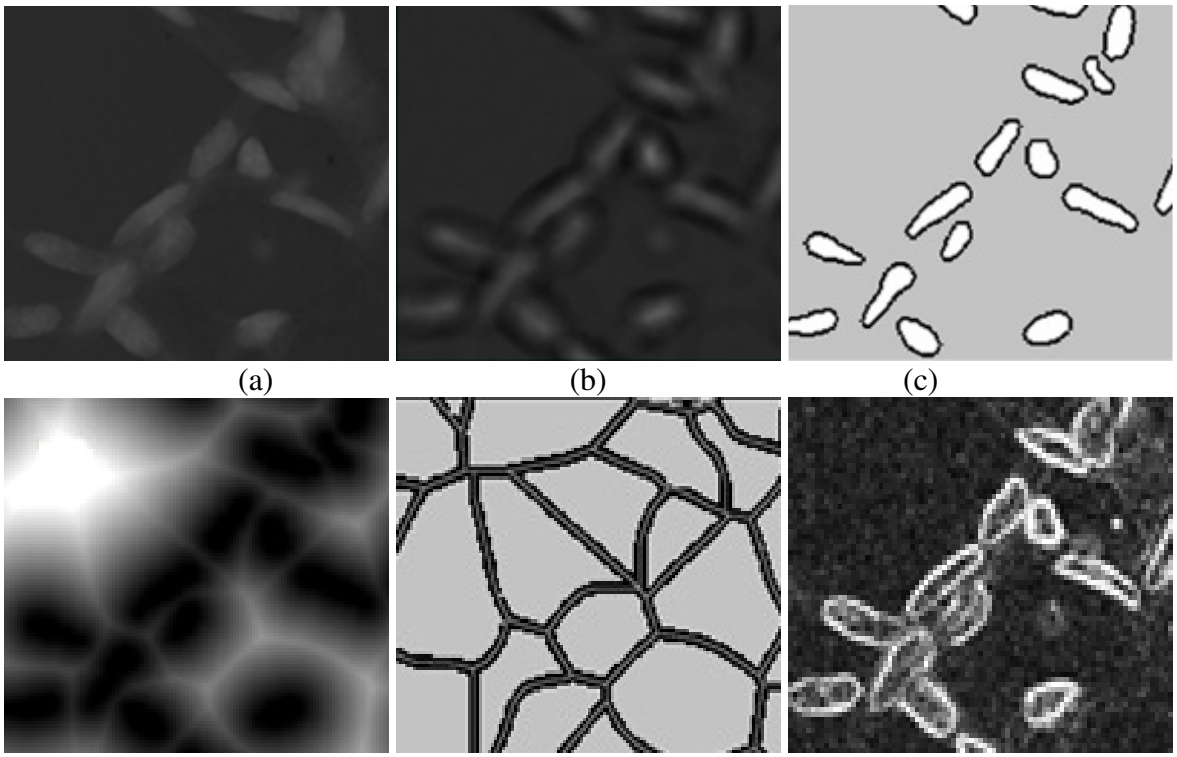

Figure 29. Step in the segmentation algorithm. a) original image b) filtered image using center and surround filter c) thresholding the filtered image d) distance transform of the threshold image e) watershed transform of part d f) gradient of the image

4.4.1. live cells

Using the segmentation algorithm described above, the borders of the cells are detected in the first slide of the time-lapse stack and the intensity of images in both red and green channels is calculated and plotted as the intensity profile over time. These graphs help us

monitor the dynamics of calcium concentration in green channel, and mitochondrial membrane potential or ROS in red channel.

4.5. Results

4.5.1. fixed cells

Automatic cell segmentation resulted in an accuracy of ~90% compared to manual cell detection and counting (which is the gold standard for cell detection). Figure 30 shows two images from two different groups of mice and figure 31 shows the overall results of cell detection for four fields of view from each slide. Since BCL-2 is an apoptosis inhibitor, this feature is expected to have different values in different classes as can be seen in figures 30 and 31.

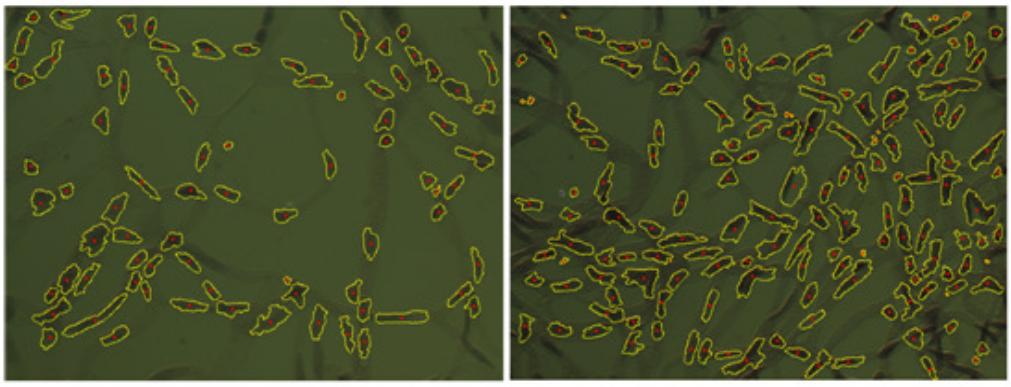

(a) (b)

Figure 30. Cell detection example. a) low number of cells (80, p42 BCL -/-). b) high number of cells (152, P21 -/+).

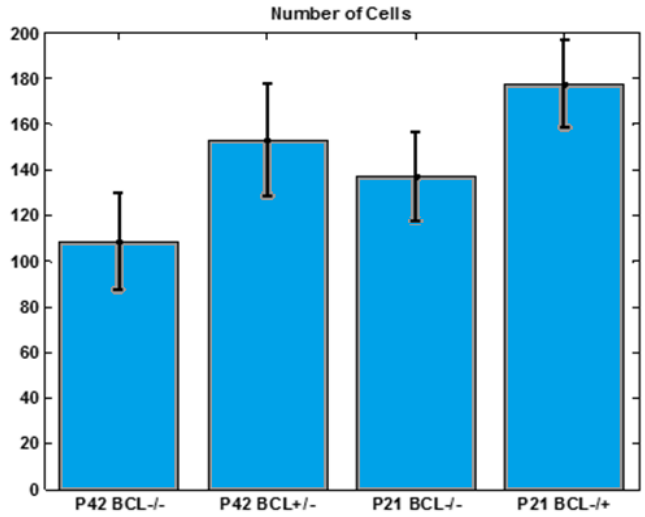

Figure 31. Cell Count Statistics. Mean values and Standard Deviations of cell counts of retinal vasculature. P42 is 6 weeks, P21 is 3 weeks, BCL -/- indicates complete knockout, whereas BCL -/+ or +/- indicates partial knockout.

4.5.2. CRAC channels in NIH 3T3 fibroblasts

In order to study the properties of CRAC in fibroblasts, the cells were loaded with Fluo-3 AM, imaged in GFP and treated with tapsigargin, calcium, and ionomycin for one set, and with DNP, thapsigardin, calcium, and ionomycin for another set. The changes in the intensity of a single cell is shown in figure 32 and the results of segmentation of cell borders in green channel is shown in figure 33.

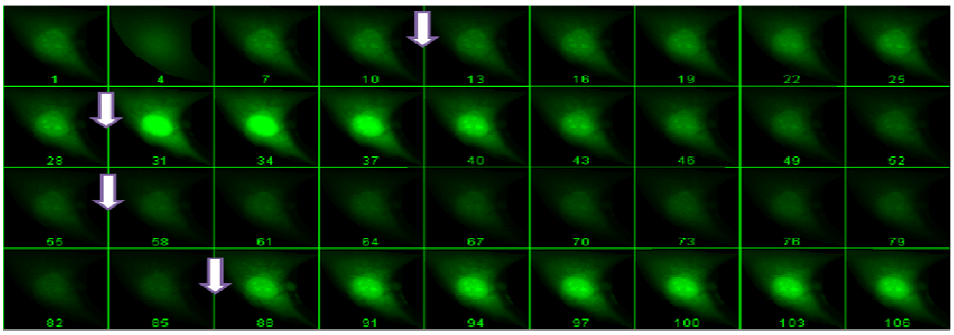

Figure 32. Dynamics of fluo-3 intensity for one cell over time with the addition of DNP, tapsigargin, calcium, and ionomycin shown with arrows in the figure.

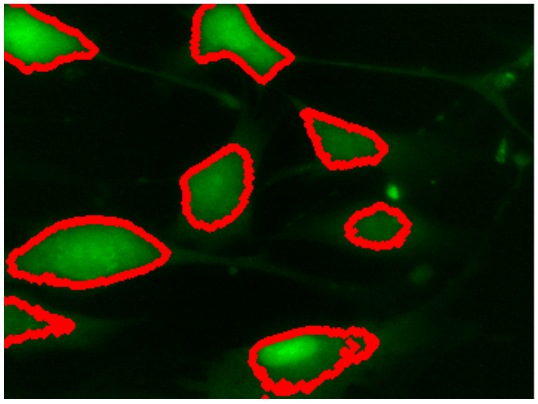

Figure 33. Result of segmentation on the GFP channel images of the cells. For the initial image the cells are automatically detected and the borders are saved and are applied to all the images in the time lapse, to be further used for time-lapse profile intensity.

The dynamics of the calcium concentration over time for segmented cells is also calculated and plotted over time in figure 34 for the two experimental scenarios.

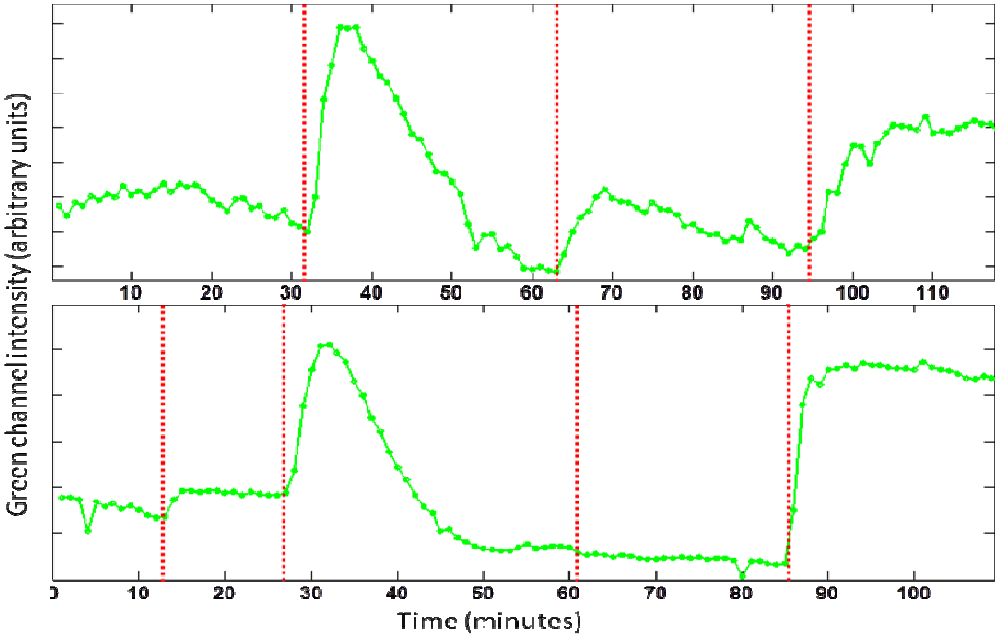

Figure 34. Plotting the profile of the segmented cells over time. Red dotted lines shows addition of thapsigargin, calcium, and ionomycin in top, and DNP, thapsigargin, calcium, and ionomycin in the bottom panels over time.

4.5.3. ROS production in NIH3T3 Fibroblasts

KCN and PCP were added to the cells loaded just with Mito-SOX and the dynamics of the cells in red channel (ROS production) were studied, as shown in figures 35 and 36. Addition of Mito-SOX increase the intensity of the cell images gradually over time in the fluorescent red channel, but the slope of this increase is different in the presence of chain perturbations. As shown in figure 36, in the presence of KCN, rapid production of ROS resulted in a much steeper slope compared to control, while addition of PCP resulted in a lower slope compared to the control dish.

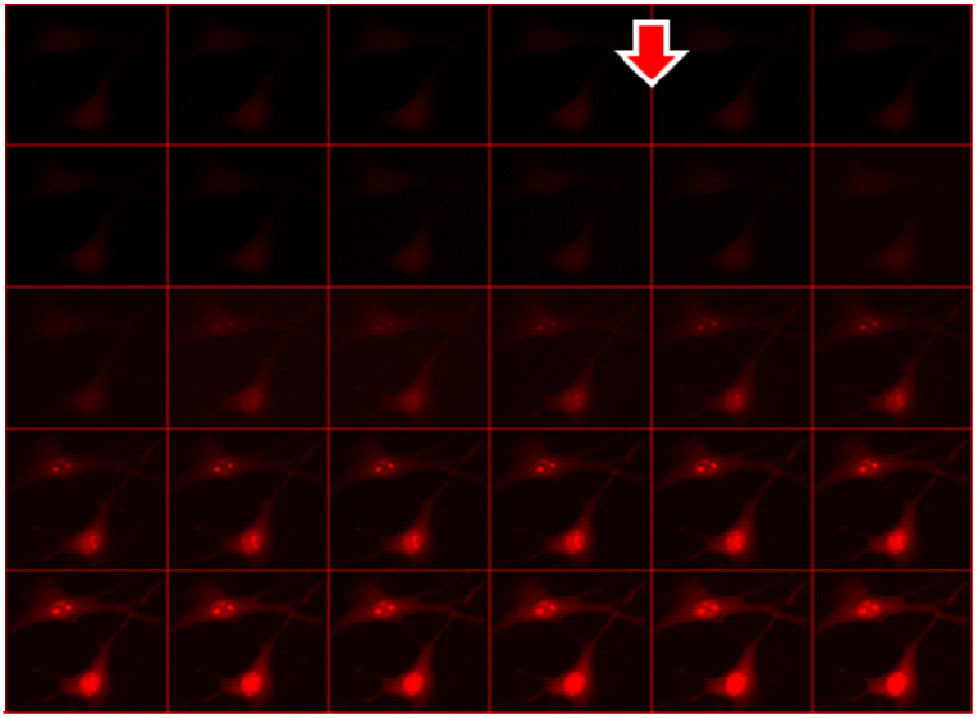

Figure 35. Dynamics of red channel (Mito-SOX) intensity for two cells over time. Addition of Mito-SOX is shown in the figure with an arrow.

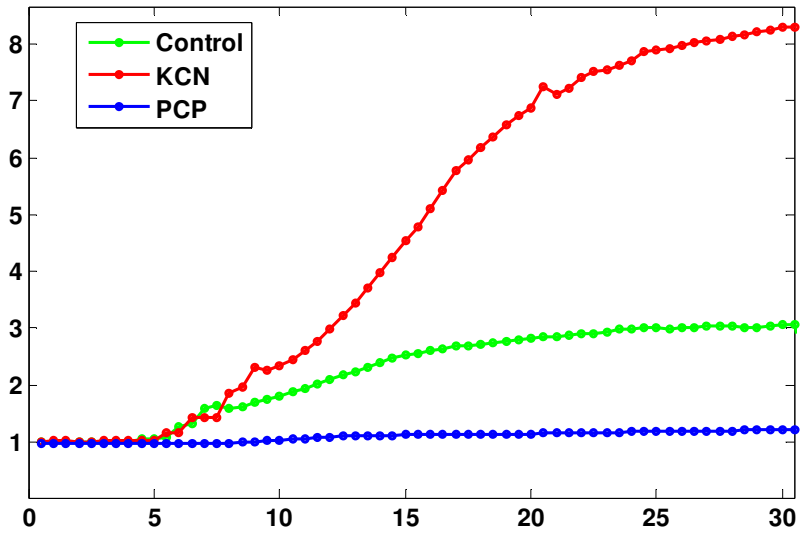

Figure 36. The profile of the cells in red channel over time. Mito-SOX is added to the dish 5 minute after the start of the imaging. The first dish (green) is imaged in the presence of Mito-SOX only while for the second and third dishes Mito-SOX is added at the same time with 3mM KCN (red) and 3nM PCP (blue), respectively.

4.5.4. ROS production in PAEC

The drugs were added to PAEC with a different protocol that instead of adding them right after Mito-SOX, they were added 20 minutes later giving time to Mito-SOX to attach to the superoxide. Different concentration of drugs were used to study the proper concentration which cause the maximum effect but not yet is lethal for the cells. The same way as fibroblasts the dynamics of the cells in red channel (ROS production) were studied, as shown in figure 37 for rotenone.

Addition of Mito-SOX increase the intensity of the cell images gradually over time in the fluorescent red channel, but the rate of this increase changes later after addition of different chain perturbations. As shown in figure 37, in the presence of rotenone, the rate of the superoxide production is increasing comparing to the wells without rotenone. Also by increasing the concentration of the drug, the change in the rate increases as well.

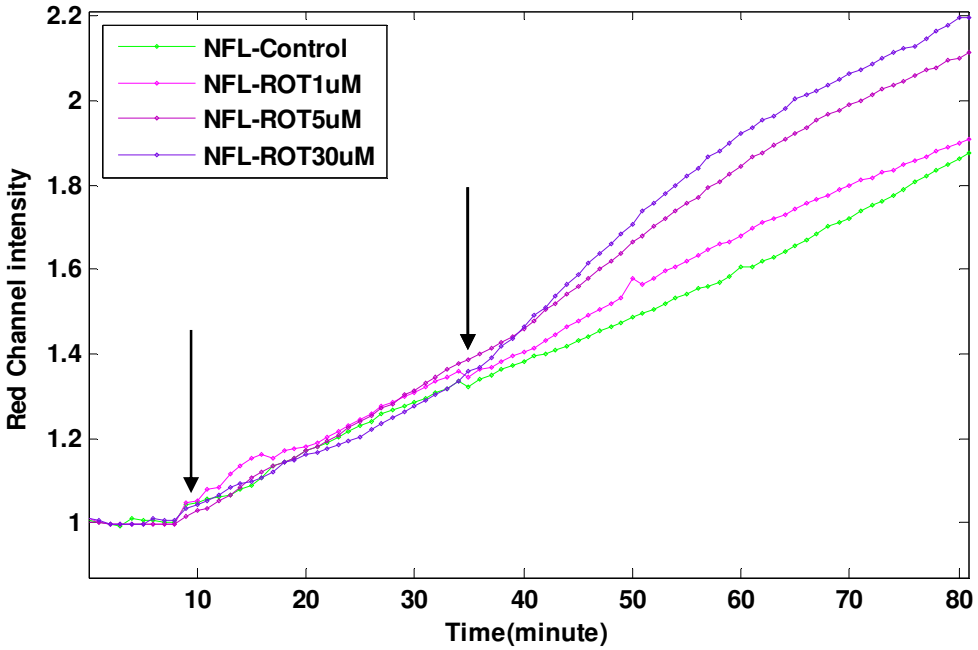

Figure 37. Dynamics of red channel (Mito-SOX) intensity of cells over time. Addition of Mito-SOX (first) and Rotenone are shown in the figure with arrows.

4.6. Discussion

Optical image processing and cytometry techniques including segmentation can be used to quantify injury using cellular morphology for fixed microscopic slides of retina, and the results of the analysis allow for statistical determination of injury. The current gold standard method for quantifying the parameters (namely the number of cells) is the tedious process of manual counting, which cannot be used for real-time measurements and suffers from human error. However, the segmentation algorithm developed here automates this process and reduces the potential for human error in

making these measurements. Furthermore, objective processing using the automated algorithm removes the subjective processing errors and makes the process reproducible.

Thapsigargin, calcium, and ionomycin are all expected to increase the level of cytosolic calcium concentration (but through different mechanisms), which can be seen in the top panel of figure 33. Thapsigargin raises the concentration of cytosolic (intracellular) calcium by blocking the ability of the cell to pump calcium into the sarcoplasmic and endoplasmic reticula, which causes these stores to become depleted. Store depletion can secondarily activate plasma membrane calcium channels, allowing an influx of calcium into the cytosol. Ionomycin is an ionophore which is used in research to mark the upper limit of the calcium concentration in the cells. Addition of DNP uncouples oxidative phosphorylation, causing a release of calcium from mitochondrial stores and preventing calcium re-uptake{Barker, 2006 #1476} [151]. In the presence of DNP, thapsigargin and ionomycin are expected to increase the cytosolic calcium levels, but the addition of calcium itself is expected not to affect the level of calcium in the cytosol, which is the case in the bottom panel of figure 34.

As previously discussed, KCN increases NADH and decreases FAD levels; basically blocks electron flow, maximizes the probability of losing electrons to oxygen, and causes a significant increase in the level of superoxide. On the other hand, PCP (which is an uncoupler) oxidizes NADH and other coenzymes, use up the oxygen and prevents the production of superoxide. The results of using Mito-SOX in fibroblast confirms these hypotheses and, as can be seen in figure 36, there is a steep slope in the production of superoxide under the influence of KCN compared to control, while the addition of PCP along with Mito-SOX shows a decrease in the level of superoxide

compared to control in fibroblasts. Rotenone is an inhibitor of complex I and we expect to see the same behavior as the one we saw for the KCN and the results shows that in the presence of rotenone, there is a increase in the production rate of rotenone as expected.

Chapter 5

Conclusion and future direction

5. Conclusion and future direction

The tools and methods designed as part of this research, namely the fluorometer instrument and the acquisition protocols combined with the software and algorithms to process the signals and images, have shown the ability to measure the amount of injury in tissue and cells due to mitochondrial dysfunction, resulting in a robust and reliable *in situ* and *in vitro* quantification of health in the presence of oxidative stress.

The conclusion is categorized into three sections for each imaging protocol below.

5.1. Frozen tissue studies

The results of this study support the utility of optical imaging of NADH and FAD signals to evaluate lung tissue mitochondrial redox state. While optical determination of RR in tissues such as brain and myocardium is accepted [72, 73, 108], the applicability of these methodologies in examination of the redox state in *lungs*, where the density of mitochondria is much lower, has not been established. The potential clinical importance of real time optical imaging of lungs in patients with critical illnesses, patients on high O_2, or patients with IR lung injury secondary to lung transplant or chest contusions, is great. Reliable fluorescence determination of the RR could be adopted in the same fashion that near-infrared spectroscopy (NIRS) is gaining favor as a non-invasive measure of tissue oxygenation in critically injured patients [118]. While NIRS is an *indirect* measure of tissue oxygenation, NADH and FAD data provide information regarding tissue redox and mitochondrial bioenergetics, a truer and more sensitive early

measure of organ function. Because NADH and FAD signals can be detected through fiber optic probes placed on the surface of the lung, RR data could be obtained either intraoperatively or through tube thoracostomies (frequently placed for clinical indications in patients with severe lung injury). Our studies support the capacity of fluorescence imaging to detect pulmonary oxidative injury, and set the stage for live tissue studies along with adaptation of the methods (use of reflectance measurements) required to translate this approach to clinical arenas.

The limitation of translation to *in vivo* and optical surface fluorescence imaging is that it may not detect changes deeper than 500 μm (the imaging depth is normally around 200-300 μm). However, this resolution is more than sufficient for determining the RR of homogeneous parenchymal tissue, which has a thickness (air to plasma) of 1.6 μm [8] for lung tissue.

Confirming the application of aforementioned technique in diagnosis of lung injuries, apart from expanding the application to a wide variety of injuries and diseases, it is possible to use this as a monitoring technique to follow the progress of the injury or even effect of therapy over time which is the next step in our cryogenic experiment.

5.2. Fluorometry for Bronchopulmonary Studies

In conclusion, the results of this study demonstrate the utility of optical fluorometry to detect a change in the redox status of lung mitochondrial coenzymes NADH and FAD in isolated perfused lungs over time. In the present study and previous studies by others and ourselves [18, 50-52], the relative change in the NADH and FAD

signals are reported instead of the actual signals, which are sensitive to various factors including probe distance from the organ surface, day-to-day variations in light intensity, and PMT gain settings. One approach to overcoming this limitation would be by imaging a phantom of known NADH and FAD concentrations at the end of a given experiment (lung), and then using this information to scale the measured NADH and FAD signals. This would allow us to compare un-normalized signals from different lungs.

The lung surface optical imaging data do not provide information about the specific types of lung cells contributing to the measured NADH and FAD signals, although endothelial cells would be expected to contribute significantly because of their relatively large surface area and fraction of total lung cells [8]. Though determining the contributions of specific lung cell types to the measured signal is potentially important, the global oxido-reductive state of the lung tissue is a highly valuable piece of information irrespective of the individual cell types contributing to the redox ratio.

Over 900,000 adults receive invasive mechanical ventilation (MV) in the United States each year [53, 54]. Many either have acute lung injury (ALI) or have conditions such as shock and severe sepsis that place them at particular risk of ALI [54-59]. Treatment with high levels of oxygen to maintain adequate tissue oxygenation may further exacerbate lung injury. However, the susceptibility to lung injury (from hyperoxia or shock) varies widely from person to person, and there are only crude and subjective means of screening for or following these injuries clinically so using such instrument developed here make the screening objective and accurate.

The results of this study suggest that hyperoxia-induced mitochondrial dysfunction occurs prior to the inflammatory phase of lung O_2 toxicity. If so, a change in

lung surface mitochondrial redox state, as measured using optical fluorescence techniques, could be used as an index of lung O_2 toxicity in patients with ALI requiring high oxygen therapy, or to monitor the progression of ALI and its most severe form Acute Respiratory Distress Syndrome (ARDS), one of the most frequent causes of admission to the intensive care unit [60]. The fiber optic probe could be placed on the lung pleural surface through a small thoracotomy incision or a thoracostomy tube in patients with these devices in place. Alternatively, the probe might be introduced through an endotracheal tube, and positioned against airway epithelium. The same probe could be used to evaluate the efficacy of novel or existing interventions on lung tissue mitochondrial redox state and energy homeostasis in real time.

An individual with enhanced susceptibility to ARDS would be a strong candidate for strategies such as scrupulous attention to ventilation with low tidal volumes, deliberate tolerance of lower arterial oxygen, or higher carbon dioxide tensions to limit oxygen toxicity or barotrauma, avoidance of transfusions, etc [53-59]. These interventions decrease injury but incur additional risks (increased sedation, impairment of vital organ functions, etc.) that limit their universal and strict application in ALI patients. The diagnostic and therapeutic monitoring applications of this tool are important not only for ALI/ARDS, but also for other lung conditions, including lung cancer which is characterized by mitochondrial impairment (so called Warburg effect) [61], lung transplant related ischemia-reperfusion injury [62], or other animal models of human ALI [63]. Additional applications include diagnostic and therapeutic monitoring of conditions in other organs with high energy flux, such as heart ischemia-reperfusion injury and heart failure management, or intraoperative identification of ischemic intestine and others.

5.3. Cell cultures and microscopy

The current methods for detection of the retinal features from images obtained from fixed retina slides involve tedious manual counting and analysis. By automating this task, using the developed algorithm, the throughput of retinal image analysis, as well as the accuracy, can be increased. Manual analysis is tedious and time consuming and due to fatigue, leads to a high probability of errors in the detection process. As for clinical translation, the algorithm developed for cytometry and cell segmentation and vasculature processing, through further refinement, has the potential to be used in fundus camera, a common noninvasive method of eyes' imaging. While using this type of camera, the vasculature is often stained to fluoresce using a common dye, indocyanine green. Using the fundus camera with this stain allows for one to obtain fluorescent images of the retina. Although these images are of lower resolution than the images studied here, and the contrast between the vasculature and background is decreased, improvements in image processing will allow the algorithm to overcome these deficits and permit it to obtain similar results to those shown here.

The next step for fixed cell studies is to extract other features regarding the vasculature and also improving the segmentation algorithm so that it will be able to distinguish between different cells types which is a project in progress by other graduate students in the lab.

Live cell studies enable us to look at the previously studied injuries at the cellular level. In the next step, it is intended to model injuries such as hyperoxia and hypoxia using controlled environment incubator and microscope gas levels. It is predicted that

hyperoxic condition may exacerbates the severity of lung injury in PAEC by regulating superoxide levels produced.

It is also intended to compare injured cells to control ones. The cells are being prepared by inducing pulmonary hypertension in the lamb fetus in utero by pulling out the fetus, and occluding the ductus arteriosus by 50%, then putting the fetus back in the mother for one more week. The PAECs are then being harvested from the hypertensive lamb lungs and are grown in culture. They are expected to produce more free radicals comparing to control PAECs. Also monitoring the behavior of these cells under long hypoxic conditions followed by hyperoxic conditions is advantageous since it is a good model of injuries happening to the fetus at birth. The cell injuries will be studied in Biophotonics lab by other graduate students.

6. References

[1] A. Mayevsky and G. G. Rogatsky, "Mitochondrial function in vivo evaluated by NADH fluorescence: from animal models to human studies," *American journal of physiology. Cell physiology,* vol. 292, pp. C615-40, Feb 2007.

[2] (4/25/2012). *Modes of Action*. Available: http://chemweb.calpoly.edu/cbailey/377/PapersW07/AndrewB/Modes_of_Action.html

[3] (4/25/2012). *Cell Structure & Function*. Available: http://people.eku.edu/ritchisong/301notes1.htm

[4] (4/25/2012). *Basic Concepts in Fluorescence*. Available: http://micro.magnet.fsu.edu/primer/techniques/fluorescence/fluorescenceintro.html

[5] M. W. Davidson. (2000). *http://micro.magnet.fsu.edu/cells/mitochondria/mitochondria.html*.

[6] A. B. Fisher, L. Furia, and B. Chance, "Evaluation of redox state of isolated perfused rat lung," *Am J Physiol,* vol. 230, pp. 1198-1204, May 1976.

[7] T. Vo-Dinh, *Biomedical photonics handbook*. Boca Raton, Fla.: CRC Press, 2003.

[8] L. V. Wang and H.-i. Wu, *Biomedical optics : principles and imaging*. Hoboken, N.J.: Wiley-Interscience, 2007.

[9] B. Alberts, *Molecular biology of the cell*, 4th ed. New York: Garland Science, 2002.

[10] E. N. Marieb and K. Hoehn, *Human anatomy & physiology*, 8th ed. San Francisco: Benjamin Cummings, 2010.

[11] K. Henze and W. Martin, "Evolutionary biology: essence of mitochondria," *Nature,* vol. 426, pp. 127-8, Nov 13 2003.

[12] D. Voet, J. G. Voet, and C. W. Pratt, *Fundamentals of biochemistry : life at the molecular level*, 2nd ed. Hoboken, N.J.: Wiley, 2006.

[13] N. R. Pace, "The universal nature of biochemistry," *Proc Natl Acad Sci U S A,* vol. 98, pp. 805-8, Jan 30 2001.

[14] N. A. Campbell, B. Williamson, and R. J. Heyden, *Biology: Exploring Life*. Boston, Massachusetts: Pearson Prentice Hall, 2006.

[15] H. Lodish, *Molecular cell biology*, 7th ed. New York, NY: W. H. Freeman and Co., 2012.

[16] T. M. Devlin, *Textbook of biochemistry : with clinical correlations*, 7th ed. Hoboken, NJ: John Wiley & Sons, 2011.

[17] N. Kango, *Textbook of Microbiology*. New Delhi: I.K. International Publishing House Pvt. Ltd., 2010.

[18] A. B. Fisher, "Intermediary metabolism of the lung," *Environ Health Perspect,* vol. 55, pp. 149-58, Apr 1984.

[19] B. Halliwell and J. M. C. Gutteridge, *Free radicals in biology and medicine*, 4th ed. Oxford ; New York: Oxford University Press, 2007.
[20] T. M. Buttke and P. A. Sandstrom, "Oxidative Stress as a Mediator of Apoptosis," *Immunology Today,* vol. 15, pp. 7-10, Jan 1994.
[21] K. Staniszewski, "OPTICAL INSTRUMENTATION AND IMAGE CYTOMETRY OF LUNG AND EYE INJURIES: STUDIES IN THE RODENT MODEL," Masters, Electrical Engineering, University of wisconsin Milwaukee, Milwaukee, 2012.
[22] M. Ranji, S. Kanemoto, M. Matsubara, M. A. Grosso, J. H. Gorman, R. C. Gorman, D. L. Jaggard, and B. Chance, "Fluorescence spectroscopy and imaging of myocardial apoptosis," *Journal of Biomedical Optics,* vol. 11, Nov-Dec 2006.
[23] M. Ranji, M. Matsubara, B. G. Leshnower, R. H. Hinmon, D. L. Jaggard, B. Chance, R. C. Gorman, and J. H. Gorman, "Quantifying Acute Myocardial Injury Using Ratiometric Fluorometry," *Ieee Transactions on Biomedical Engineering,* vol. 56, pp. 1556-1563, May 2009.
[24] M. Matsubara, M. Ranji, B. G. Leshnower, M. Noma, S. J. Ratcliffe, B. Chance, R. C. Gorman, and J. H. Gorman, "In Vivo Fluorometric Assessment of Cyclosporine on Mitochondrial Function During Myocardial Ischemia and Reperfusion," *Annals of Thoracic Surgery,* vol. 89, pp. 1532-1537, May 2010.
[25] B. Chance and H. Baltscheffsky, "Respiratory enzymes in oxidative phosphorylation. VII. Binding of intramitochondrial reduced pyridine nucleotide," *J Biol Chem,* vol. 233, pp. 736-9, Sep 1958.
[26] C. H. Barlow, W. R. Harden, 3rd, A. H. Harken, M. B. Simson, J. C. Haselgrove, B. Chance, M. O'Connor, and G. Austin, "Fluorescence mapping of mitochondrial redox changes in heart and brain," *Crit Care Med,* vol. 7, pp. 402-6, Sep 1979.
[27] R. S. Balaban and L. J. Mandel, "Coupling of aerobic metabolism to active ion transport in the kidney," *J Physiol,* vol. 304, pp. 331-48, Jul 1980.
[28] E. Meirovithz, J. Sonn, and A. Mayevsky, "Effect of hyperbaric oxygenation on brain hemodynamics, hemoglobin oxygenation and mitochondrial NADH," *Brain Res Rev,* vol. 54, pp. 294-304, Jun 2007.
[29] R. Sepehr, K. Staniszewski, S. Maleki, E. R. Jacobs, S. Audi, and M. Ranji, "Optical imaging of tissue mitochondrial redox state in intact rat lungs in two models of pulmonary oxidative stress," *Journal of biomedical optics,* vol. 17, p. 046010, Apr 2012.
[30] R. Sepehr, S. Audi, K. Staniszewski, S. Maleki, and M. Ranji, "Fluorescence Spectroscopy and Cryoimaging of Rat Lung Tissue Mitochondrial Redox State," in *SPIE*, Munich, 2011.
[31] R. Sepehr, K. Staniszewski, E. R. Jacobs, S. Audi, and M. Ranji, "Optical Studies of tissue mitochondrial redox in isolated perfused rat lungs," in *SPIE*, San Francisco, 2012.
[32] J. R. Lakowicz, *Principles of fluorescence spectroscopy*, 3rd ed. New York: Springer, 2006.
[33] J. Ribas Gispert, *Coordination chemistry*. Weinheim: Wiley-VCH, 2008.
[34] J. M. Christie, M. Salomon, K. Nozue, M. Wada, and W. R. Briggs, "LOV (light, oxygen, or voltage) domains of the blue-light photoreceptor phototropin (nph1):

Binding sites for the chromophore flavin mononucleotide," *Proceedings of the National Academy of Sciences of the United States of America,* vol. 96, pp. 8779-8783, Jul 20 1999.

[35] G. H. Patterson, S. M. Knobel, P. Arkhammar, O. Thastrup, and D. W. Piston, "Separation of the glucose-stimulated cytoplasmic mitochondrial NAD(P)H responses in pancreatic islet beta cells," *Proceedings of the National Academy of Sciences of the United States of America,* vol. 97, pp. 5203-5207, May 9 2000.

[36] B. Chance, B. Schoener, R. Oshino, F. Itshak, and Y. Nakase, "Oxidation-reduction ratio studies of mitochondria in freeze-trapped samples. NADH and flavoprotein fluorescence signals," *J Biol Chem,* vol. 254, pp. 4764-71, Jun 10 1979.

[37] J. D. Crapo, B. E. Barry, H. A. Foscue, and J. Shelburne, "Structural and biochemical changes in rat lungs occurring during exposures to lethal and adaptive doses of oxygen," *Am Rev Respir Dis,* vol. 122, pp. 123-43, Jul 1980.

[38] W. A. Altemeier and S. E. Sinclair, "Hyperoxia in the intensive care unit: why more is not always better," *Curr Opin Crit Care,* vol. 13, pp. 73-8, Feb 2007.

[39] A. B. Fisher and M. F. Beers, "Hyperoxia and acute lung injury," *Am J Physiol Lung Cell Mol Physiol,* vol. 295, p. L1066; author reply L1067, Dec 2008.

[40] A. H. Jobe and E. Bancalari, "Bronchopulmonary dysplasia," *Am J Respir Crit Care Med,* vol. 163, pp. 1723-9, Jun 2001.

[41] J. J. Coalson, V. Winter, and R. A. deLemos, "Decreased alveolarization in baboon survivors with bronchopulmonary dysplasia," *Am J Respir Crit Care Med,* vol. 152, pp. 640-6, Aug 1995.

[42] J. J. Coalson, V. T. Winter, T. Siler-Khodr, and B. A. Yoder, "Neonatal chronic lung disease in extremely immature baboons," *Am J Respir Crit Care Med,* vol. 160, pp. 1333-46, Oct 1999.

[43] N. R. Aggarwal, F. R. D'Alessio, K. Tsushima, D. C. Files, M. Damarla, V. K. Sidhaye, M. M. Fraig, V. Y. Polotsky, and L. S. King, "Moderate oxygen augments lipopolysaccharide-induced lung injury in mice," *Am J Physiol Lung Cell Mol Physiol,* vol. 298, pp. L371-81, Mar 2010.

[44] X. Qiu, H. Li, H. Tang, Y. Jin, W. Li, YuSun, PingFeng, X. Sun, and Z. Xia, "Hydrogen inhalation ameliorates lipopolysaccharide-induced acute lung injury in mice," *Int Immunopharmacol,* vol. 11, pp. 2130-7, Dec 2011.

[45] F. Chabot, J. A. Mitchell, J. M. Gutteridge, and T. W. Evans, "Reactive oxygen species in acute lung injury," *Eur Respir J,* vol. 11, pp. 745-57, Mar 1998.

[46] K. F. Udobi, E. Childs, and K. Touijer, "Acute respiratory distress syndrome," *Am Fam Physician,* vol. 67, pp. 315-22, Jan 15 2003.

[47] S. Jeyaseelan, H. W. Chu, S. K. Young, and G. S. Worthen, "Transcriptional profiling of lipopolysaccharide-induced acute lung injury," *Infect Immun,* vol. 72, pp. 7247-56, Dec 2004.

[48] M. Bhatia and S. Moochhala, "Role of inflammatory mediators in the pathophysiology of acute respiratory distress syndrome," *J Pathol,* vol. 202, pp. 145-56, Feb 2004.

[49] W. L. Lee and G. P. Downey, "Neutrophil activation and acute lung injury," *Curr Opin Crit Care,* vol. 7, pp. 1-7, Feb 2001.

[50] V. Sampath, A. C. Radish, A. L. Eis, K. Broniowska, N. Hogg, and G. G. Konduri, "Attenuation of lipopolysaccharide-induced oxidative stress and apoptosis in fetal pulmonary artery endothelial cells by hypoxia," *Free Radic Biol Med,* vol. 46, pp. 663-71, Mar 1 2009.

[51] K. Sato, M. B. Kadiiska, A. J. Ghio, J. Corbett, Y. C. Fann, S. M. Holland, R. G. Thurman, and R. P. Mason, "In vivo lipid-derived free radical formation by NADPH oxidase in acute lung injury induced by lipopolysaccharide: a model for ARDS," *FASEB J,* vol. 16, pp. 1713-20, Nov 2002.

[52] N. W. Kooy, J. A. Royall, Y. Z. Ye, D. R. Kelly, and J. S. Beckman, "Evidence for in vivo peroxynitrite production in human acute lung injury," *Am J Respir Crit Care Med,* vol. 151, pp. 1250-4, Apr 1995.

[53] C. L. Wu, L. Y. Lin, J. S. Yang, M. C. Chan, and C. M. Hsueh, "Attenuation of lipopolysaccharide-induced acute lung injury by treatment with IL-10," *Respirology,* vol. 14, pp. 511-21, May 2009.

[54] T. M. Wizemann, C. R. Gardner, J. D. Laskin, S. Quinones, S. K. Durham, N. L. Goller, S. T. Ohnishi, and D. L. Laskin, "Production of nitric oxide and peroxynitrite in the lung during acute endotoxemia," *J Leukoc Biol,* vol. 56, pp. 759-68, Dec 1994.

[55] L. Liaudet, P. Pacher, J. G. Mabley, L. Virag, F. G. Soriano, G. Hasko, and C. Szabo, "Activation of poly(ADP-Ribose) polymerase-1 is a central mechanism of lipopolysaccharide-induced acute lung inflammation," *Am J Respir Crit Care Med,* vol. 165, pp. 372-7, Feb 1 2002.

[56] K. Irani, "Oxidant signaling in vascular cell growth, death, and survival : a review of the roles of reactive oxygen species in smooth muscle and endothelial cell mitogenic and apoptotic signaling," *Circ Res,* vol. 87, pp. 179-83, Aug 4 2000.

[57] S. Zhuang, M. C. Lynch, and I. E. Kochevar, "Caspase-8 mediates caspase-3 activation and cytochrome c release during singlet oxygen-induced apoptosis of HL-60 cells," *Exp Cell Res,* vol. 250, pp. 203-12, Jul 10 1999.

[58] C. S. Ng, S. Wan, and A. P. Yim, "Pulmonary ischaemia-reperfusion injury: role of apoptosis," *Eur Respir J,* vol. 25, pp. 356-63, Feb 2005.

[59] http://www.infoplease.com/science/health/us-transplants-year

[60] T. Vo-Dinh, *Biomedical Photonics Handbook*: CRS PRESS, 2000.

[61] A. P. Michalopoulou, J. T. Fitzgerald, C. Troppmann, and S. G. Demos, "Spectroscopic imaging for detection of ischemic injury in rat kidneys by use of changes in intrinsic optical properties," *Applied Optics,* vol. 44, pp. 2024-2032, Apr 10 2005.

[62] B. Vollmar, M. Burkhardt, T. Minor, H. Klauke, and M. D. Menger, "A correlation of intravital microscopically assessed NADH fluorescence, tissue oxygenation, and organ function during shock and resuscitation of the rat liver," *Adv Exp Med Biol,* vol. 454, pp. 95-101, 1998.

[63] S. Nioka, D. J. Wang, J. Im, T. Hamaoka, Z. J. Wang, J. S. Leigh, and B. Chance, "Simulation of Mb/Hb in NIRS and oxygen gradient in the human and canine skeletal muscles using H-NMR and NIRS," *Adv Exp Med Biol,* vol. 578, pp. 223-8, 2006.

[64] N. Ramanujam, M. F. Mitchell, A. Mahadevan, S. Warren, S. Thomsen, E. Silva, and R. Richards-Kortum, "In vivo diagnosis of cervical intraepithelial neoplasia using 337-nm-excited laser-induced fluorescence," *Proc Natl Acad Sci U S A,* vol. 91, pp. 10193-7, Oct 11 1994.

[65] M. A. Mycek, K. T. Schomacker, and N. S. Nishioka, "Colonic polyp differentiation using time-resolved autofluorescence spectroscopy," *Gastrointest Endosc,* vol. 48, pp. 390-4, Oct 1998.

[66] N. Ramanujam, J. Chen, K. Gossage, R. Richards-Kortum, and B. Chance, "Fast and noninvasive fluorescence imaging of biological tissues in vivo using a flying-spot scanner," *IEEE Trans Biomed Eng,* vol. 48, pp. 1034-41, Sep 2001.

[67] G. A. Wagnieres, W. M. Star, and B. C. Wilson, "In vivo fluorescence spectroscopy and imaging for oncological applications," *Photochem Photobiol,* vol. 68, pp. 603-32, Nov 1998.

[68] N. Ramanujam, R. Richards-Kortum, S. Thomsen, A. Mahadevan-Jansen, M. Follen, and B. Chance, "Low Temperature Fluorescence Imaging of Freeze-trapped Human Cervical Tissues," *Opt Express,* vol. 8, pp. 335-43, Mar 12 2001.

[69] B. Chance and G. R. Williams, "A method for the localization of sites for oxidative phosphorylation," *Nature,* vol. 176, pp. 250-4, Aug 6 1955.

[70] A. Mayevsky, "Brain NADH redox state monitored in vivo by fiber optic surface fluorometry," *Brain Res,* vol. 319, pp. 49-68, Mar 1984.

[71] M. Ranji, S. Kanemoto, M. Matsubara, M. A. Grosso, J. H. Gorman, 3rd, R. C. Gorman, D. L. Jaggard, and B. Chance, "Fluorescence spectroscopy and imaging of myocardial apoptosis," *J Biomed Opt,* vol. 11, p. 064036, Nov-Dec 2006.

[72] M. Matsubara, M. Ranji, B. G. Leshnower, M. Noma, S. J. Ratcliffe, B. Chance, R. C. Gorman, and J. H. Gorman, 3rd, "In vivo fluorometric assessment of cyclosporine on mitochondrial function during myocardial ischemia and reperfusion," *Ann Thorac Surg,* vol. 89, pp. 1532-7, May 2010.

[73] M. Ranji, M. Matsubara, B. G. Leshnower, R. H. Hinmon, D. L. Jaggard, B. Chance, R. C. Gorman, and J. H. Gorman Iii, "Quantifying acute myocardial injury using ratiometric fluorometry," *IEEE Trans Biomed Eng,* vol. 56, pp. 1556-63, May 2009.

[74] B. Chance, C. P. Lee, and B. Schoener, "High and low energy states of cytochromes. II. In submitochondrial particles," *Journal of Biological Chemistry,* vol. 241, pp. 4574-6, Oct 25 1966.

[75] B. Chance, B. Schoener, R. Oshino, F. Itshak, and Y. Nakase, "Oxidation-reduction ratio studies of mitochondria in freeze-trapped samples. NADH and flavoprotein fluorescence signals," *Journal of Biological Chemistry,* vol. 254, pp. 4764-71, Jun 10 1979.

[76] A. Shiino, M. Haida, B. Beauvoit, and B. Chance, "Three-dimensional redox image of the normal gerbil brain," *Neuroscience,* vol. 91, pp. 1581-5, 1999.

[77] B. Quistorff, J. C. Haselgrove, and B. Chance, "High spatial resolution readout of 3-D metabolic organ structure: an automated, low-temperature redox ratio-scanning instrument," *Anal Biochem,* vol. 148, pp. 389-400, Aug 1 1985.

[78] M. A. O'Reilly, R. J. Staversky, R. H. Watkins, and W. M. Maniscalco, "Accumulation of p21(Cip1/WAF1) during hyperoxic lung injury in mice," *Am J Respir Cell Mol Biol,* vol. 19, pp. 777-85, Nov 1998.

[79] X. I. Couroucli, S. E. Welty, R. S. Geske, and B. Moorthy, "Regulation of pulmonary and hepatic cytochrome P4501A expression in the rat by hyperoxia: implications for hyperoxic lung injury," *Mol Pharmacol,* vol. 61, pp. 507-15, Mar 2002.

[80] H. Y. Cho, A. E. Jedlicka, S. P. Reddy, T. W. Kensler, M. Yamamoto, L. Y. Zhang, and S. R. Kleeberger, "Role of NRF2 in protection against hyperoxic lung injury in mice," *Am J Respir Cell Mol Biol,* vol. 26, pp. 175-82, Feb 2002.

[81] C. C. Dos Santos, "Hyperoxic acute lung injury and ventilator-induced/associated lung injury: new insights into intracellular signaling pathways," *Crit Care,* vol. 11, p. 126, 2007.

[82] M. Kawasaki, K. Kuwano, N. Hagimoto, T. Matsuba, R. Kunitake, T. Tanaka, T. Maeyama, and N. Hara, "Protection from lethal apoptosis in lipopolysaccharide-induced acute lung injury in mice by a caspase inhibitor," *Am J Pathol,* vol. 157, pp. 597-603, Aug 2000.

[83] R. Sepehr, K. Staniszewski, S. Maleki, E. R. Jacobs, S. Audi, and M. Ranji, "Optical imaging of tissue mitochondrial redox state in intact rat lungs in two models of pulmonary oxidative stress," *J Biomed Opt,* vol. 17, p. 046010, Apr 2012.

[84] I. Ali, S. Gruenloh, Y. Gao, A. V. Clough, J. R. Falck, M. Medhora, and E. R. Jacobs, "Protection by 20-5,14-HEDGE Against Surgically-Induced Ischemia Reperfusion Lung Injury in Rats," *Annals of Thoracic Surgery,* 2011.

[85] A. Leke-Tambo, E. R. Jacobs, M. Medhora, S. Gruenloh, Y. Gao, and I. Ali, "The role of TLR4 and HMGB1 in the ischemia/reperfusion-mediated mitochondrial dysfunction," *Chest,* vol. 140, 2011.

[86] S. H. Abman, "Bronchopulmonary dysplasia: "a vascular hypothesis"," *Am J Respir Crit Care Med,* vol. 164, pp. 1755-6, Nov 15 2001.

[87] A. J. Jobe, "The new BPD: an arrest of lung development," *Pediatr Res,* vol. 46, pp. 641-3, Dec 1999.

[88] S. G. Kallapur and A. H. Jobe, "Contribution of inflammation to lung injury and development," *Arch Dis Child Fetal Neonatal Ed,* vol. 91, pp. F132-5, Mar 2006.

[89] A. Vadivel, J. L. Aschner, G. J. Rey-Parra, J. Magarik, H. Zeng, M. Summar, F. Eaton, and B. Thebaud, "L-citrulline attenuates arrested alveolar growth and pulmonary hypertension in oxygen-induced lung injury in newborn rats," *Pediatr Res,* vol. 68, pp. 519-25, Dec 2010.

[90] J. T. Powell and P. L. Whitney, "Postnatal development of rat lung. Changes in lung lectin, elastin, acetylcholinesterase and other enzymes," *Biochem J,* vol. 188, pp. 1-8, Apr 15 1980.

[91] N. Sheibani, E. A. Scheef, T. A. Dimaio, Y. J. Wang, S. Kondo, and C. M. Sorenson, "Bcl-2 expression modulates cell adhesion and migration promoting branching of ureteric bud cells," *Journal of Cellular Physiology,* vol. 210, pp. 616-625, Mar 2007.

[92] C. M. Sorenson, "Bcl-2 family members and disease," *Biochimica Et Biophysica Acta-Molecular Cell Research,* vol. 1644, pp. 169-177, Mar 1 2004.

[93] C. Grutzmacher, S. Park, T. L. Elmergreen, Y. X. Tang, E. A. Scheef, N. Sheibani, and C. M. Sorenson, "Opposing effects of bim and bcl-2 on lung endothelial cell migration," *American Journal of Physiology-Lung Cellular and Molecular Physiology,* vol. 299, pp. L607-L620, Nov 2010.

[94] P. M. Hassoun, F. S. Yu, C. G. Cote, J. J. Zulueta, R. Sawhney, K. A. Skinner, H. B. Skinner, D. A. Parks, and J. J. Lanzillo, "Upregulation of xanthine oxidase by lipopolysaccharide, interleukin-1, and hypoxia. Role in acute lung injury," *Am J Respir Crit Care Med,* vol. 158, pp. 299-305, Jul 1998.

[95] C. M. Sorenson, B. J. Padanilam, and M. R. Hammerman, "Abnormal postpartum renal development and cystogenesis in the bcl-2(-/-)mouse," *American Journal of Physiology-Renal Fluid and Electrolyte Physiology,* vol. 271, pp. F184-F193, Jul 1996.

[96] C. M. Sorenson, S. A. Rogers, S. J. Korsmeyer, and M. R. Hammerman, "Fulminant Metanephric Apoptosis and Abnormal Kidney Development in Bcl-2-Deficient Mice," *American Journal of Physiology-Renal Fluid and Electrolyte Physiology,* vol. 268, pp. F73-F81, Jan 1995.

[97] D. J. Veis, C. M. Sorenson, J. R. Shutter, and S. J. Korsmeyer, "Bcl-2-Deficient Mice Demonstrate Fulminant Lymphoid Apoptosis, Polycystic Kidneys, and Hypopigmented Hair," *Cell,* vol. 75, pp. 229-240, Oct 22 1993.

[98] Z. Gan, D. L. Roerig, A. V. Clough, and S. H. Audi, "Differential responses of targeted lung redox enzymes to rat exposure to 60 or 85% oxygen," *J Appl Physiol,* vol. 111, pp. 95-107, Jul 2011.

[99] S. H. Audi, M. P. Merker, G. S. Krenz, T. Ahuja, D. L. Roerig, and R. D. Bongard, "Coenzyme Q1 redox metabolism during passage through the rat pulmonary circulation and the effect of hyperoxia," *J Appl Physiol,* vol. 105, pp. 1114-26, Oct 2008.

[100] W. S. Kunz and F. N. Gellerich, "Quantification of the content of fluorescent flavoproteins in mitochondria from liver, kidney cortex, skeletal muscle, and brain," *Biochemical medicine and metabolic biology,* vol. 50, pp. 103-10, Aug 1993.

[101] A. Mayevsky and B. Chance, "Oxidation-reduction states of NADH in vivo: from animals to clinical use," *Mitochondrion,* vol. 7, pp. 330-9, Sep 2007.

[102] J. J. Kelly, J. R. Ewen, S. L. Bernard, R. W. Glenny, and C. H. Barlow, "Regional blood flow measurements from fluorescent microsphere images using an Imaging CryoMicrotome," *Review of Scientific Instruments,* vol. 71, pp. 228-234, Jan 2000.

[103] S. L. Bernard, J. R. Ewen, C. H. Barlow, J. J. Kelly, S. McKinney, D. A. Frazer, and R. W. Glenny, "High spatial resolution measurements of organ blood flow in small laboratory animals," *Am J Physiol Heart Circ Physiol,* vol. 279, pp. H2043-52, Nov 2000.

[104] S. Maleki, R. Sepehr, K. Staniszewski, N. Sheibani, C. M. Sorenson, and M. Ranji, "Mitochondrial redox studies of oxidative stress in kidneys from diabetic mice," *Biomed Opt Express,* vol. 3, pp. 273-81, Feb 1 2012.

[105] H. N. Xu, B. H. Wu, S. Nioka, B. Chance, and L. Z. Li, "Quantitative Redox Scanning of Tissue Samples Using a Calibration Procedure," *Journal of Innovative Optical Health Sciences,* vol. 2, pp. 375-385, Oct 2009.

[106] B. Chance and H. Baltscheffsky, "Respiratory enzymes in oxidative phosphorylation. VII. Binding of intramitochondrial reduced pyridine nucleotide," *Journal of Biological Chemistry,* vol. 233, pp. 736-9, Sep 1958.

[107] B. Chance, B. Schoener, R. Oshino, F. Itshak, and Y. Nakase, "Oxidation-reduction ratio studies of mitochondria in freeze-trapped samples. NADH and flavoprotein fluorescence signals," *The Journal of biological chemistry,* vol. 254, pp. 4764-71, Jun 10 1979.

[108] A. Mayevsky and G. G. Rogatsky, "Mitochondrial function in vivo evaluated by NADH fluorescence: from animal models to human studies," *Am J Physiol Cell Physiol,* vol. 292, pp. C615-40, Feb 2007.

[109] A. Mayevsky, R. Walden, E. Pewzner, A. Deutsch, E. Heldenberg, J. Lavee, S. Tager, E. Kachel, E. Raanani, S. Preisman, V. Glauber, and E. Segal, "Mitochondrial function and tissue vitality: bench-to-bedside real-time optical monitoring system," *Journal of Biomedical Optics,* vol. 16, Jun 2011.

[110] K. Staniszewski, S. H. Audi, R. Sepehr, E. R. Jacobs, and M. Ranji, "Surface fluorescence studies of tissue mitochondrial redox state in isolated perfused rat lungs," *Annals of biomedical engineering,* vol. 41, pp. 827-36, Apr 2013.

[111] A. B. Fisher, L. Furia, and B. Chance, "Evaluation of redox state of isolated perfused rat lung," *The American journal of physiology,* vol. 230, pp. 1198-1204, May 1976.

[112] B. Chance, P. Cohen, F. Jobsis, and B. Schoener, "Intracellular oxidation-reduction states in vivo," *Science,* vol. 137, pp. 499-508, Aug 17 1962.

[113] Y. Avi-Dor, J. Olson, M. Doherty, and N. Kaplan, "Fluorescence of pyridine nucleotides in mitochondria," *Biol. Chem,* vol. 237, p. 7, 1962.

[114] L. K. Klaidman, A. C. Leung, and J. D. Adams, Jr., "High-performance liquid chromatography analysis of oxidized and reduced pyridine dinucleotides in specific brain regions," *Anal Biochem,* vol. 228, pp. 312-7, Jul 1 1995.

[115] M. O'Connor, F. Welsh, L. Komarnicky, L. Davis, J. Stevens, D. Lewis, and C. Herman, "Origin of labile NADH tissue fluorescence," *Oxygen Physiol. Function,* p. 10, 1977.

[116] I. Georgakoudi, B. C. Jacobson, M. G. Muller, E. E. Sheets, K. Badizadegan, D. L. Carr-Locke, C. P. Crum, C. W. Boone, R. R. Dasari, J. Van Dam, and M. S. Feld, "NAD(P)H and collagen as in vivo quantitative fluorescent biomarkers of epithelial precancerous changes," *Cancer Res,* vol. 62, pp. 682-7, Feb 1 2002.

[117] N. Ramanujam, M. F. Mitchell, A. Mahadevan, S. Warren, S. Thomsen, E. Silva, and R. Richardskortum, "In-Vivo Diagnosis of Cervical Intraepithelial Neoplasia Using 337-Nm-Excited Laser-Induced Fluorescence," *Proceedings of the National Academy of Sciences of the United States of America,* vol. 91, pp. 10193-10197, Oct 11 1994.

[118] N. I. Shapiro, R. Arnold, R. Sherwin, J. O'Connor, G. Najarro, S. Singh, D. Lundy, T. Nelson, S. W. Trzeciak, A. E. Jones, and E. M. Emshocknet, "The association of near-infrared spectroscopy derived tissue oxygenation

measurements with sepsis syndromes, organ dysfunction, and mortality in emergency department patients with sepsis," *Critical Care,* vol. 15, p. R223, Sep 22 2011.

[119] A. Mayevsky and G. G. Rogatsky, "Mitochondrial function in vivo evaluated by NADH fluorescence: from animal models to human studies," *American Journal of Physiology-Cell Physiology,* vol. 292, pp. C615-C640, Feb 2007.

[120] J. J. Kelly, D. A. Rorvik, K. N. Richmond, and C. H. Barlow, "Videofluorometer for Imaging Tissue Metabolism," *Review of Scientific Instruments,* vol. 60, pp. 3498-3502, Nov 1989.

[121] J. T. Fitzgerald, A. Michalopoulou, C. D. Pivetti, R. N. Raman, C. Troppmann, and S. G. Demos, "Real-time assessment of in vivo renal ischemia using laser autofluorescence imaging," *Journal of Biomedical Optics,* vol. 10, Jul-Aug 2005.

[122] F. Sedlic, D. Pravdic, N. Hirata, Y. Mio, A. Sepac, A. K. Camara, T. Wakatsuki, Z. J. Bosnjak, and M. Bienengraeber, "Monitoring mitochondrial electron fluxes using NAD(P)H-flavoprotein fluorometry reveals complex action of isoflurane on cardiomyocytes," *Biochimica Et Biophysica Acta-Bioenergetics,* vol. 1797, pp. 1749-1758, Oct 2010.

[123] M. Ranji, "Fluorescent images of mitochondrial redox states of in situ mouse hypoxic ischemic intestines," *Journal of Innovative Optical Health Sciences (JIOHS),* vol. 2, pp. 365-374, 2009.

[124] M. Boldt, K. Harbig, G. Weidemann, and D. W. Lubbers, "A sensitive dual wavelength microspectrophotometer for the measurement of tissue fluorescence and reflectance," *Pflugers Arch,* vol. 385, pp. 167-73, May 1980.

[125] Q. Liu, G. Grant, and T. Vo-Dinh, "Investigation of Synchronous Fluorescence Method in Multicomponent Analysis in Tissue," *IEEE J. of selected Topics in Quantum Electronics,* vol. 16, p. 14, 2010.

[126] S. H. Audi, D. L. Roerig, S. T. Haworth, and A. V. Clough, "Role of Glutathione in Lung Retention of 99mTc-Hexamethylpropyleneamine Oxime in Two Unique Rat Models of Hyperoxic Lung Injury," *J Appl Physiol,* vol. 113, pp. 658-65, May 24 2012.

[127] K. Staniszewski, S. H. Audi, R. Sepehr, E. R. Jacobs, and M. Ranji, "Surface fluorescence studies of tissue mitochondrial redox state in isolated perfused rat lungs," *Ann Biomed Eng,* vol. 41, pp. 827-36, Apr 2013.

[128] J. V. Rocheleau, W. S. Head, and D. W. Piston, "Quantitative NAD(P)H/flavoprotein autofluorescence imaging reveals metabolic mechanisms of pancreatic islet pyruvate response," *J Biol Chem,* vol. 279, pp. 31780-7, Jul 23 2004.

[129] L. Xia, M. Bjornstedt, T. Nordman, L. C. Eriksson, and J. M. Olsson, "Reduction of ubiquinone by lipoamide dehydrogenase. An antioxidant regenerating pathway," *Eur J Biochem,* vol. 268, pp. 1486-90, Mar 2001.

[130] B. Commoner and D. Lipkin, "The Application of the Beer-Lambert Law to Optically Anisotropic Systems," *Science,* vol. 110, pp. 41-3, Jul 8 1949.

[131] Z. Gan, S. H. Audi, R. D. Bongard, K. M. Gauthier, and M. P. Merker, "Quantifying mitochondrial and plasma membrane potentials in intact pulmonary

arterial endothelial cells based on extracellular disposition of rhodamine dyes," *Am J Physiol Lung Cell Mol Physiol,* vol. 300, pp. L762-72, May 2011.

[132] P. L. Else and A. J. Hulbert, "Mammals: an allometric study of metabolism at tissue and mitochondrial level," *Am J Physiol,* vol. 248, pp. R415-21, Apr 1985.

[133] J. Eng, R. M. Lynch, and R. S. Balaban, "Nicotinamide adenine dinucleotide fluorescence spectroscopy and imaging of isolated cardiac myocytes," *Biophys J,* vol. 55, pp. 621-30, Apr 1989.

[134] E. M. Nuutinen, "Subcellular origin of the surface fluorescence of reduced nicotinamide nucleotides in the isolated perfused rat heart," *Basic Res Cardiol,* vol. 79, pp. 49-58, Jan-Feb 1984.

[135] R. Brandes and D. M. Bers, "Increased work in cardiac trabeculae causes decreased mitochondrial NADH fluorescence followed by slow recovery," *Biophys J,* vol. 71, pp. 1024-35, Aug 1996.

[136] C. B. Allen and C. W. White, "Glucose modulates cell death due to normobaric hyperoxia by maintaining cellular ATP," *Am J Physiol,* vol. 274, pp. L159-64, Jan 1998.

[137] M. R. Owen, E. Doran, and A. P. Halestrap, "Evidence that metformin exerts its anti-diabetic effects through inhibition of complex 1 of the mitochondrial respiratory chain," *Biochem J,* vol. 348 Pt 3, pp. 607-14, Jun 15 2000.

[138] T. K. Aldrich, A. B. Fisher, and H. J. Forman, "Paraquat inhibits mixed-function oxidation by rat lung," *J Appl Physiol,* vol. 54, pp. 1089-93, Apr 1983.

[139] A. B. Fisher, N. Itakura, C. Dodia, and R. G. Thurman, "Pulmonary mixed-function oxidation: stimulation by glucose and the effects of metabolic inhibitors," *Biochem Pharmacol,* vol. 30, pp. 379-83, Feb 15 1981.

[140] M. Aldakkak, D. F. Stowe, E. J. Lesnefsky, J. S. Heisner, Q. Chen, and A. K. Camara, "Modulation of mitochondrial bioenergetics in the isolated Guinea pig beating heart by potassium and lidocaine cardioplegia: implications for cardioprotection," *J Cardiovasc Pharmacol,* vol. 54, pp. 298-309, Oct 2009.

[141] W. S. Kunz and W. Kunz, "Contribution of different enzymes to flavoprotein fluorescence of isolated rat liver mitochondria," *Biochimica Et Biophysica Acta,* vol. 841, pp. 237-46, Sep 6 1985.

[142] W. S. Kunz and F. N. Gellerich, "Quantification of the content of fluorescent flavoproteins in mitochondria from liver, kidney cortex, skeletal muscle, and brain," *Biochem Med Metab Biol,* vol. 50, pp. 103-10, Aug 1993.

[143] F. J. Gerich, S. Hepp, I. Probst, and M. Muller, "Mitochondrial inhibition prior to oxygen-withdrawal facilitates the occurrence of hypoxia-induced spreading depression in rat hippocampal slices," *J Neurophysiol,* vol. 96, pp. 492-504, Jul 2006.

[144] R. A. De Blasi, M. Ferrari, A. Natali, G. Conti, A. Mega, and A. Gasparetto, "Noninvasive measurement of forearm blood flow and oxygen consumption by near-infrared spectroscopy," *J Appl Physiol,* vol. 76, pp. 1388-93, Mar 1994.

[145] Reyhaneh Sepehr, Said Audi, Sepideh Maleki, Kevin Staniszewski, Annie L. Eis, Girija G. Konduri, Mahsa Ranji ," Optical Imaging of Lipopolysaccharide-induced Oxidative Stress in Acute Lung Injury from Hyperoxia and Sepsis" JIOHS, Vol. 06, No. 03, 2013.

[146] Reyhaneh Sepehr, Said Audi, Kevin Staniszewski, Elizabeth R. Jacobs, and Mahsa Ranji, " Novel Flurometric Tool to Assess Mitochondrial Redox State of Isolated Perfused Rat Lungs after Exposure to Hyperoxia," to be published in IEEE Journal of Translational Engineering in Health and Medicine, 2013.

[147] Reyhaneh Sepehr, Kevin Staniszewski, Elizabeth R. Jacobs, Said Audi, and Mahsa Ranji, “Fluorometry of ischemia reperfused rat lungs in vivo”, accepted for presentation in SPIE photonices 2013.

[148] Anant B. Parekh, "Mitochondrial regulation of store-operated CRAC channels," Cell Calcium, vol. 44, pp. 6-13, 2008

[149] J. Kelly, J. Ewen, S. Bernard, R. Glenny, C. Barlow , "Mitochondrial Regional blood flow measurements from fluorescent microsphere images using an imaging CryoMicrotome," Rev Sci Instrum, vol. 71, pp. 228-234, 2000

[150] S. Bernard, J. Ewen, C. Barloe, J. Kelly, S. McKinney, D. Frazer, R. Glenny, "High spatial resolution measurements of organ blood flow in small laboratory animals," Am J Physiol Heart Circ Physiol , vol. 279, pp. 2043-2052, 2000

[151] Barker K, Seger D, Kumar S (2006). "Comment on "Pediatric fatality following ingestion of Dinitrophenol: postmortem identification of a 'dietary supplement'. Clin Toxicol (Phila) 44 (3): 351

7. Appendix I: Curriculum Vitae

Reyhaneh Sepehr

Place of birth: Abadeh, Iran

Education:

- B.Sc., Amir Kabir University of Technology, Tehran, Iran., May 2005
  Major: Biomedical Engineering

- M.Sc., Amir Kabir University of Technology, Tehran, Iran., Spring 2008
  Major: Biomedical Engineering

Dissertation Title:

- Optical Studies Of Oxidative Stress In Lung Tissue: Rodent Models

Affiliations/Memberships:

- SPIE member since January 2012

Teaching Experience:

- Teaching Assistant for the course "DSP", Fall Semester 2008
- Tutoring English and Mathematics.

Research Experience:

- Researcher in Biophotonics Lab since Aug 2010. Projects:
  - Evaluate oxidative stress and redox state of tissue in different models of lung injuries *in situ* using image processing and fluorescent imaging in cryogenic temperatures.
  - Optical techniques in determining the dynamics of mitochondrial redox state of the normal and injured lung tissue *ex vivo*.
  - *In vivo* experiments and signal processing to evaluate the effect of acute ischemia and other lung injury models using optical fluorometry for real-time disease diagnosis.
  - *In vitro* studies of chemical perturbations to alter the ionic channels and ROS production in both cellular and subcellular membranes.

- Researcher in R&D Department of Pooyandegan-Rah-Saadat Co. Tehran, Iran, February 2009-August 2010. Projects:
    - Artifact removal of plethysmographic signals.
    - Measure of depth of anesthesia from EEG signals
    - ECG noise measurement and index

- Medical Engineer in BNM Co. Tehran, Iran, Summer 2008, Working on the Cell Separator Devices.

- Medical Engineer in the Medical Engineering Center of Madaen Hospital, Tehran, Iran, summer 2002.

- Biomedical Engineering Magazine Team Member Nov 2007-Apr 2010.

Awards/Honors:

- **2013** Nominated for the distinguished dissertation fellowship from the electrical engineering department, UW Milwaukee

- **2012** Ranked **3rd** in the research day poster competition held by collage of engineering and applied science, UW Milwaukee.

- **2011** Ranked **1st** in the PhD qualifying exam, electrical engineering, UW Milwaukee.

- **2010-2013** Recipient of UWM Research Foundation Fellow Award, Chancellor's Award and travel award.

- **2005-2008** Ranked as **2nd** among the students of Biomedical Msc. Engineering of Amir Kabir University of Technology.

- **2004** Granted fellowship to study Masters on biomedical engineering in Amir Kabir University of Technology without taking the entrance exam.

- **2002** Granted fellowship to study two majors simultaneously in Amir Kabir University of Technology (second major: Electrical Engineering, Electronics)

- **2001** Ranked **301th** among the 450,000 participants in the nationwide ‘Universities Entrance Exam’ and rewarded as an outstanding student of Amir Kabir University of Technology.

- **2000** Accepted in the first stage of Physics & Mathematics Olympiads of Iran.

Journal Publications and Conference Abstracts:

Peer-Reviewed Journal Papers

- **Reyhaneh Sepehr**, Kevin Staniszewski, Said Audi, Elizabeth R. Jacobs, and Mahsa Ranji, "Surface Fluorescence Studies of Tissue Mitochondrial Redox State in Isolated Perfused Rat Lungs," Ann Biomed Eng, Dec 13 2012.

- **Reyhaneh Sepehr**, Kevin Staniszewski, Sepideh Maleki, Elizabeth R. Jacobs, Said Audi, and Mahsa Ranji, "Optical imaging of tissue mitochondrial redox state in intact rat lungs in two models of pulmonary oxidative stress" Journal of Biomedical Optics, Vol 17, No. 4, April 2012.

- **Reyhaneh Sepehr**, Said Audi, Sepideh Maleki, Kevin Staniszewski, Annie L. Eis, Girija G. Konduri, Mahsa Ranji ," Optical Imaging of Lipopolysaccharide-induced Oxidative Stress in Acute Lung Injury from Hyperoxia and Sepsis" JIOHS, Vol. 06, No. 03, 2013.

- **Reyhaneh Sepehr**, Said Audi, Kevin Staniszewski, Elizabeth R. Jacobs, and Mahsa Ranji, " Novel Flurometric Tool to Assess Mitochondrial Redox State of Isolated Perfused Rat Lungs after Exposure to Hyperoxia," to be published in IEEE Journal of Translational Engineering in Health and Medicine, 2013.

- Sepideh Maleki, **Reyhaneh Sepehr**, Kevin Staniszewski, Nader Sheibani, Christine M. Sorenson, and Mahsa Ranji, "Mitochondrial redox studies of oxidative stress in kidneys from diabetic mice." Journal of Biomedical Optics Express, Vol. 3, No. 2, pp. 273-281, Feb 2012.

- Sepideh Maleki, Sandeep Gopalakrishnan, Zahra Ghanian, **Reyhaneh Sepehr**, Heather Schmitt, Janis Eells, Mahsa Ranji, "Optical Imaging of Mitochondrial Redox State in Rodent Model of Retinitis Pigmentosa ", accepted for publication in Journal of Biomedical Optics.

Conference Papers

- **Reyhaneh Sepehr**, Kevin Staniszewski, Elizabeth R. Jacobs, Said Audi, and Mahsa Ranji, "*Fluorometry of ischemia reperfused rat lungs in vivo*", accepted for presentation in SPIE photonices 2013.

- Zahra Ghanian, Sepideh Maleki, Sandeep Gopalakrishnan, **Reyhaneh Sepehr**, Heather Schmitt, Janis Eells, Mahsa Ranji, "*Optical Imaging of Oxidative Stress in Rodent Model of Retinitis Pigmentosa*", accepted as poster presentation to SPIE photonices west 2013

- **R. Sepehr,** K. Staniszewski, E. R. Jacobs, S. Audi, M. Ranji, "*Optical studies of tissue mitochondrial redox in isolated perfused rat lungs*", in Proceedings of SPIE 8207D, San Fransisco, 2012; doi: 10.1117/12.909474

- **R. Sepehr**, K. Staniszewski, C. M. Sorenson, N. Sheibani, M. Ranji, "*Classification of retinopathic injury using image cytometry and vasculature complexity*", in Proceedings of SPIE 8225, San Fransisco, 2012; doi: 10.1117/12.908598

- S. Maleki, **R. Sepehr**, K. Staniszewski, N. Sheibani, C.M. Sorenson, M. Ranji, "*Optical cryoimaging of kidney mitochondrial redox state in diabetic mice models*", in Proceedings of SPIE 8225, San Fransisco, 2012.

- K. Staniszewski, **R. Sepehr**, S. Maleki, C.M. Sorenson, N. Sheibani, M. Ranji, " *Automated Evaluation of Retinopathies Using Image Cytometry*", DAMOR Workshop, Feb 2012.

- **R. Sepehr**, K. Staniszewski, S. Maleki, M. Ranji, "*Optical Cryoimaging of Kidney Mitochondrial Redox State and the Effect of BCL-2 Family Expression*", BMES Oct 2011.

- **R. Sepehr**, S. Audi, K. Staniszewski, S Maleki, M. Ranji, "*Fluorescence Spectroscopy and Cryoimaging of Rat Lung Tissue Mitochondrial Redox State*", in Proceedings of SPIE 80870, Munich, 2011; doi:10.1117/12.890019.

University Services:

- Organizing Committee Member of the 16th Iranian Conference on Electrical Engineering (icee2008) Tarbiat Modares University, Tehran, Iran.

- President of Persian Sports club (an student organization at UW Milwaukee)

8. Appendix II: Abstracts of Journal Papers

Journal of Biomedical Optics 17(4), 046010 (April 2012)

Optical imaging of tissue mitochondrial redox state in intact rat lungs in two models of pulmonary oxidative stress

Reyhaneh Sepehr, Kevin Staniszewski, Sepideh Maleki, Elizabeth R. Jacobs, Said Audi, and Mahsa Ranji
University of Wisconsin Milwaukee, Biophotonics Lab, Department of Electrical Engineering, Milwaukee, Wisconsin 53211
Pulmonary Division, Zablocki VA Medical Center, Milwaukee, Wisconsin 53295
Marquette University, Department of Biomedical Engineering, Milwaukee, Wisconsin 53233

Abstract. Ventilation with enhanced fractions of O_2 (hyperoxia) is a common and necessary treatment for hypoxemia in patients with lung failure, but prolonged exposure to hyperoxia causes lung injury. Ischemia-reperfusion (IR) injury of lung tissue is common in lung transplant or crush injury to the chest. These conditions are associated with apoptosis and decreased survival of lung tissue. The objective of this work is to use cryoimaging to evaluate the effect of exposure to hyperoxia and IR injury on lung tissue mitochondrial redox state in rats. The autofluorescent mitochondrial metabolic coenzymes nicotinamide adenine dinucleotide (NADH) and flavin adenine dinucleotide (FAD) are electron carriers in ATP generation. These intrinsic fluorophores were imaged for rat lungs using lowtemperature fluorescence imaging (cryoimaging). Perfused lungs from four groups of rats were studied: normoxia (control), control perfused with an mitochondrial complex IV inhibitor (potassium cyanide, KCN), rats exposed to hyperoxia (85% O2) for seven days, and from rats subjected to lung IR in vivo 24 hours prior to study. Each lung was sectioned sequentially in the transverse direction, and the images were used to reconstruct a three-dimensional (3-D) rendering. In KCN perfused lungs the respiratory chain was more reduced, whereas hyperoxic and IR lung tissue have a more oxidized respiratory chain than control lung tissue, consistent with previously measured
mitochondrial dysfunction in both hyperoxic and IR lungs.
 [DOI: 10.1117/1.JBO.17.4.046010]
Keywords: optical imaging; nicotinamide adenine dinucleotide; flavin adenine dinucleotide; mitochondrial redox; lung tissue; hyperoxia; ischemia-reperfusion.
Paper 11581 received Oct. 7, 2011; revised manuscript received Feb. 3, 2012; accepted for publication Feb. 14, 2012; published online Apr. 19, 2012.

Annals of Biomedical Engineering (2012) DOI: 10.1007/s10439-012-0716-z

Surface Fluorescence Studies of Tissue Mitochondrial Redox State in Isolated Perfused Rat Lungs

Kevin Staniszewski, Said H. Audi, Reyhaneh Sepehr, Elizabeth R. Jacobs, Mahsa Ranji

Biophotonics Lab, Department of Electrical Engineering, University of Wisconsin Milwaukee, 3200 N Cramer St., Milwaukee,WI 53211, USA;
Department of Biomedical Engineering, Marquette University, 1515 West Wisconsin Avenue, Milwaukee,WI 53233, USA;
Research and Development, Clement J. Zablocki VA Medical Center, 5000 W. National Avenue, Milwaukee,WI 5329, USA;
Medical College of Wisconsin, Milwaukee, WI, USA

(Received 18 July 2012; accepted 28 November 2012)

Abstract—We designed a fiber-optic-based optoelectronic fluorometer to measure emitted fluorescence from the auto-fluorescent electron carriers NADH and FAD of the mitochondrial electron transport chain (ETC). The ratio of NADH to FAD is called the redox ratio (RR = NADH/FAD) and is an indicator of the oxidoreductive state of tissue. We evaluated the fluorometer by measuring the fluorescence intensities of NADH and FAD at the surface of isolated, perfused rat lungs. Alterations of lung mitochondrial metabolic state were achieved by the addition of rotenone (complex I inhibitor), potassium cyanide (KCN, complex IV inhibitor) and/or pentachlorophenol (PCP, uncoupler) into the perfusate recirculating through the lung. Rotenone- or KCN-containing perfusate increased RR by 21and 30%, respectively. In contrast, PCP-containing perfusate decreased RR by 27%. These changes are consistent with the established effects of rotenone, KCN, and PCP on the redox status of the ETC. Addition of blood to perfusate quenched NADH and FAD signal, but had no effect of RR. This study demonstrates the capacity of fluorometry to detect a change in mitochondrial redox state in isolated perfused lungs, and suggests the potential of fluorometry for use in in vivo experiments to extract a sensitive measure of lung tissue's health in real-time.

Keywords—Lung surface fluorometry, Nicotinamide Adenine Dinucleotide (NADH), Flavin Adenine Dinucleotide (FADH2), Mitochondrial redox

Journal of Innovative Optical Health Sciences
Vol. 6, No. 3 (2013) 1350017 (10 pages)
DOI: 10.1142/S179354581350017X

Optical Imaging Of Lipopolysaccharide induced Oxidative Stress In Acute Lung Injury From Hyperoxia And Sepsis

Reyhaneh Sepehr, Said H. Audi, Sepideh Maleki And Kevin Staniszewski, Annie L. Eis, Girija G. Konduri, Mahsa Ranji

Biophotonics Laboratory, Department of Electrical Engineering and Computer Science, University of Wisconsin Milwaukee
Department of Biomedical Engineering Marquette University
Department of Pediatrics, Cardiovascular Research Center Medical College of Wisconsin
ranji@uwm.edu

Received 21 February 2013
Accepted 2 May 2013

Abstract. Reactive oxygen species (ROS) have been implicated in the pathogenesis of many acute and chronic pulmonary disorders such as acute lung injury (ALI) in adults and bronchopulmonary dysplasia (BPD) in premature infants. Bacterial infection and oxygen toxicity, which result in pulmonary vascular endothelial injury, contribute to impaired vascular growth and alveolar simplification seen in the lungs of premature infants with BPD. Hyperoxia induces ALI, reduces cell proliferation, causes DNA damage and promotes cell death by causing mitochondrial dysfunction. The objective of this study was to use an optical imaging technique to evaluate the variations in °uorescence intensities of the auto-°uorescent mitochondrial metabolic coenzymes, NADH and FAD in four di®erent groups of rats. The ratio of these °uorescence signals (NADH/FAD), referred to as NADH redox ratio (NADH RR) has been used as an indicator of tissue metabolism in injuries. Here, we investigated whether the changes in metabolic state can be used as a marker of oxidative stress caused by hyperoxia and bacterial lipopolysaccharide (LPS) exposure in neonatal rat lungs. We examined the tissue redox states of lungs from four groups of rat pups: normoxic (21% O2) pups, hyperoxic (90% O2) pups, pups treated with LPS (normoxic þ LPS), and pups treated with LPS and hyperoxia (hyperoxic þ LPS). Our results show that hyperoxia oxidized the respiratory chain as re°ected by a _43% decrease in lung tissue NADH RR as compared to that for normoxic lungs. LPS treatment alone or with hyperoxia had no significant effect on lung tissue NADH RR as compared to that for normoxic or hyperoxic lungs, respectively. Thus, NADH RR serves as a quantitative marker of oxidative stress level in lung injury caused by two clinically important conditions: hyperoxia and LPS exposure.

Keywords: Fluorescence imaging; NADH; FAD; LPS; Hyperoxia.

IEEE Journal of Translational Engineering in Health and Medicine
Vol. 1, No. 1 (2013) 1500210
DOI: 10.1109/JTEHM.2013.2285916

Novel Flurometric Tool to Assess Mitochondrial Redox State of Isolated Perfused Rat Lungs after Exposure to Hyperoxia

R. Sepehr, S. H. Audi[‡], K. S. Staniszewski, S. T. Haworth, E. R. Jacobs, M. Ranji[‡,*]

[‡]Co-Senior authors, *Corresponding author

Abstract[1] Recently we demonstrated the utility of optical fluorometry to detect a change in the redox status of mitochondrial autofluorescent coenzymes NADH (Nicotinamide Adenine Dinucleotide) and FAD (oxidized form of Flavin Adenine Dinucleotide (FADH2,)) as a measure of mitochondrial function in isolated perfused rat lungs (IPL). The objective of this study was to utilize optical fluorometry to evaluate the effect of rat exposure to hyperoxia (>95% O2 for 48 hours) on lung tissue mitochondrial redox status of NADH and FAD in a nondestructive manner in IPL. Surface NADH and FAD signals were measured before and after lung perfusion with perfusate containing rotenone (ROT, complex I inhibitor), potassium cyanide (KCN, complex IV inhibitor), and/or pentachlorophenol (PCP, uncoupler). ROT- or KCN-induced increase in NADH signal is considered a measure of complex I activity, and KCN-induced decrease in FAD signal is considered a measure of complex II activity. The results show that hyperoxia decreased complex I and II activities by 63% and 55%, respectively, as compared to lungs of rats exposed to room air (normoxic rats). Mitochondrial complex I and II activities in lung homogenates were also lower (77% and 63%, respectively) for hyperoxic than for normoxic lungs. These results suggest that the mitochondrial matrix is more reduced in hyperoxic lungs than in normoxic lungs, and demonstrate the ability of optical fluorometry to detect a change in mitochondrial redox state of hyperoxic lungs prior to histological changes characteristic of hyperoxia.

Index Terms— NADH dehydrogenase (complex I), succinate dehydrogenase (complex II), Flavin Adenine Dinucleotide ($FADH_2$), Nicotinamide Adenine Dinucleotide (NADH), lung surface fluorometry, mitochondrial redox

---

Manuscript received 2013. This work was supported in part by the support of University of Wisconsin Milwaukee RGI 7 Grant, Clinical and Translational Science Institute KL2 Grant: NIH 8Kl2TR000056, Wisconsin Applied Research grant (Wi-ARG), NIH grant 8UL1TR000055 (CTSI), VA Merit Review Award BX001681, and the Department of Veterans Affairs that provided resources essential to the completion of these investigations.

Biomed Opt Express
Vol. 3, No. 2 (2012) 273-281
DOI: 10.1364/BOE.3.000273

Mitochondrial Redox Studies of Oxidative Stress in Kidneys of Diabetic Akita Mice and Bcl-2 Deficient Mice

S Maleki[a], R. Sepehr[a], K. Staniszewski[a], N Sheibani[b], C.M. Sorenson[c], M. Ranji[a,*]
[a]Biophotonics laboratory, University of Wisconsin Milwaukee, Department of Electrical Engineering and Computer Science
Departments of [b]Ophthalmology and Visual Sciences, and [c]Pediatrics,
University of Wisconsin School of Medicine and Public Health
*: Corresponding author

Abstract: Diabetic nephropathy (DN) represents the most common cause of end stage renal disease (ESRD) and is known as a major risk factor in developing cardiovascular disease. Chronic hyperglycemia which occurs during diabetes, leads to overproduction of free radicals especially reactive oxygen species (ROS) by the mitochondria electron transport chain. Overproduction of ROS as a consequence of hyperglycemia, causes an increase in oxidative stress (OS) which then exacerbates the development and progression of diabetes and its complications such as renal vascular and proximal tubule cell dysfunction [1-3]. Here, we investigate the change in the metabolic state of the tissue which can be used as a hallmark of OS in different tissues in two groups of mice kidneys including a group of Akita diabetic mice kidneys, its corresponding wild type (WT) and one group of bcl-2 deficient (bcl-2 -/-) mice, its corresponding WT (bcl-2 +/+). Bcl-2 family of proteins act as an anti-apoptotic protein with anti-oxidant effects, which are considered as a regulator of OS. bcl-2 expression decreases during diabetes. Akita mice, which have a mutation in the insulin 2 gene, develop type 1 diabetes as early as 4-weeks of age and a more sever diabetes by 5-6 weeks of age We also have used a novel model , Akita/TSP mice which lack thrombospondin-1 that develops much more sever diabetic nephropathy compared to its control mice, TSP-/-[4, 5]. In this study, 3D cryoimaging was utilized to obtain the fluorescence images of kidney extracted from bcl-2 -/- mice, Akita diabetic mice and their WTs as well as Akita/TSP and their WTs. Redox Ratio (RR) was used as a quantitative marker of OS in bcl-2 -/- mice as well as Akita diabetic mice of different ages.

Keywords: Oxidative stress markers, diabetes, hyperglycemia, Bcl-2 family protein, Akita diabetic mouse model, redox ratio, fluorescence imaging.

Journal of Biomedical Optics
Vol. 18, No. 1 (2013) 16004
DOI: 10.1117/1.JBO.18.1.016004

Optical Imaging of Mitochondrial Redox State in Rodent Model of Retinitis Pigmentosa

Sepideh Maleki, Sandeep Gopalakrishnan, Zahra Ghanian, Reyhaneh Sepehr, Heather Schmitt, Janis Eells, Mahsa Ranji

Abstract: Oxidative stress (OS) and mitochondrial dysfunction contribute to photoreceptor cell loss in retinal degenerative disorders. The objective of this study was to investigate the metabolic state of the retina in a rodent model of retinitis pigmentosa using a cryofluorescence imaging technique. The mitochondrial metabolic coenzymes NADH and FAD are autofluorescent and can be monitored without exogenous labels using optical techniques. The cryofluorescence redox imaging technique provides a quantitative assessment of the metabolism. More specifically, the ratio of the fluorescence intensity of these fluorophores, (NADH/FAD), the NADH redox ratio (RR), is a marker of the metabolic state of the tissue. We examined the NADH RR and retinal function in an established rodent model of retinitis pigmentosa, the P23H rat compared to that of non-dystrophic Sprague-Dawley (SD) rats. The NADH RR mean values were 1.11 ± 0.03 in the SD normal and 0.841 ± 0.01 in the P23H retina, indicating increased OS in the P23H retina. Electroretinographic data revealed a significant reduction in photoreceptor function in P23H animals compared to SD normal rats. Thus, cryofluorescence redox imaging was used as a quantitative marker of OS in eyes from transgenic rats and demonstrated that alterations in the oxidative state of eyes occur during the early stages of RP.

Keywords: Optical imaging, NADH, FAD, NADH redox ratio, Oxidative stress, Inherited retinal degeneration, Mitochondrial dysfunction.